iemn Institut d'Electronique, de Microélectronique et de Nanotechnologie

Introduction to Phononic Crystals and Metamaterials

B. Djafari Rouhani

University of Lille, France

School « METAgenierie »

July 2-7, Oléron (*France)*

ePov

Université de Lille 1 Sciences et Technologies

Outline

1.Simple analytical models to introduce basic notions

- Band gaps and localized modes associated to defects
- Zeros of transmission and Fano resonances

2. One-dimensional (1D) multilayer structures

- Theoretical methods
- Dispersion curves, band gaps and localized modes
- Transmission coefficient: tunnelling (fast)transmission and resonant (slow) transmission

3. Two-dimensional (2D) Phononic crystals

- Theoretical methods
- Dispersion curves and complete band gaps (Bragg gaps and hybridization gaps)
- Local resonances and low frequency gaps
- Waveguide and cavity modes

4. Phononic crystal slabs and nanobeams

- Array of holes in a Si membrane
- Array of pillars on a thin membrane
- Surface waves in semi-infinite phononic crystals
- Nanobeam waveguides

Phononic crystal slabs

1.Periodic array of holes in a Si membrane

- Square, honeycomb and boron nitride lattices
  - Phononic and photonic band gaps
  - Waveguides and slow modes
  - Normal transmission and sensor applications

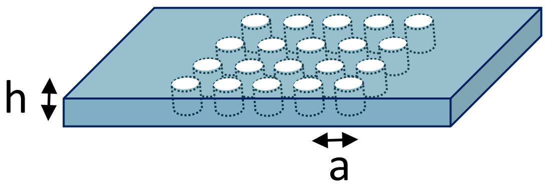

2.Periodic array of pillars on a membrane

- Phonon dispersion curves
  - Low and high frequency gaps
  - Waveguide modes, transmission and mode conversion
- Normal transmission and Fano resonances

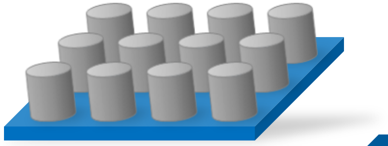

Extraordinary transmission through subwavelength pillars

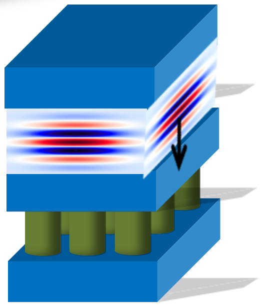

3. Strip waveguides

Band gaps, cavity modes, slow modes

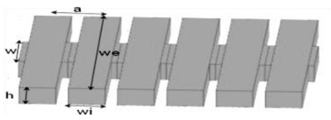

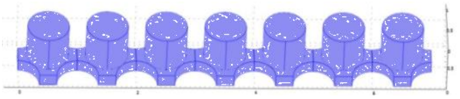

2D infinite phononic crystal: air holes in silicon matrix

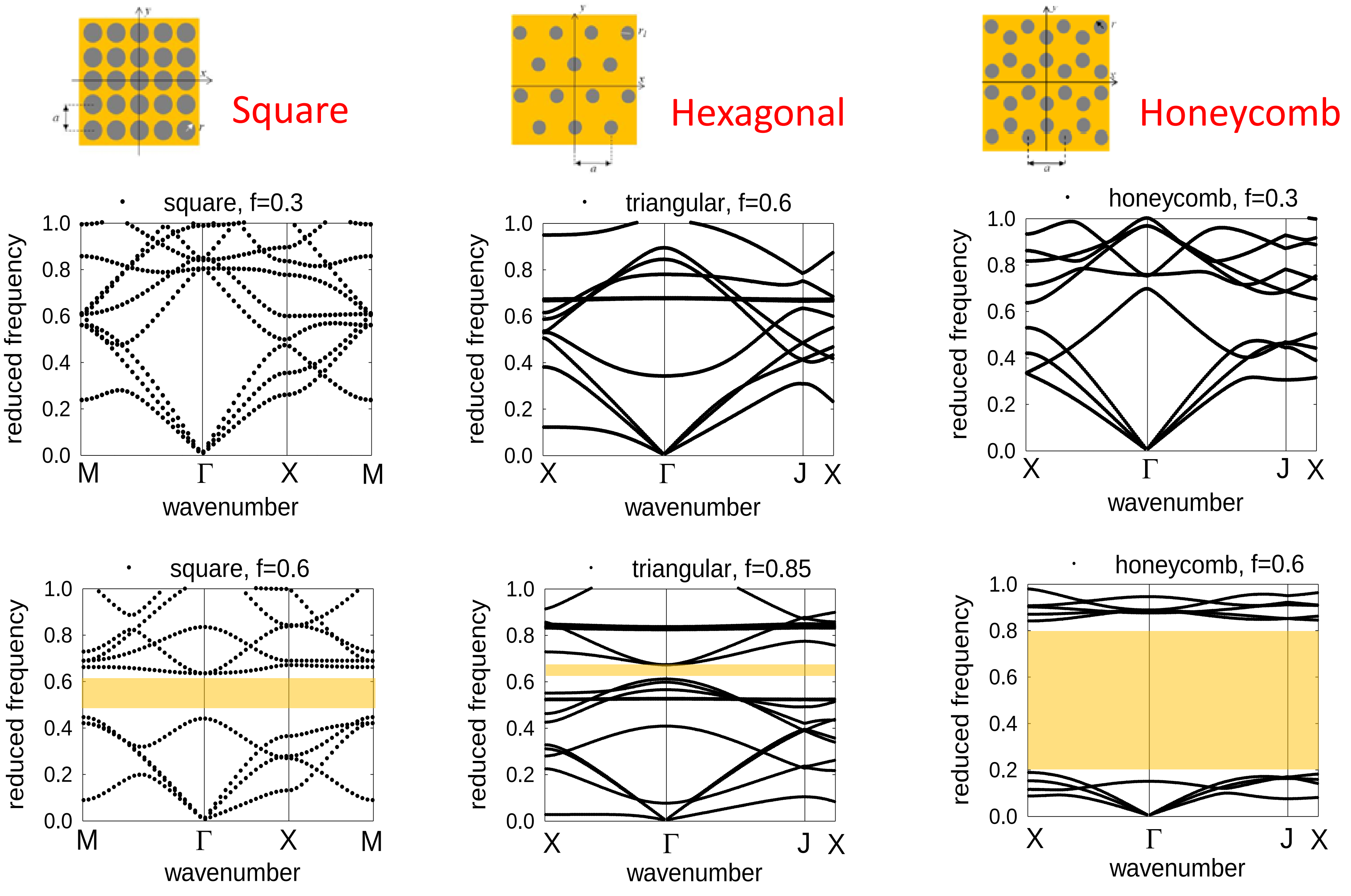

Periodic arrays of holes in a silicon membrane
Square lattice

Existence of absolute band gap

R/a = 0.47
h/a=0.1 - 0.55 - 2

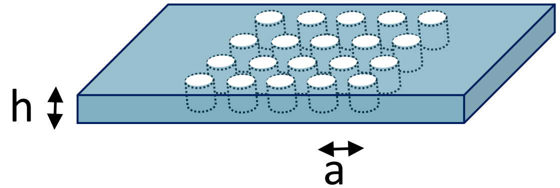

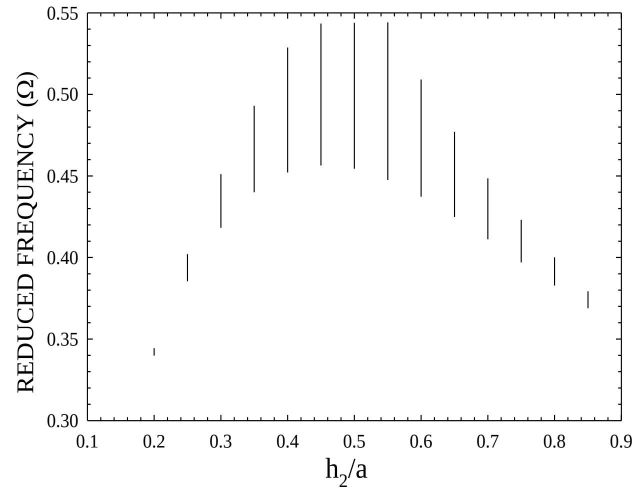

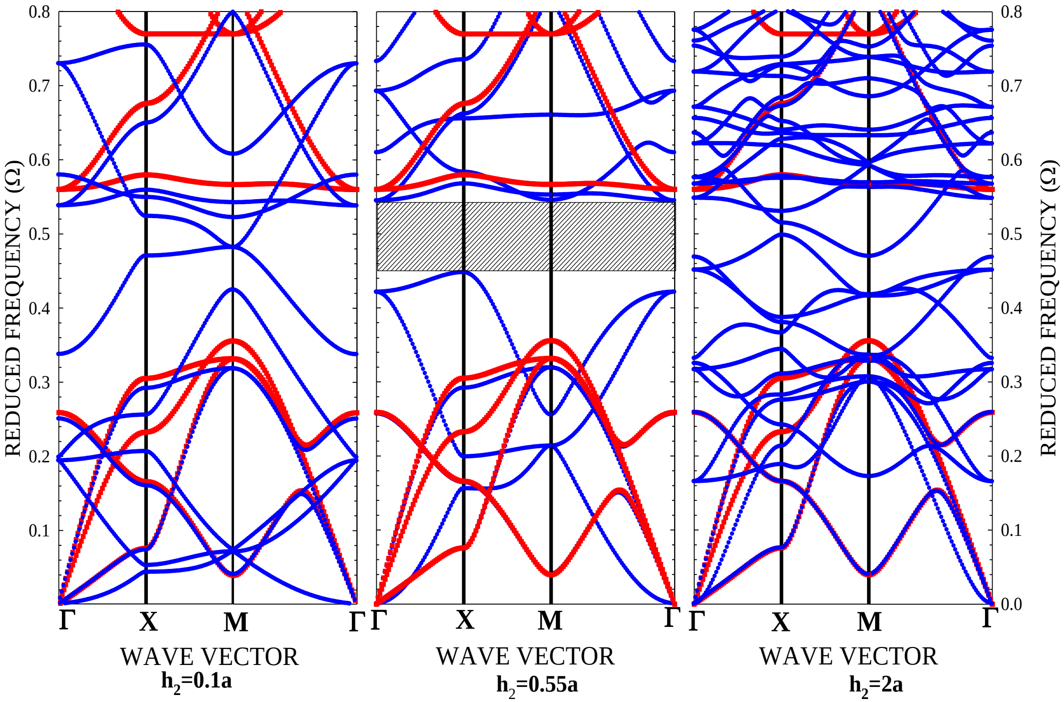

Location and width of the band gap versus the ratio **thickness/period**

Bulk modes ——
Plate modes ——

J. Vasseur, P. Deymier, B. Djafari Rouhani, Y. Pennec, A.C. Hladky-Hennion
Proceedings IMECE 2006 and Phys. Rev. B77, 085415 (2008)

Periodic arrays of holes in a silicon membrane

Honeycomb lattice

Existence of absolute band gap

Honeycomb lattice

R/a = 0.47, h/a= 0.1 - 1 - 2

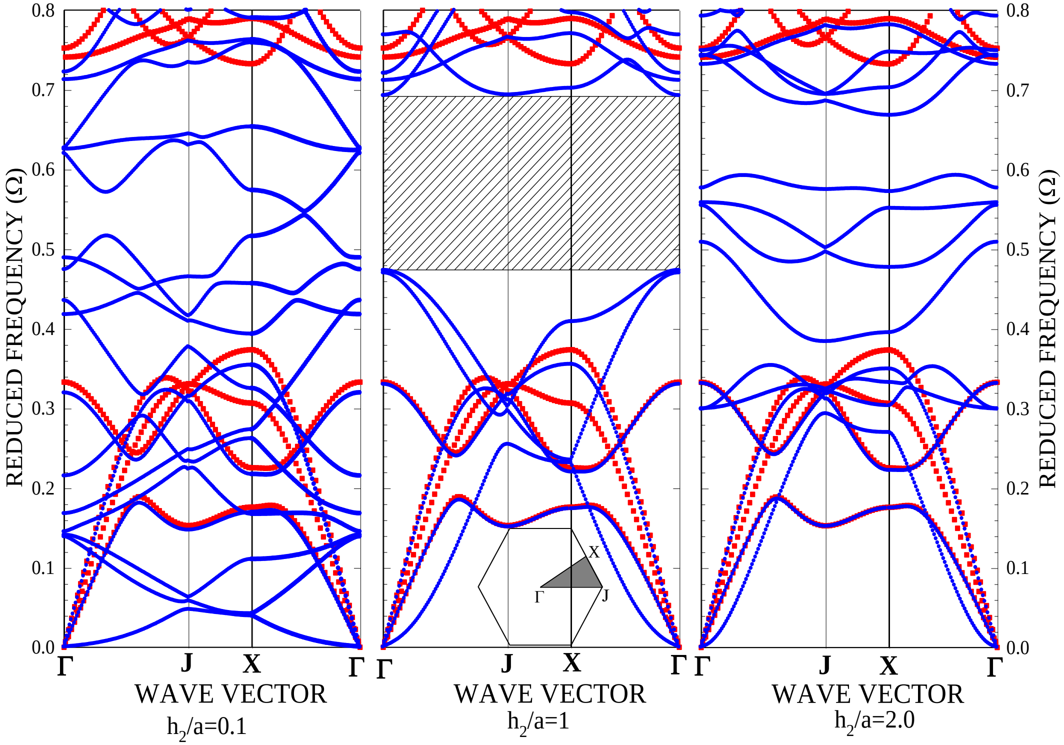

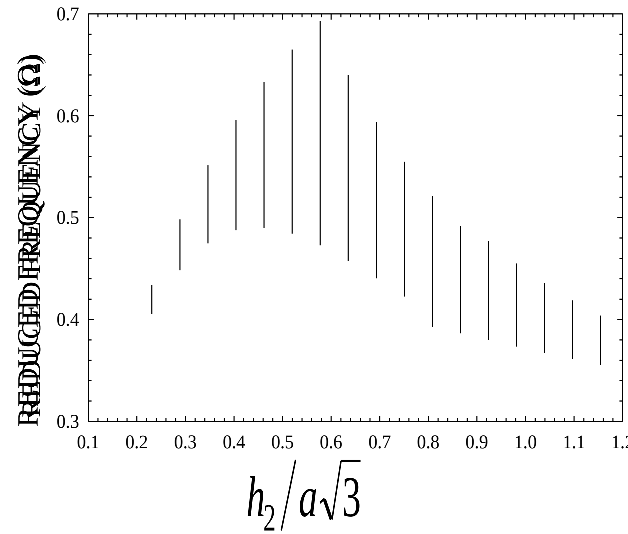

Location and width of the band gap versus the ratio : $h/a\sqrt{3}$

Bulk modes ———

Plate modes ———

J. Vasseur, P. Deymier, B. Djafari Rouhani, Y. Pennec, A.C. Hladky-Hennion
Proceedings IMECE 2006 and **Phys. Rev. B77, 085415 (2008)**

Waveguiding in a phononic crystal slab

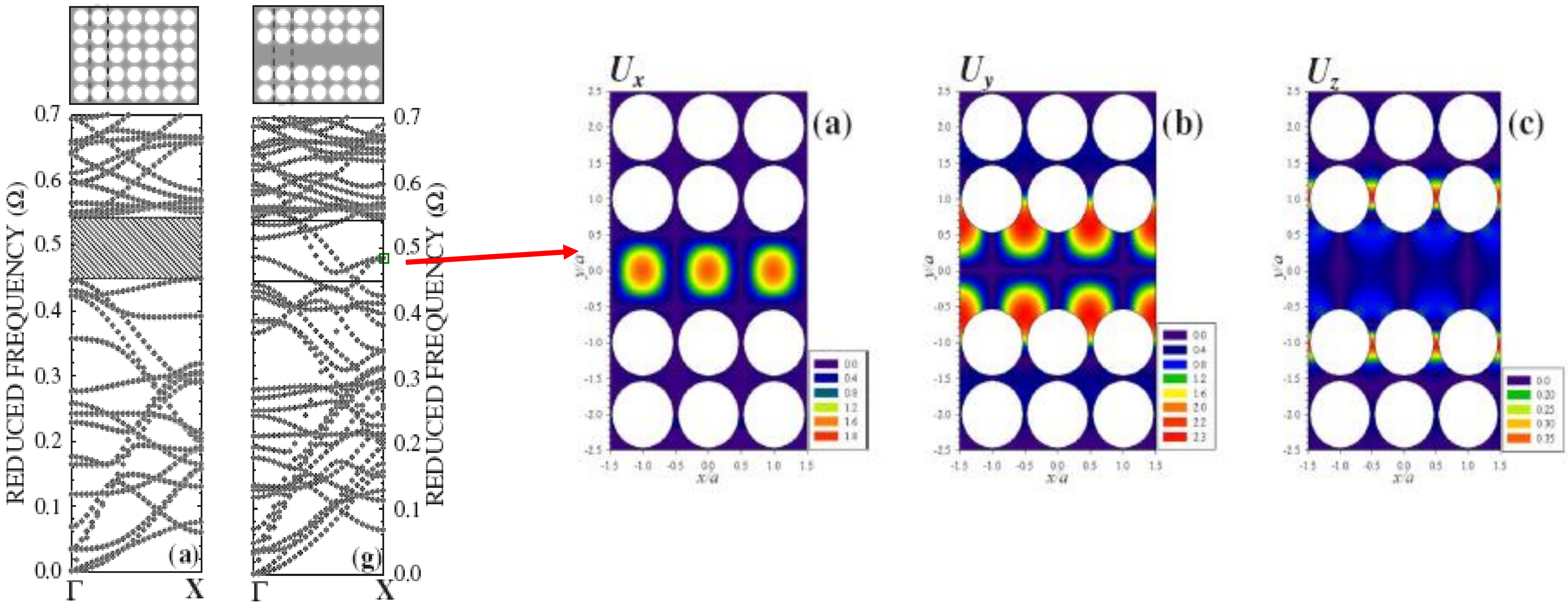

Without waveguide

With waveguide

J. Vasseur, P. Deymier, B. Djafari Rouhani, Y. Pennec, A.C. Hladky-Hennion
Phys. Rev. B77, 085415 (2008)

PZT Phononic crystal slab on a silicon substrate

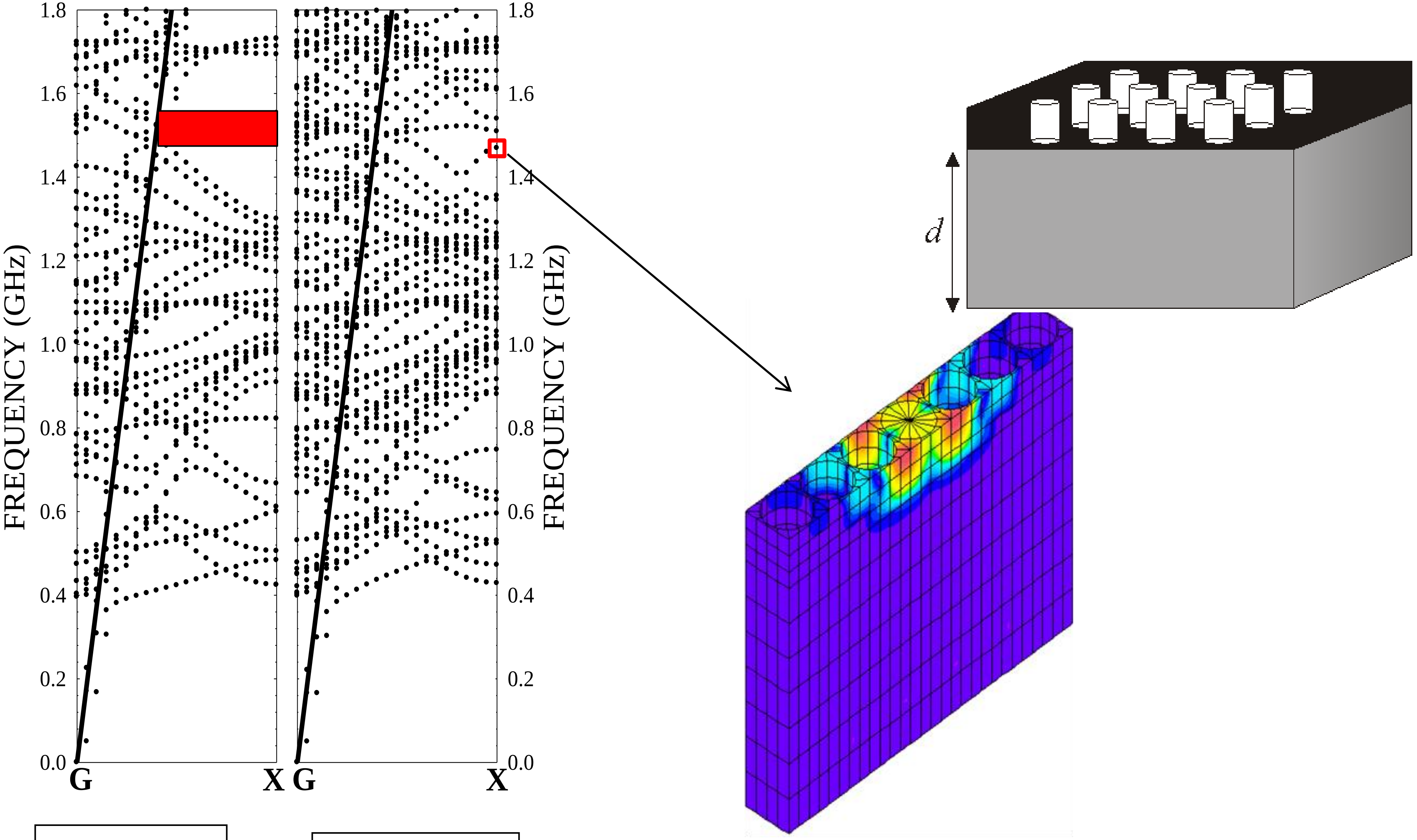

Without waveguide

With waveguide

J.O. Vasseur *et al.* , JAP 101, 114904 (2007)

Periodic arrays of holes in a silicon membrane

Dispersion Curves

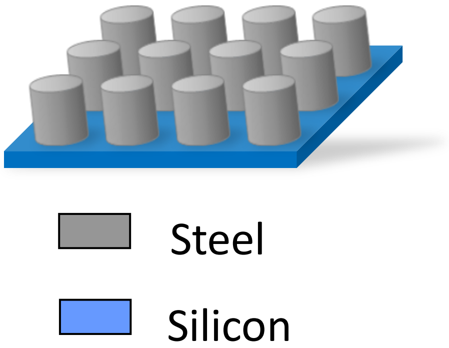

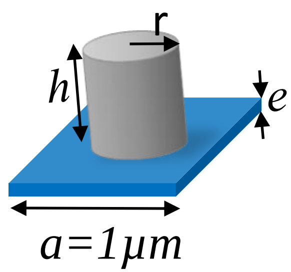

unit cell

e=0.1µm; a=1µm; h=0.6µm; r =0.42µm; $\beta = \frac{\pi . r^2}{a^2} = 56\%$

<u>Band structure</u>

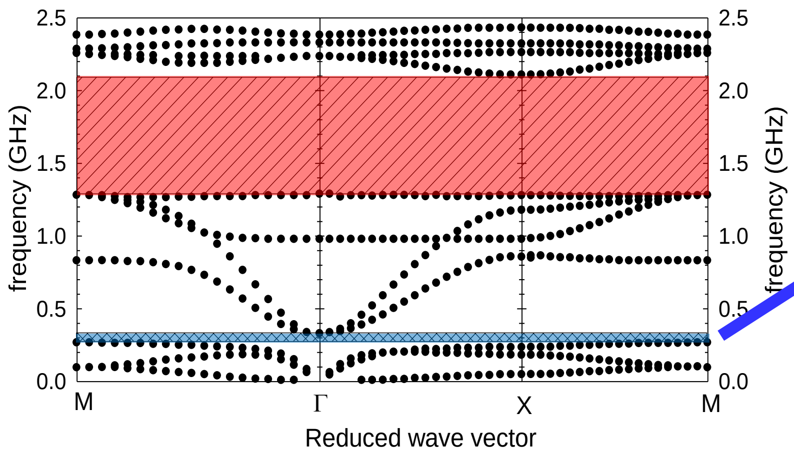

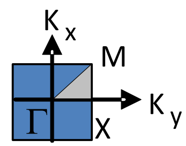

<u>Zoom of the band structure</u>

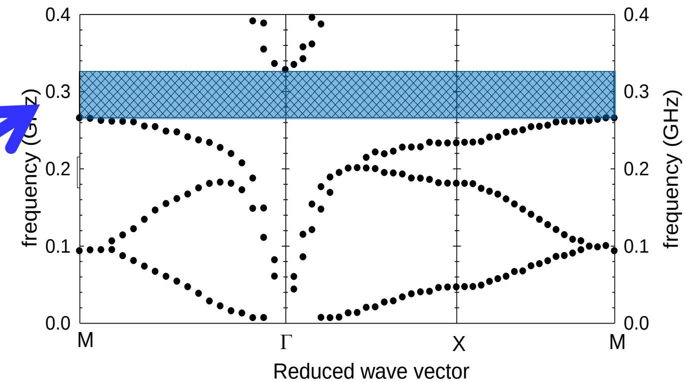

Existence of two absolute band gaps:

1. <u>At high frequency</u> **[1.28, 2.11GHz]**

2. <u>At low frequency</u> **[0.265, 0.327GHz]**
as compared to theBragg Gap :

Y. Pennec, B. Djafari Rouhani, H. Larabi et al, Phys. Rev. B 78, 104105 (2008)
B. Djafari Rouhani, Y. Pennec and H. Larabi, Proc. SPIE Vol. 7223, 72230F (2009)

High Frequency Gaps (HFG)

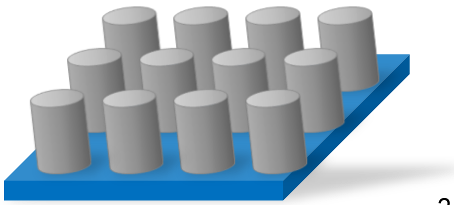

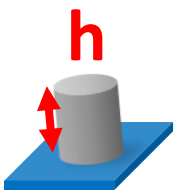

e = 0.2 µm
r = 0.42 µm

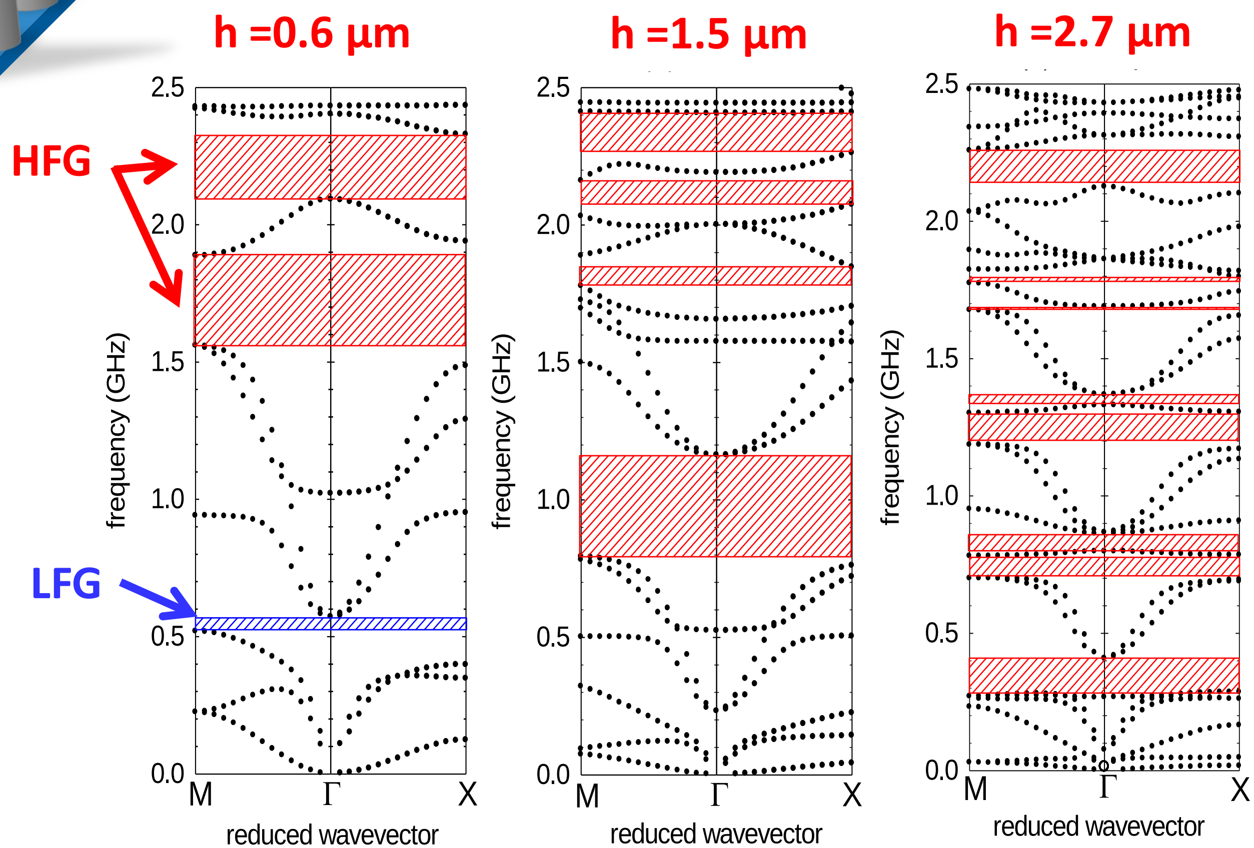

When increasing the height of the cylinders,

- The number of the gaps increases
- Their central frequencies move downward

Y. Pennec, B. Djafari Rouhani, H. Larabi et al, Phys. Rev. B 78, 104105 (2008)
B. Djafari Rouhani, Y. Pennec and H. Larabi, Proc. SPIE Vol. 7223, 72230F (2009)

Persistence of the low frequency gap as a function of the physical parameters

Steel cylinder

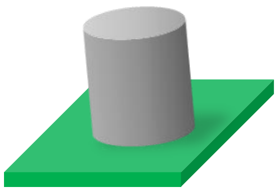

Various plates

e=0.1µm
h=0.6µm

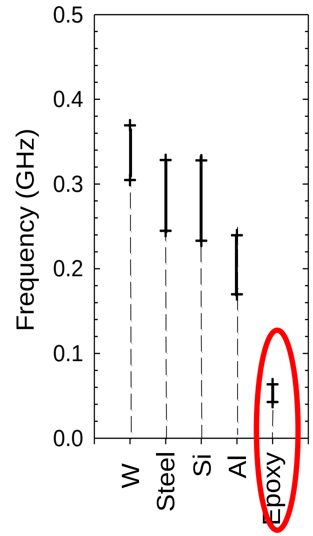

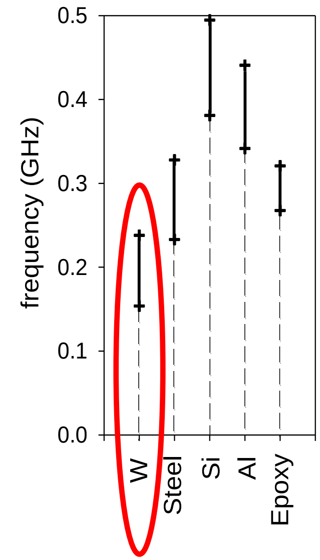

Various cylinders

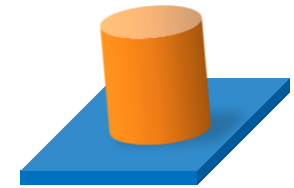

Silicon plate

Persistence of the gap upon different combinations of the constituting materials

---

Lowest gap:
high density cylinders on low density plate

Tungsten Cylinders

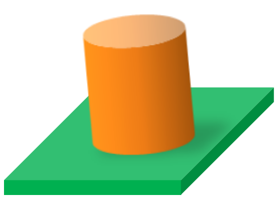

Epoxy plate

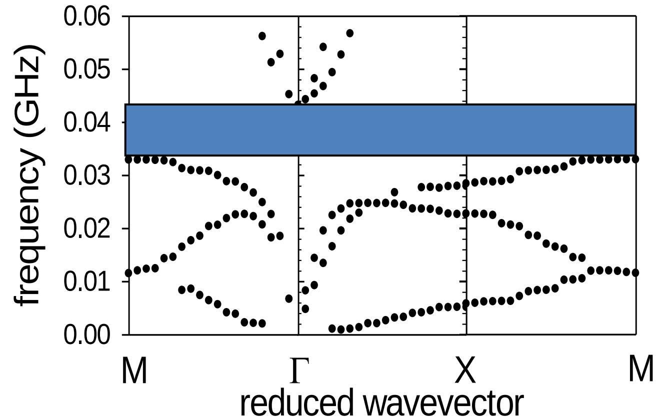

a=1µm
e=0.1µm
h=0.6µm

Nickel pillars on a $LiNbO_3$ substrate

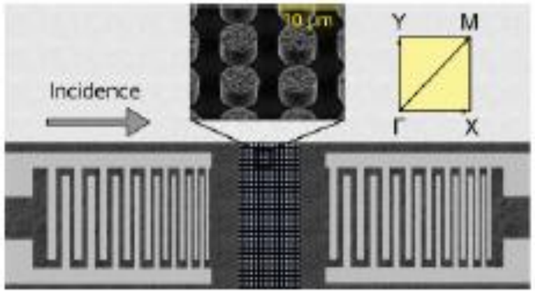

Experimental set-up

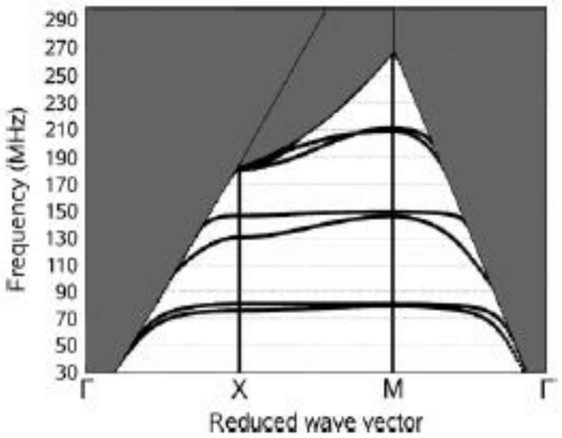

Band structure

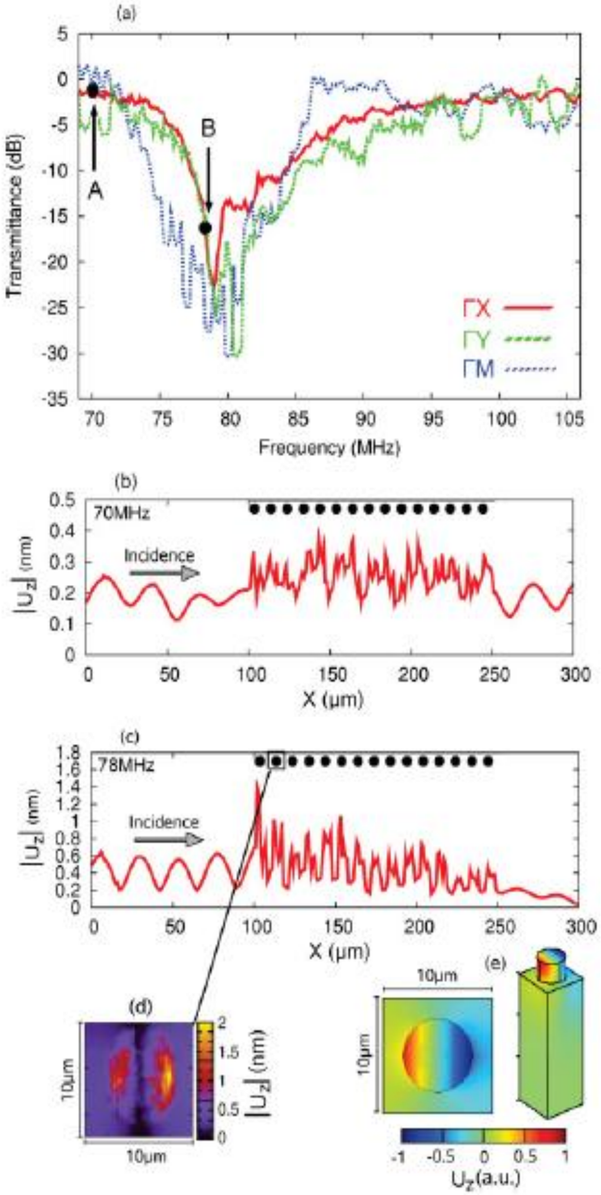

Y. Achaoui, A. Khelif, S. benchabane, L. Robert and V. Laude, Phys. Rev. B 83, 104201 (2011)

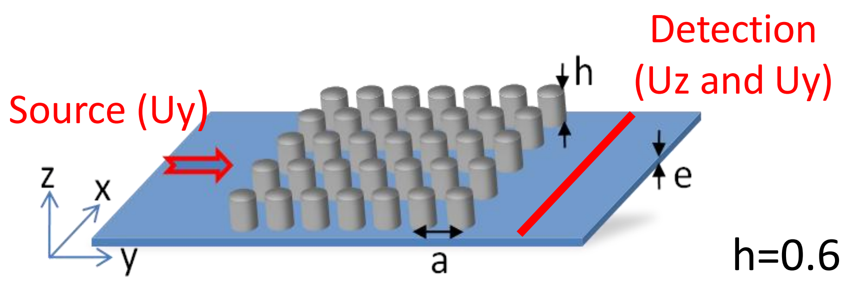

h=0.6µm
e=0.2µm
a=1.0µm

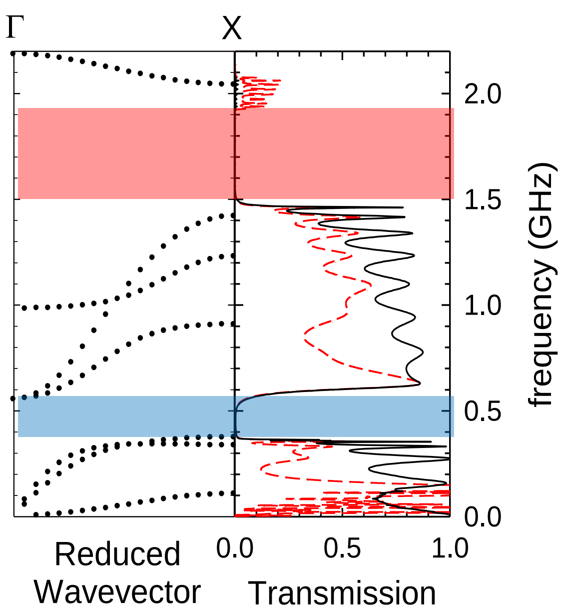

Polarization Uy
Polarization Uz

Guiding the waves

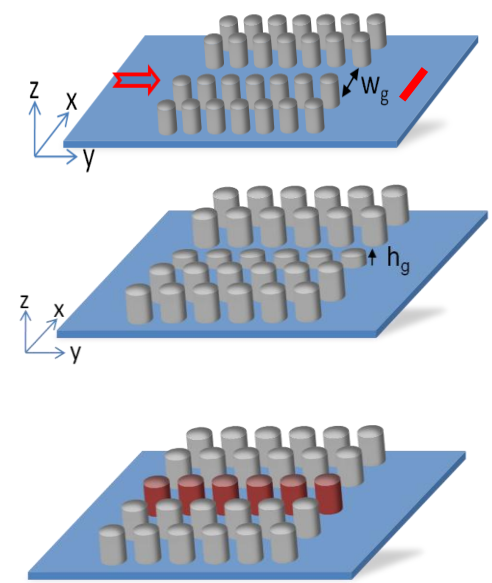

- -Number of localized branches in each gap
- -Transmitting/ non transmitting branches
- - Mode conversion/ Polarization conservation
- -Strong / weak confinement
- -Localization in the membrane or in the dots

Y. Pennec, B. Djafari Rouhani, H. Larabi et al, Phys.Rev. B 80, 144302 (2009)

Hollow Pillars and Confined Whispering Gallery Modes

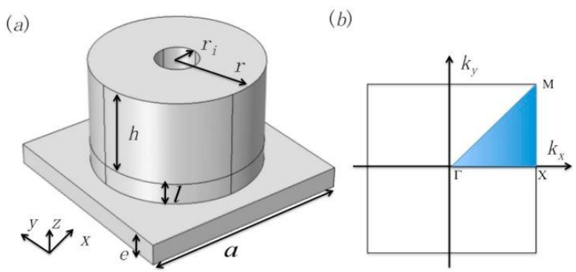

Geometry and the first Brillouin zone

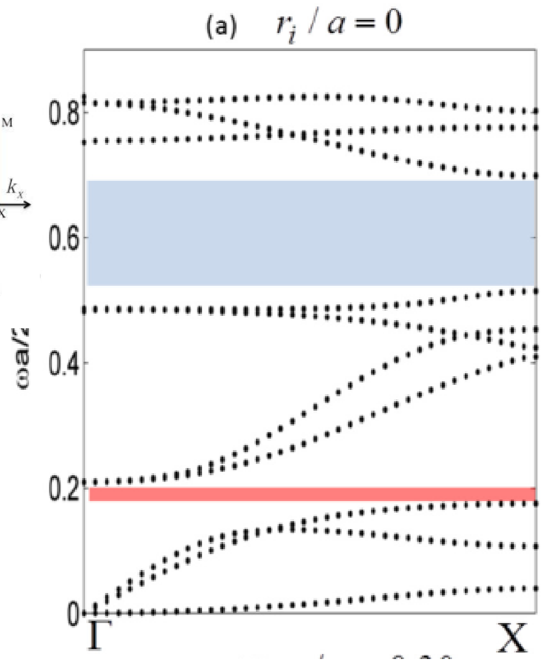

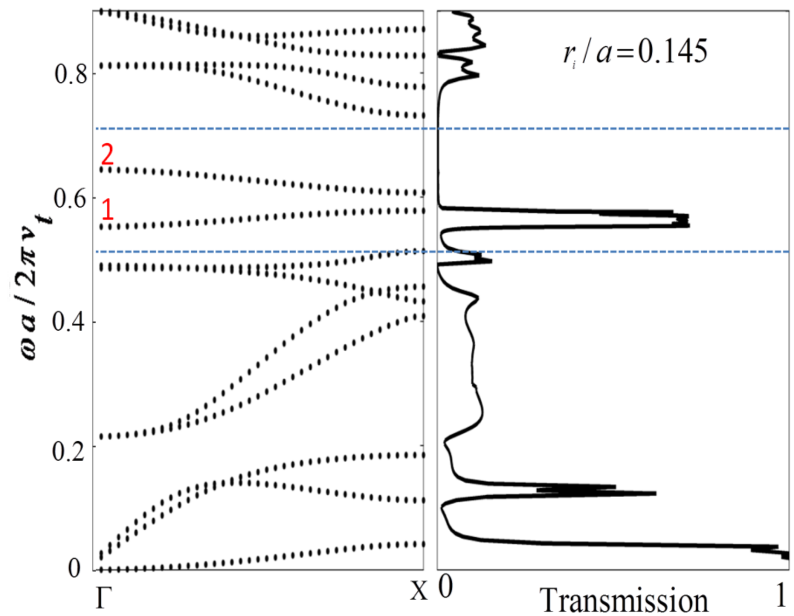

- Confined WGM modes
- Applications to waveguiding and demultiplexing
- Liquid filling: sensing applications

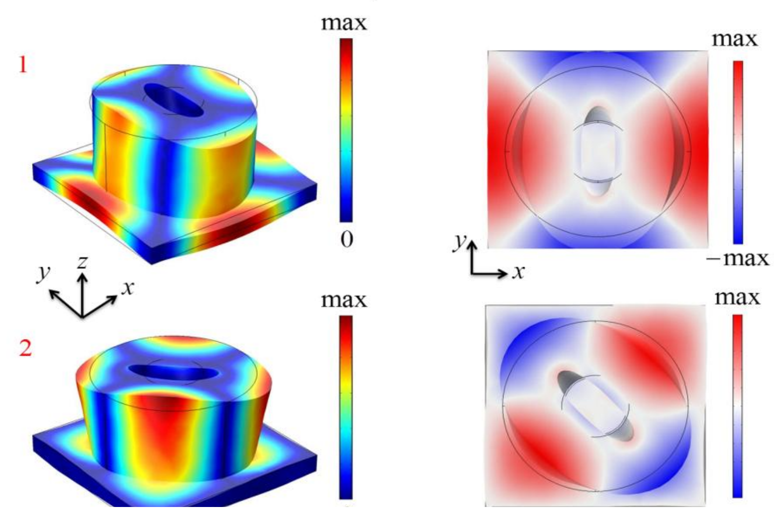

Y. Jin et al, Phys. Rev. B 93, 054109 (2016);
Crystals 6, 64 (2016);
J. Phys. D: Applied Physics 50, 035301 (2017)

Hollow pillars connected by thin bars

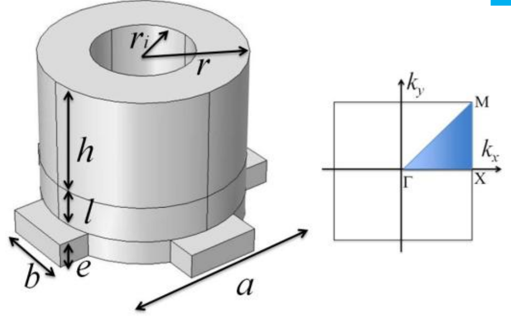

Without Hollows

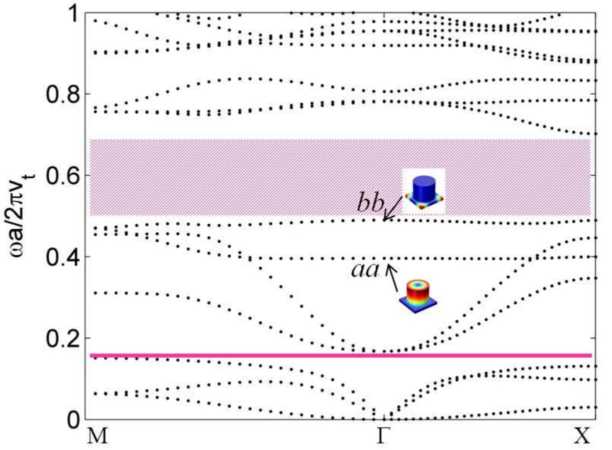

b/a=1

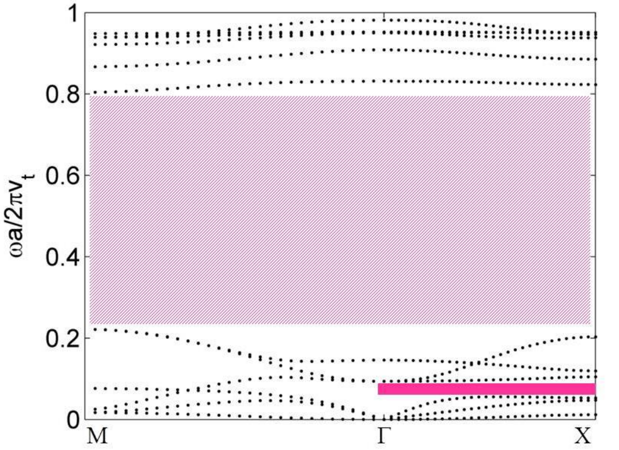

b/a=0.1

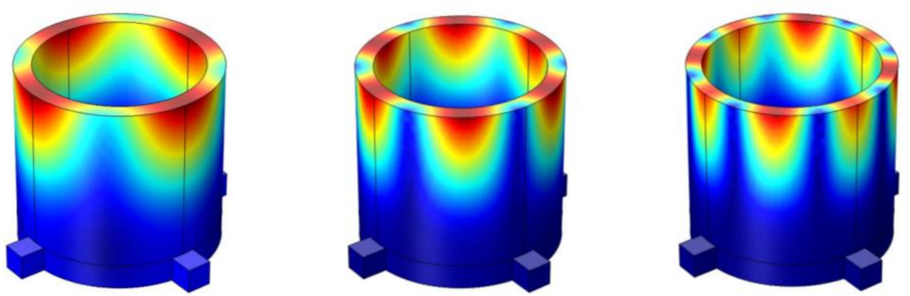

Quadrupolar WGM

Hexapolar WGM

Octopolar WGM

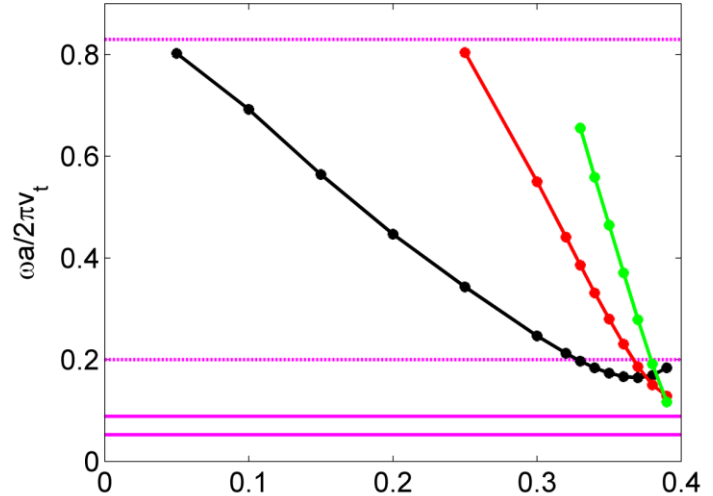

b/a=0.1, r/a=0.4, h/a=0.45, e/a=0.1, l/a=0.2

Y. Jin et al, J. Phys. D: Applied Physics 50, 035301 (2017)

Scattering of Lamb waves with a single or an array of pillars

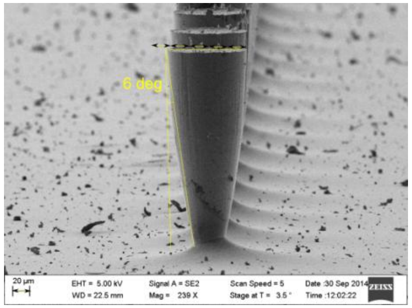

Line of conic pillar

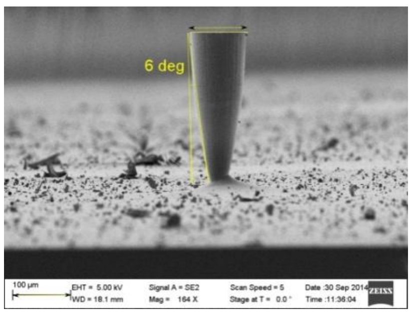

Isolated pillar

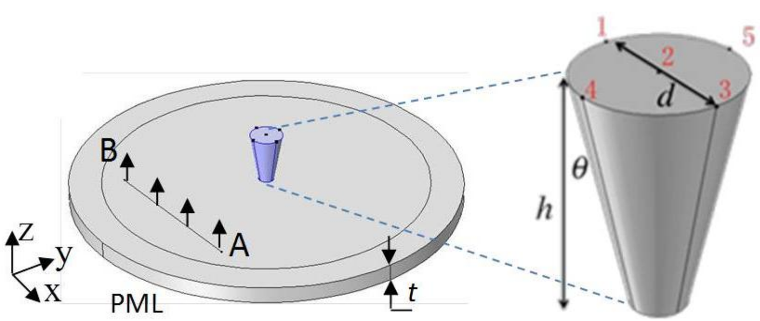

Simulation Model

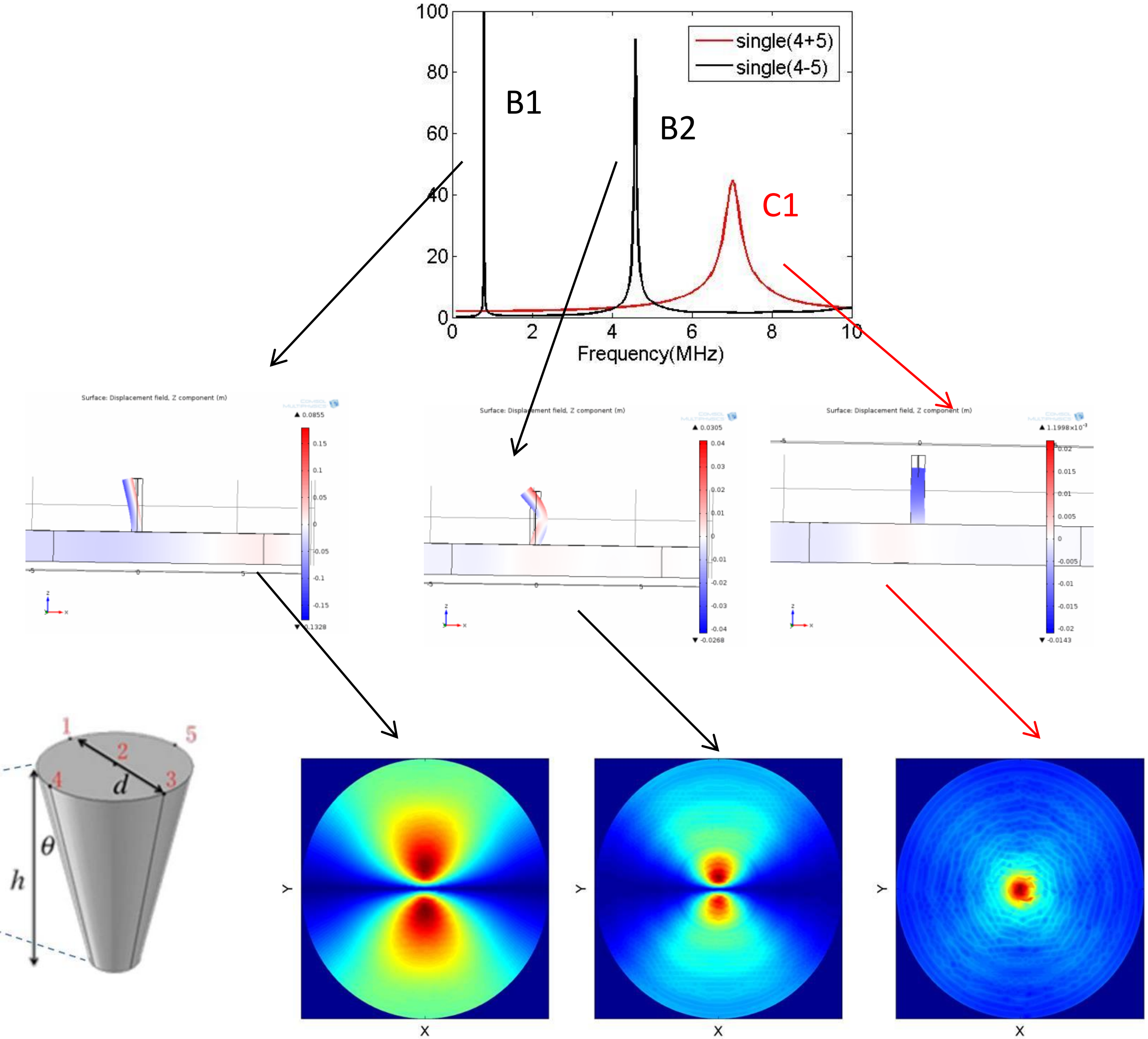

Outline

5. Brief overview of refractive properties

- Negative refraction and focusing
- Self-collimation and beam splitting

6. Subwavelength structures and applications of metamaterials

- Effective properties (positive and negative dynamic parameters)
- Focusing and imaging. Superlens and heperlens
- Cloaking
- GRIN devices
- Metasurfaces. Resonating units and space coiling. Absorption. Phase manipulation

7. Active materials and some emerging topics

Non reciprocal behaviors . Time-space periodicity. PT symmetry. Topological phononics.

8. Dual phononic-photonic crystals (phoXonic) and Optomechanics

- Simultaneous phononic-photonic band gaps.
- Waveguide modes. Slow and fast modes
- Enhanced phonon-photon interaction in a cavity. Comparison of photoelastic and optomechanic effects
- Phononic and Phoxonic sensors

Positive and negative refraction

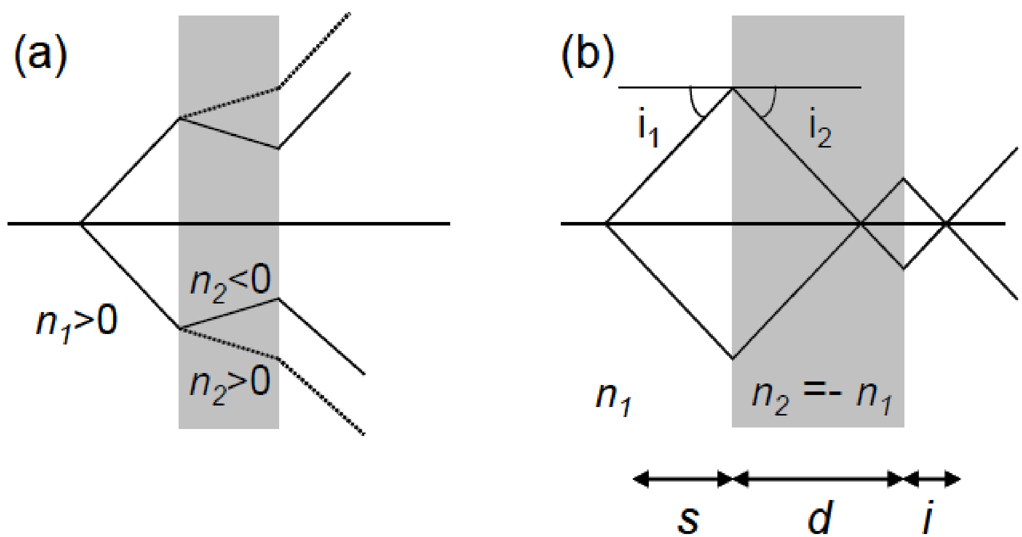

Refraction by a slab (flat lens)

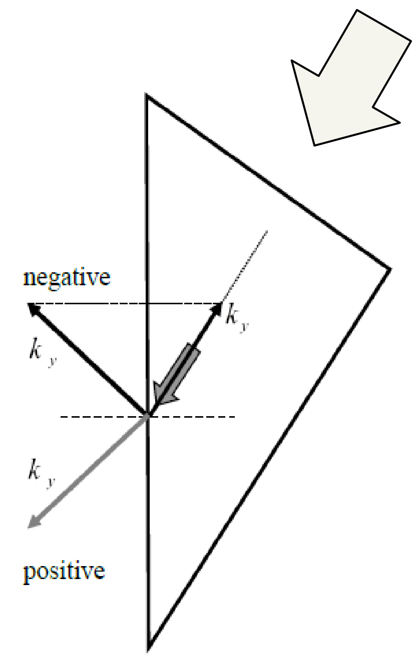

Negative refraction by a prism

Positive and negative refraction

Positive refraction

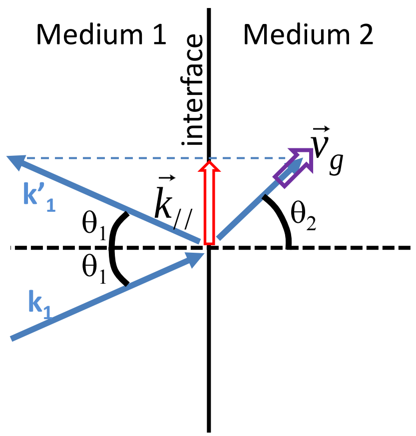

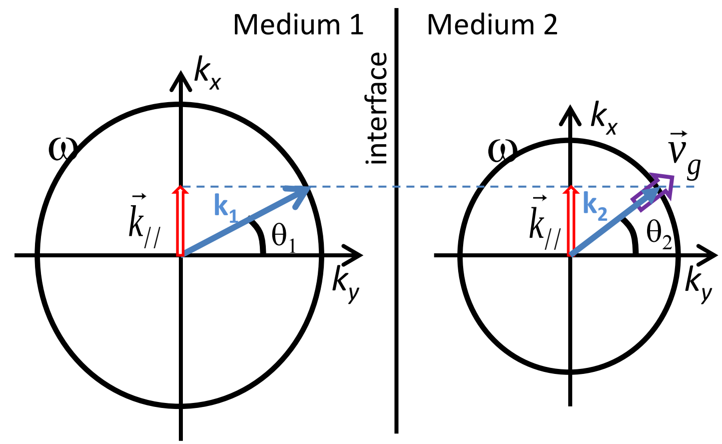

Negative refraction

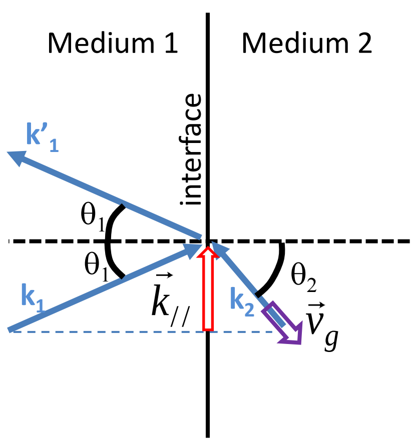

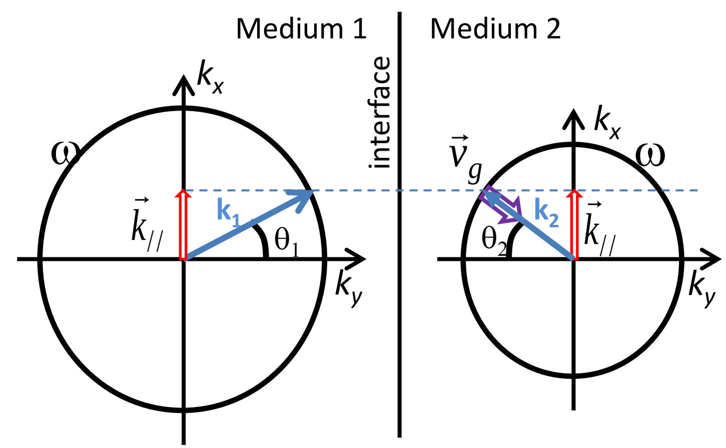

2D Phononic crystal made of a triangular lattice of steel cylinders in water (a=1.27mm, r=0.51mm)

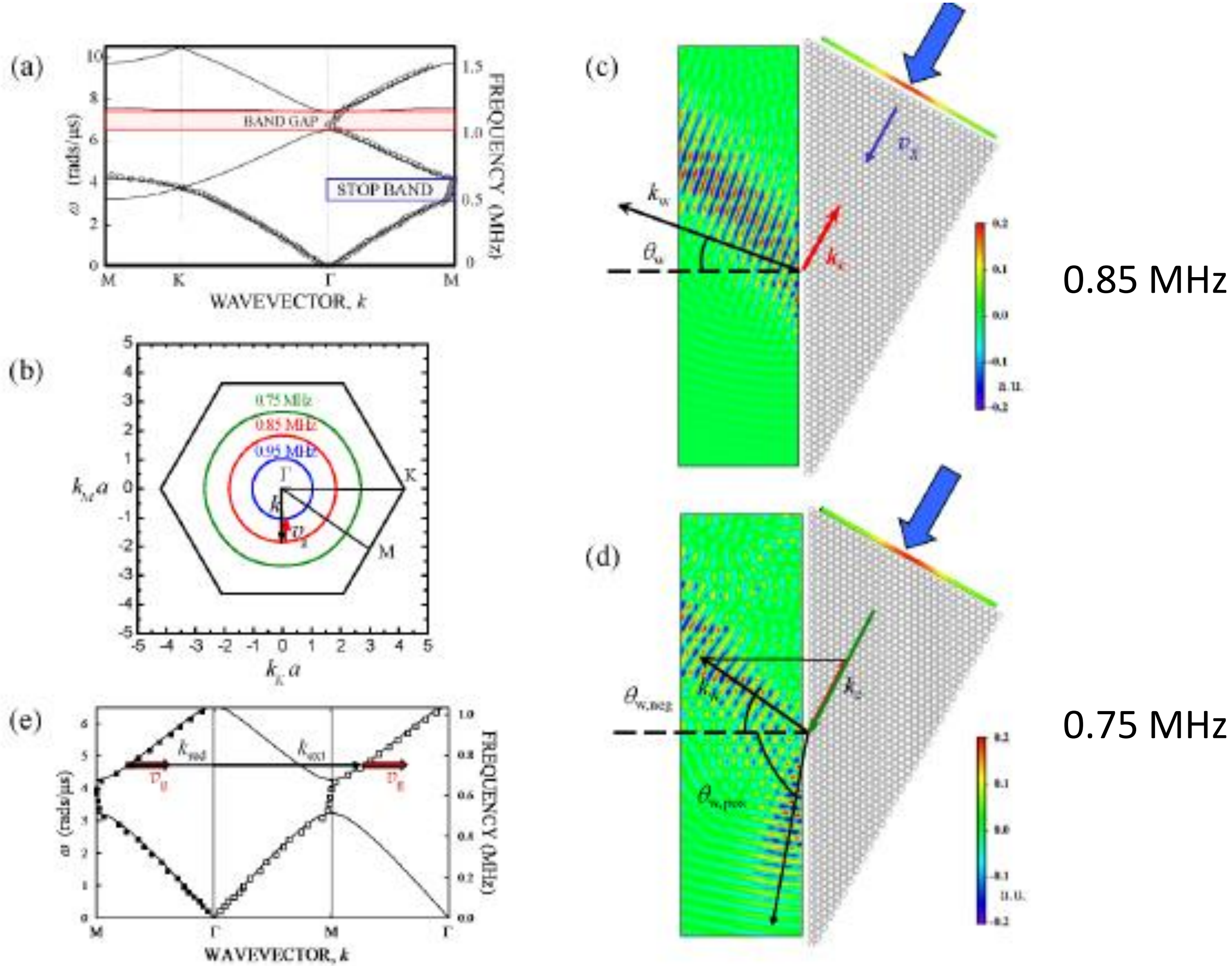

A. Sukhovitch, L. Jing and J. Page, Phys. Rev. B 77, 014301 (2008)

2D Phononic crystal made of a triangular lattice of **steel cylinders:**

in water, surrounded by **water**

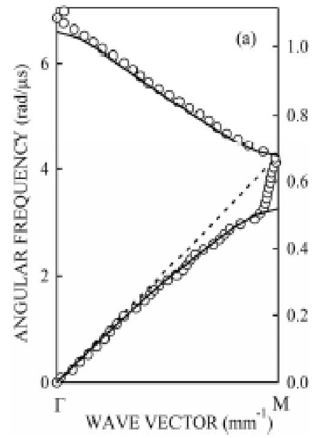

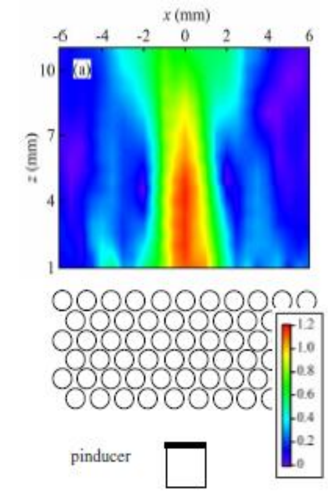

f=0.7 MHz

in methanol, surrounded by **water**

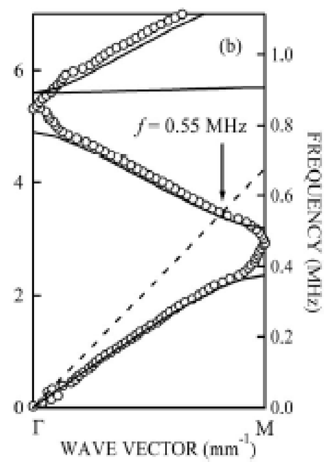

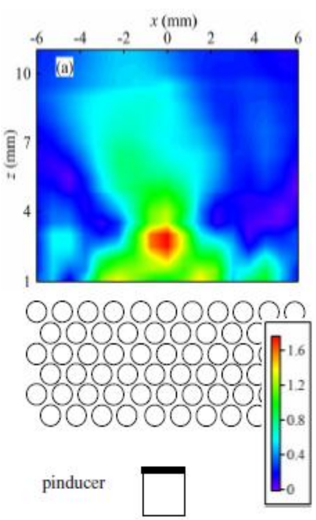

f=0.55 MHz

Regime of All Angle Negative Refraction (AANR)

a=1.27mm, r=0.51mm

A. Sukhovitch, L. Jing and J. Page, Phys. Rev. B 77, 014301 (2008)

Main conditions for optimal focusing:
(i) Circular equifrequency surfaces (in 2D)
(ii) well matched equifrequency surfaces (or contours) in the phononic crystal and in the medium outside (effective negative index of refraction = -1)
(iii) a flat band of bound modes at frequencies close to the operational frequency is needed for super resolution to be attained, so that amplification of evanescent waves from the source can occur.

NegativeRefraction

2D Phononic crystal made of a triangular lattice of steel cylinders in methanol, immersed in water

Improve the resolution by collecting part of the evanescent waves emitted by the source by means of the bound states of the phononic slab

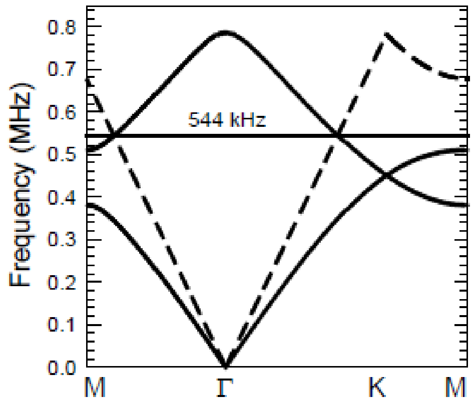

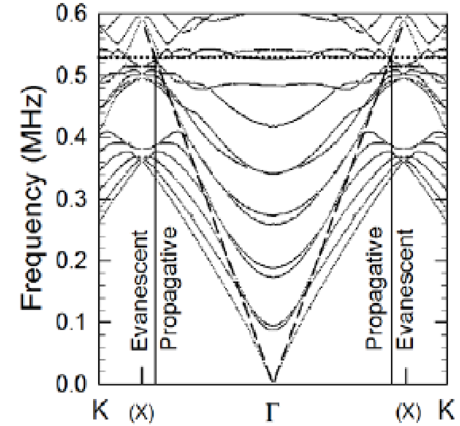

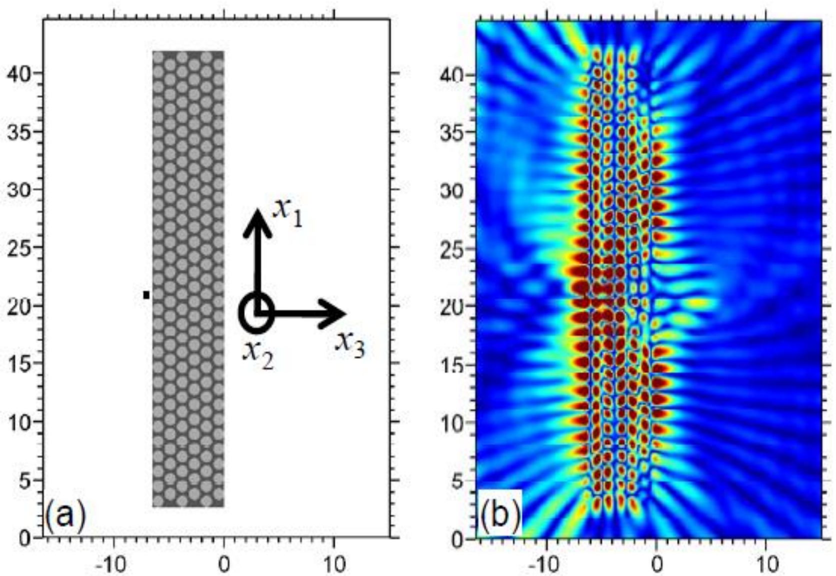

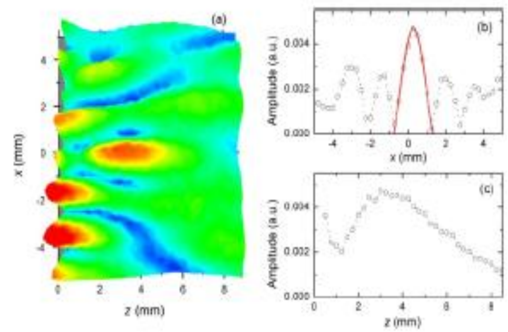

Experiment

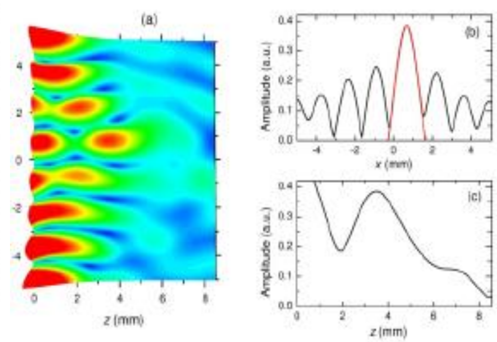

Theory

Resolution of 0.35 λ

J.F. Robillard et al, Phys. Rev. B 84, 224301 (2011)

FCC tungsten carbide beads in water, d=0.8mm

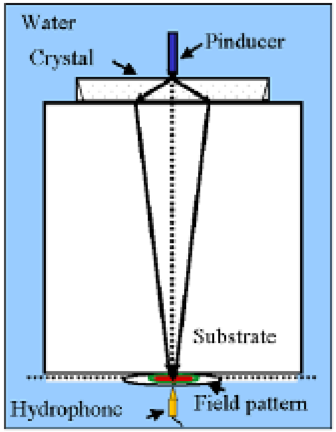

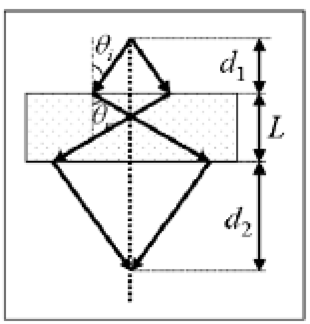

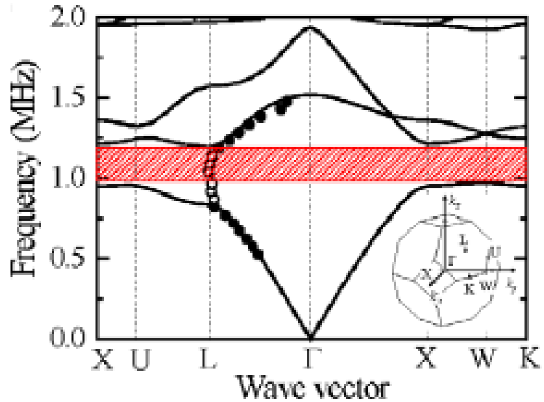

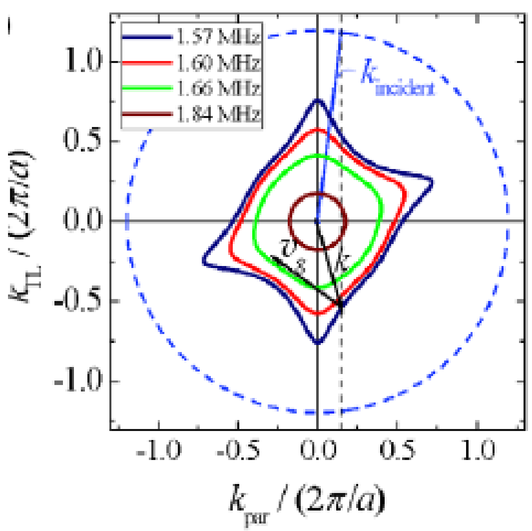

1.57 MHz 1.60 MHz

Réf.

Exp.

Th.

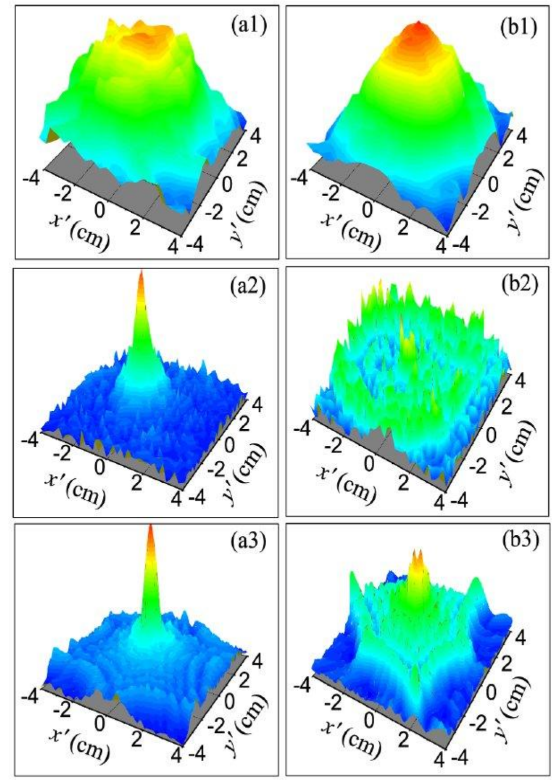

S. Yang *et al.*, Phys. Rev. Lett. **93**, 024301 (2004)

NegativeRefraction

Foam like metallic structure: Honeycomb lattice with additional masses at the corners

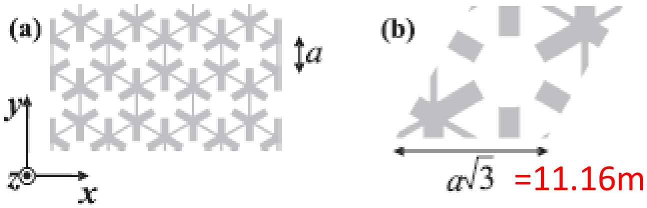

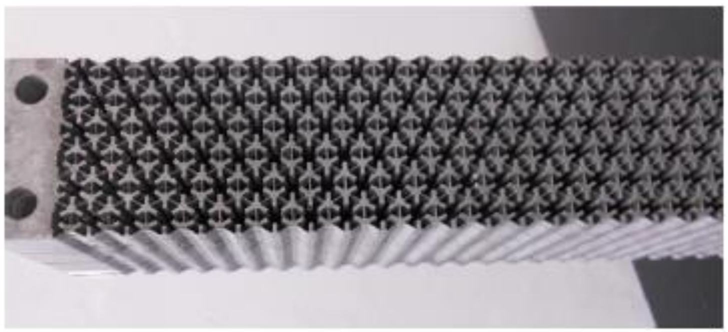

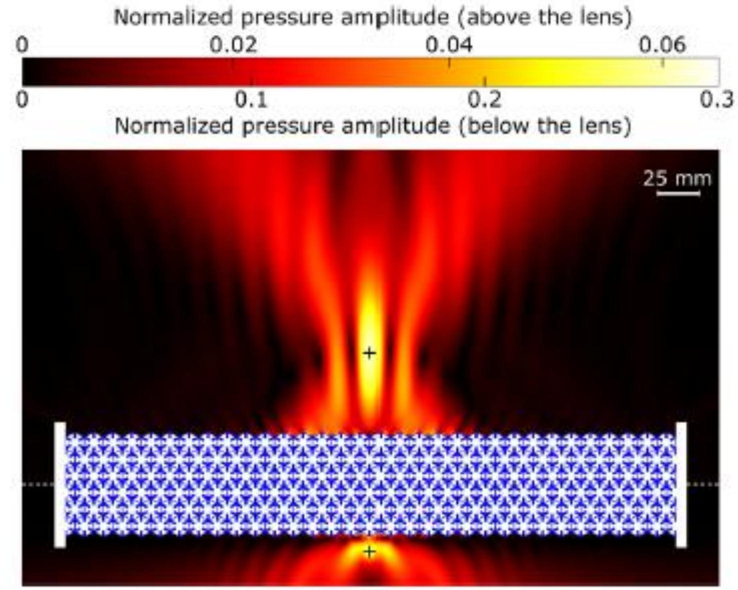

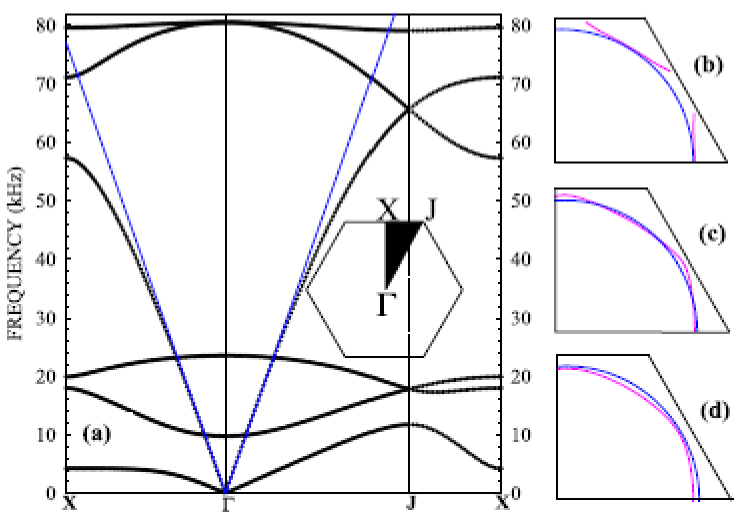

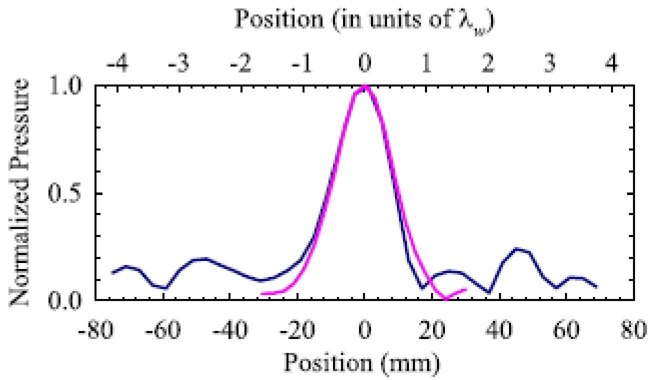

A.-C. Hladky-Hennion, J. O. Vasseur, G. Haw, C. Croënne, L. Haumesser, A. N. Norris, Appl. Phys. Lett. 102, 144103 (2013)

See also: C. Croënne, E. D. Manga, B. Morvan, A. Tinel, B. Dubus, J. Vasseur, and A.-C. Hladky-Hennion Phys. Rev. B **83**, 054301 (2011)

Negative refraction and focusing with negative index metamaterial

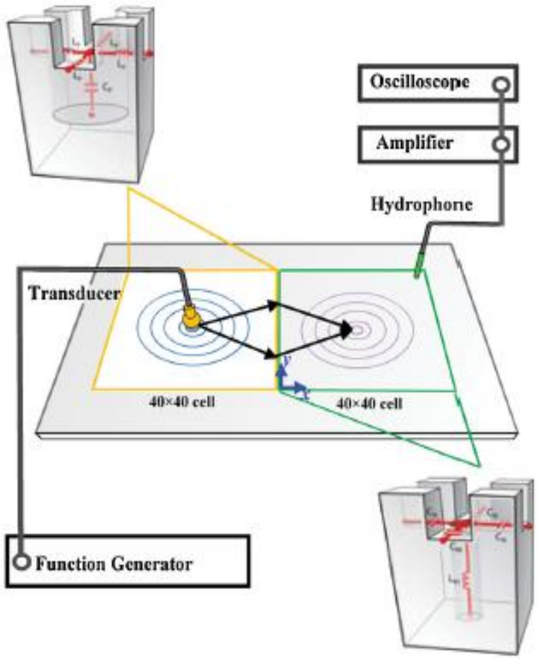

Experiment

Simulation

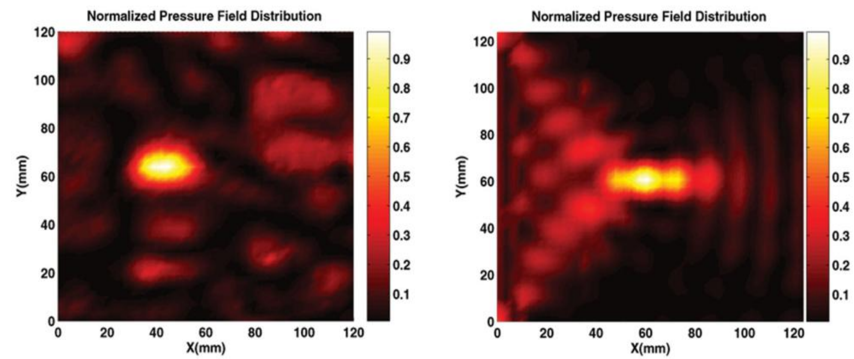

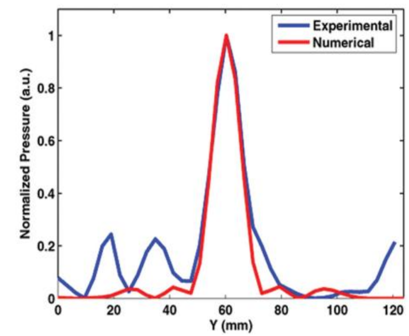

Planar network of subwavelength Helmholtz resonators. Equivalent to a circuit composed of inductors and capacitors

Positive index (left) -Negative index (right)

Pressure field in the negative material

Shu Zhang, Leilei Yin, and Nicholas Fang, Phys. Rev. Lett. 102,194301 (2009)

Anisotropic equifrequency surface

Auto-collimation and beam splitting

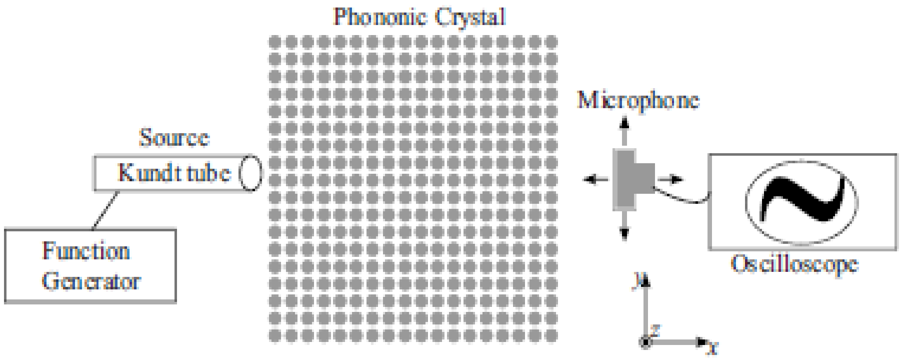

Square lattice of PVC in air (a=27mm, r= 12.9mm)

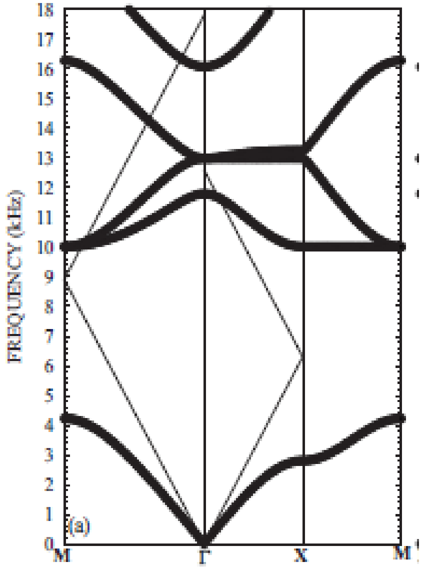

f=14.1 kHz

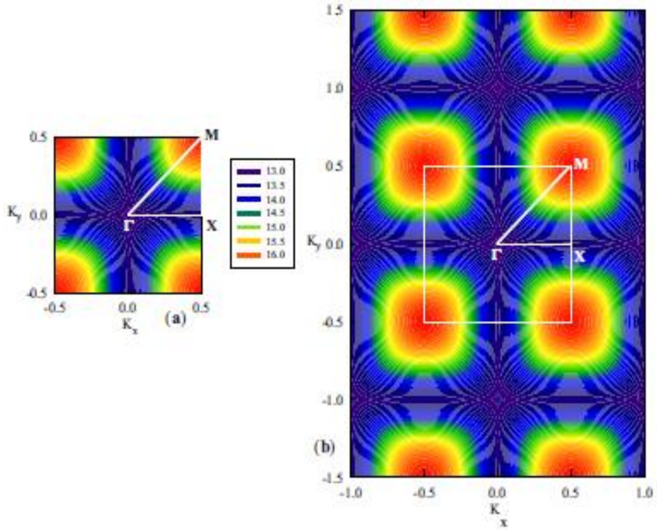

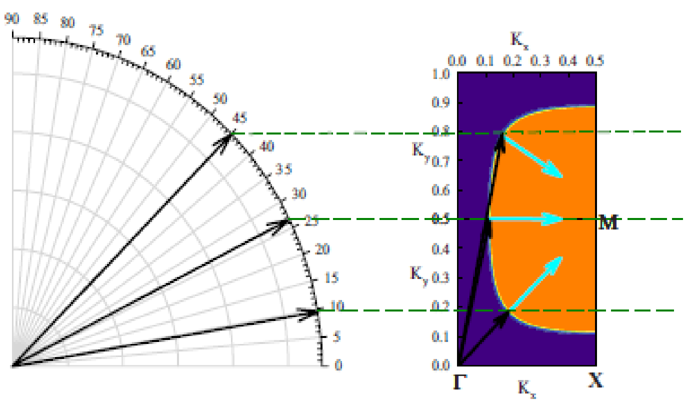

J. Bucay et al, Phys. Rev. B 79, 214305 (2009)

Anisotropic equifrequency surface

Auto-collimation and beam splitting

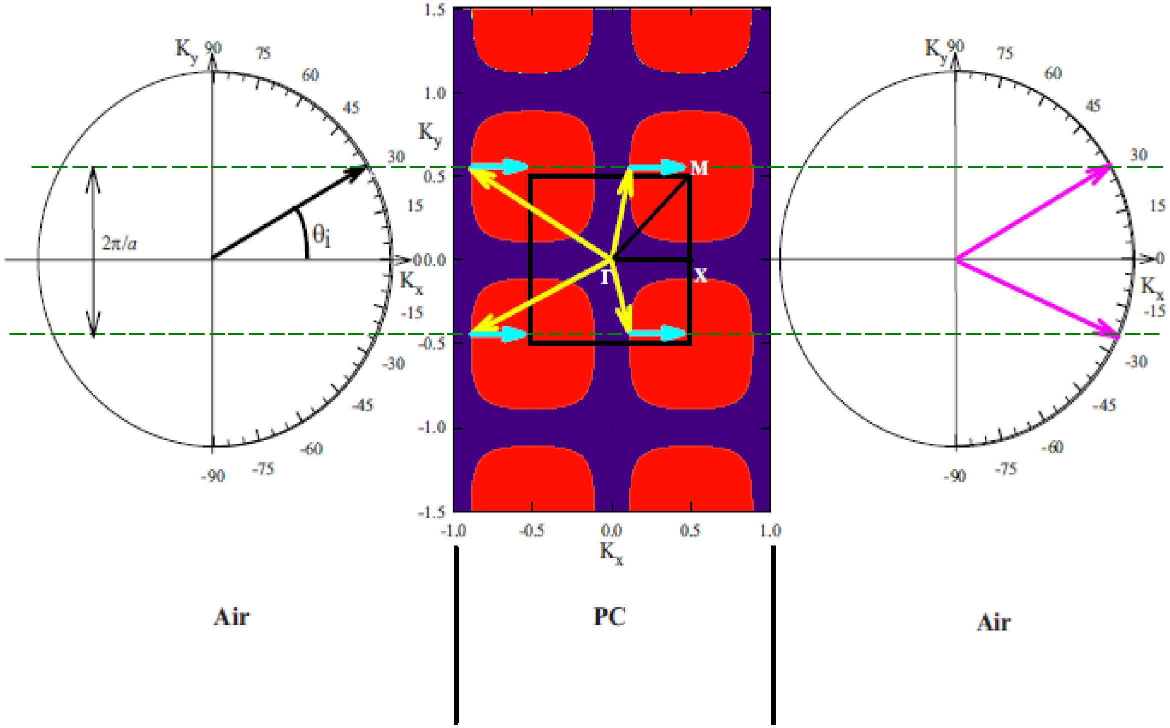

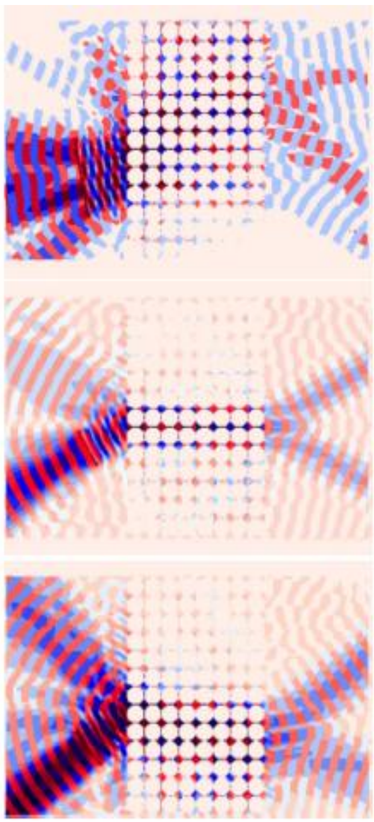

Refraction through a slab of the phononic crystal at different angles

J. Bucay et al, Phys. Rev. B 79, 214305 (2009)

Outline

5. Brief overview of refractive properties

- Negative refraction and focusing
- Self-collimation and beam splitting

6. Subwavelength structures and applications of metamaterials

- Effective properties (positive and negative dynamic parameters)
- Focusing and imaging. Superlens and heperlens
- Cloaking
- GRIN devices
- Metasurfaces. Resonating units and space coiling. Absorption. Phase manipulation

7. Active materials and some emerging topics

Non reciprocal behaviors . Time-space periodicity. PT symmetry. Topological phononics.

8. Dual phononic-photonic crystals (phoXonic) and Optomechanics

- Simultaneous phononic-photonic band gaps.
- Waveguide modes. Slow and fast modes
- Enhanced phonon-photon interaction in a cavity. Comparison of photoelastic and optomechanic effects
- Phononic and Phoxonic sensors

Negative refraction and focusing with negative index metamaterial

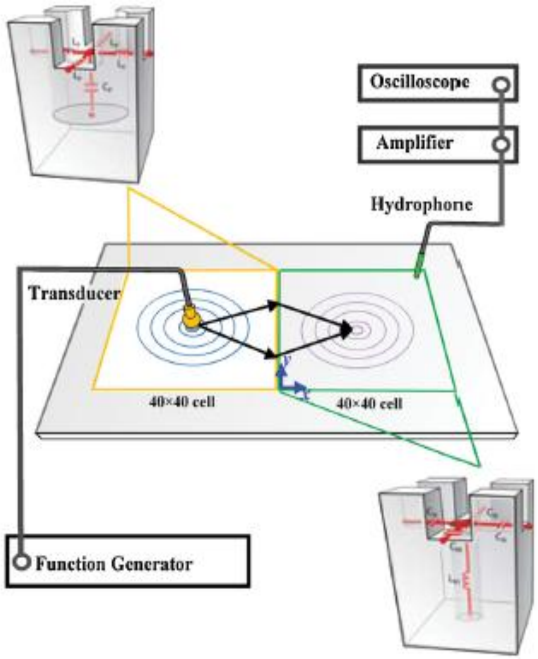

Planar network of subwavelength Helmholtz resonators. Equivalent to a circuit composed of inductors and capacitors
Positive index (left) -Negative index (right)

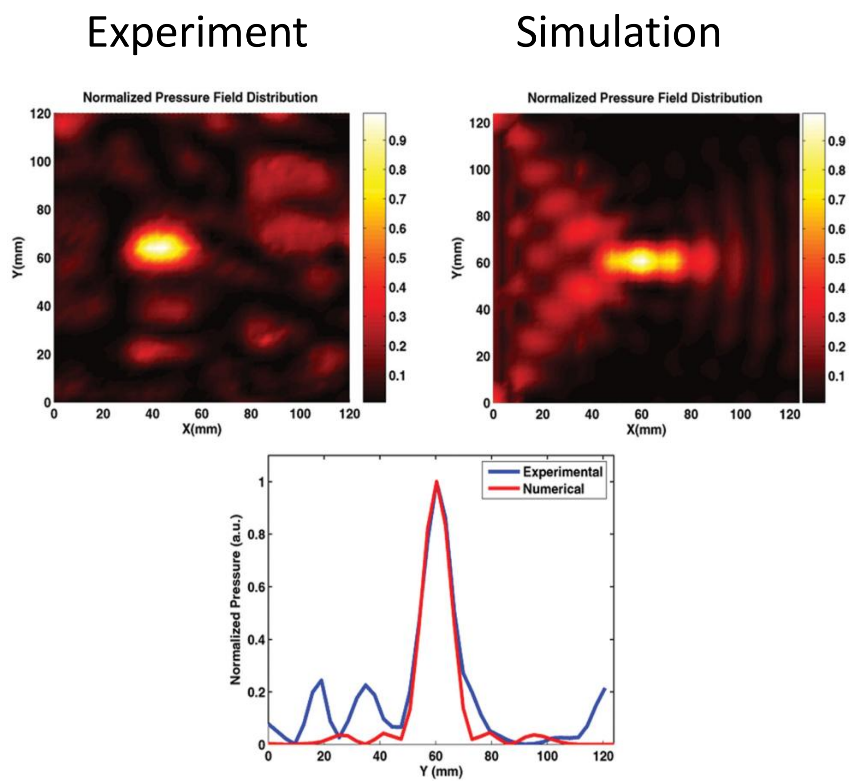

Pressure field in the negative material

Shu Zhang, Leilei Yin, and Nicholas Fang, Phys. Rev. Lett. 102,194301 (2009)

Negative refractive index and acoustic superlens from multiple scattering in single negative metamaterials

NegativeRefraction

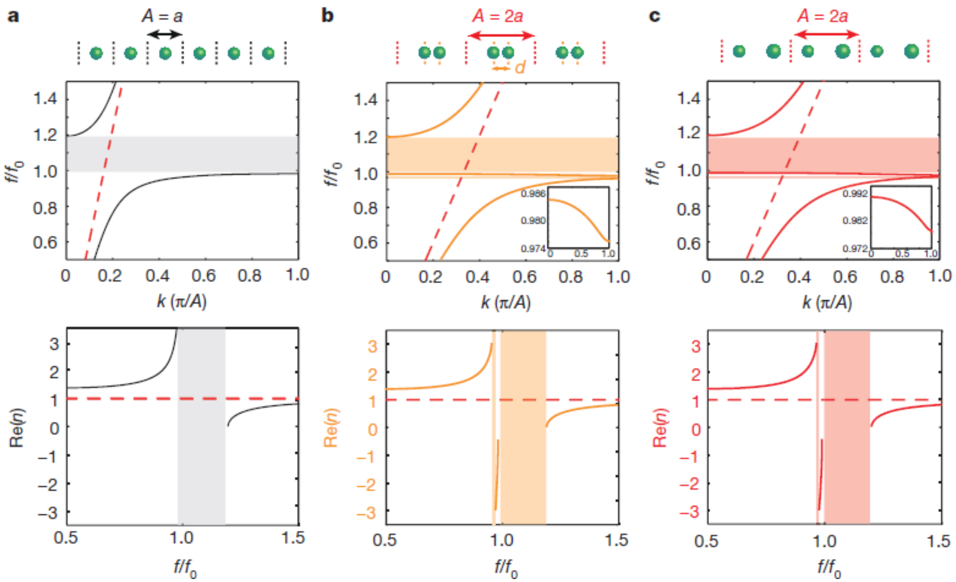

From single negativity
to double negativity

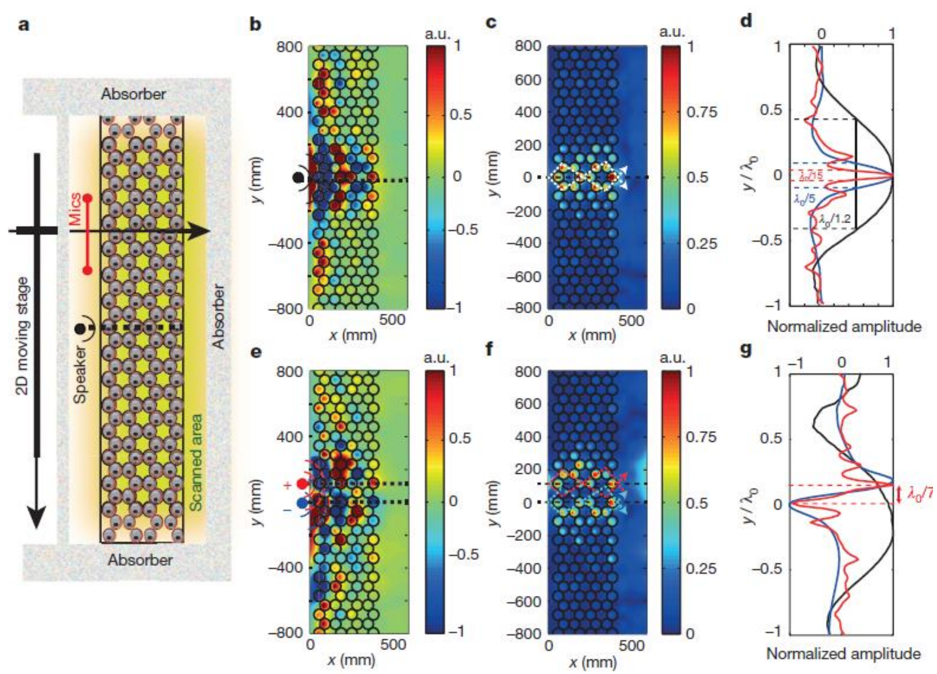

Utilization of a honeycom lattice

Focusing area of $\lambda_0/15$

Resolution of $\lambda_0/7$

N. Kaina, F. Lemoult, M. Fink and G. Lerosey, Nature 525, 77 (2015

Broadband Acoustic Hyperbolic Metamaterial

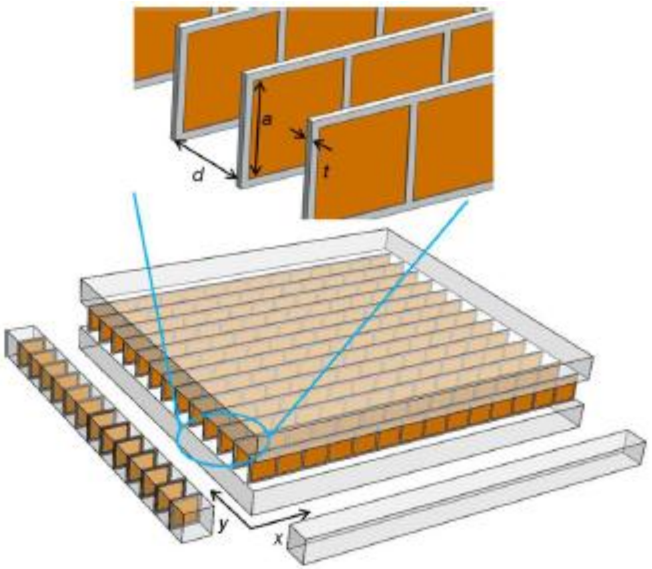

Multiple array of clamped thin plates
a=2cm, d=2cm, t=0.16cm

$$(k_x^2/\rho_x)+(k_y^2/\rho_y)=(\omega^2/B)$$

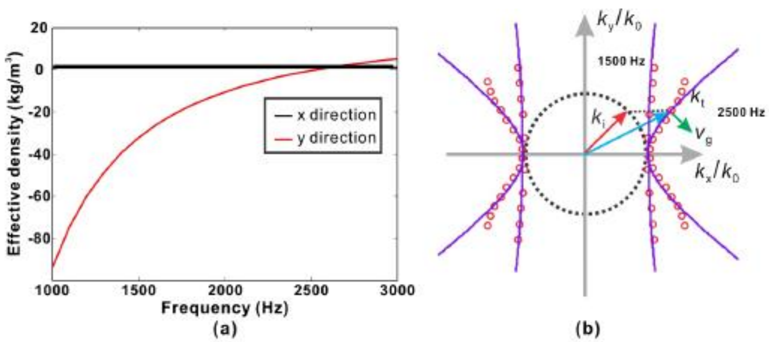

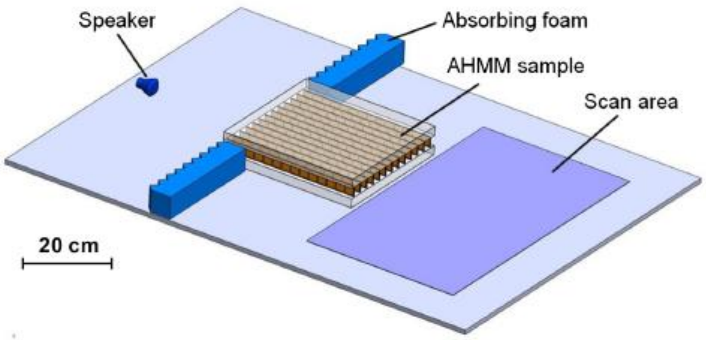

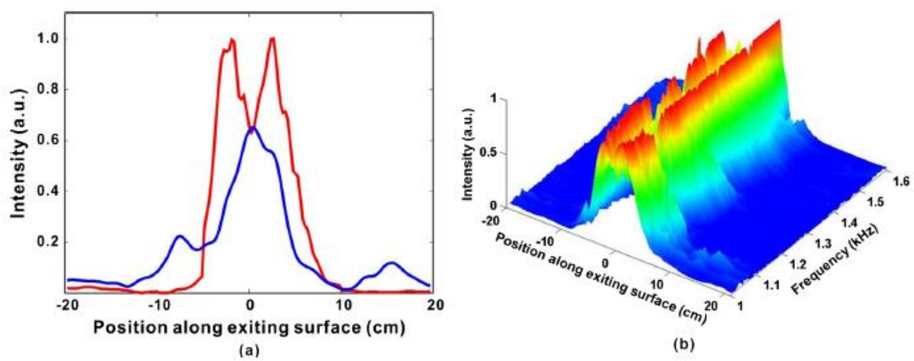

Subwavelength Imaging performance

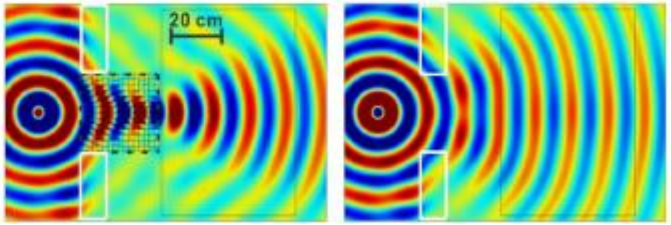

Acoustic pressure at 2440 Hz with and without the MM

C. Shen, Y. Xie, N. Sui, W. Wang, S. A. Cummer, and Y. Jing, PRL 115, 254301 (2015)

Coordinate transformation

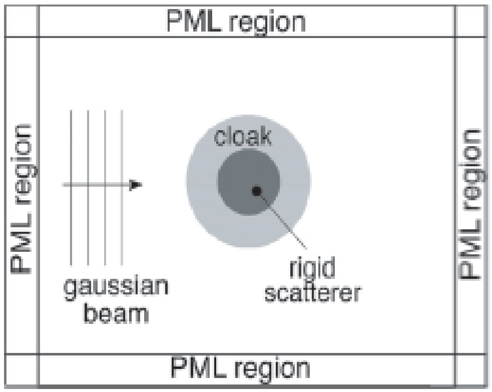

$$\rho_r = \frac{r}{r - R_1}, \qquad \rho_\phi = \frac{r - R_1}{r}, \qquad \lambda^{-1} = \left(\frac{R_2}{R_2 - R_1}\right)^2 \frac{r - R_1}{r}$$

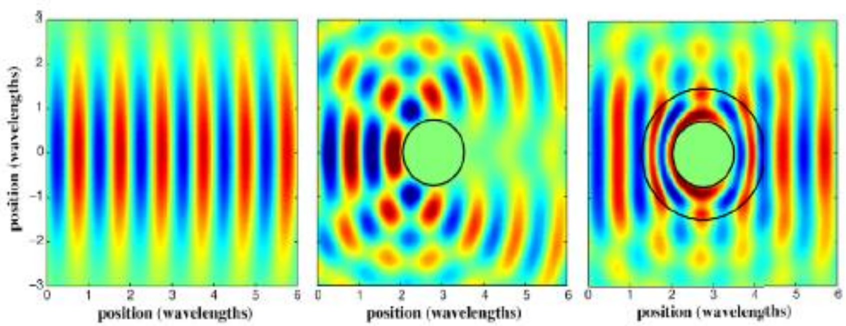

S.A. Cummer and D. Shurig, N.J. Phys. 9, 45 (2007)

Principle of transformation acoustic

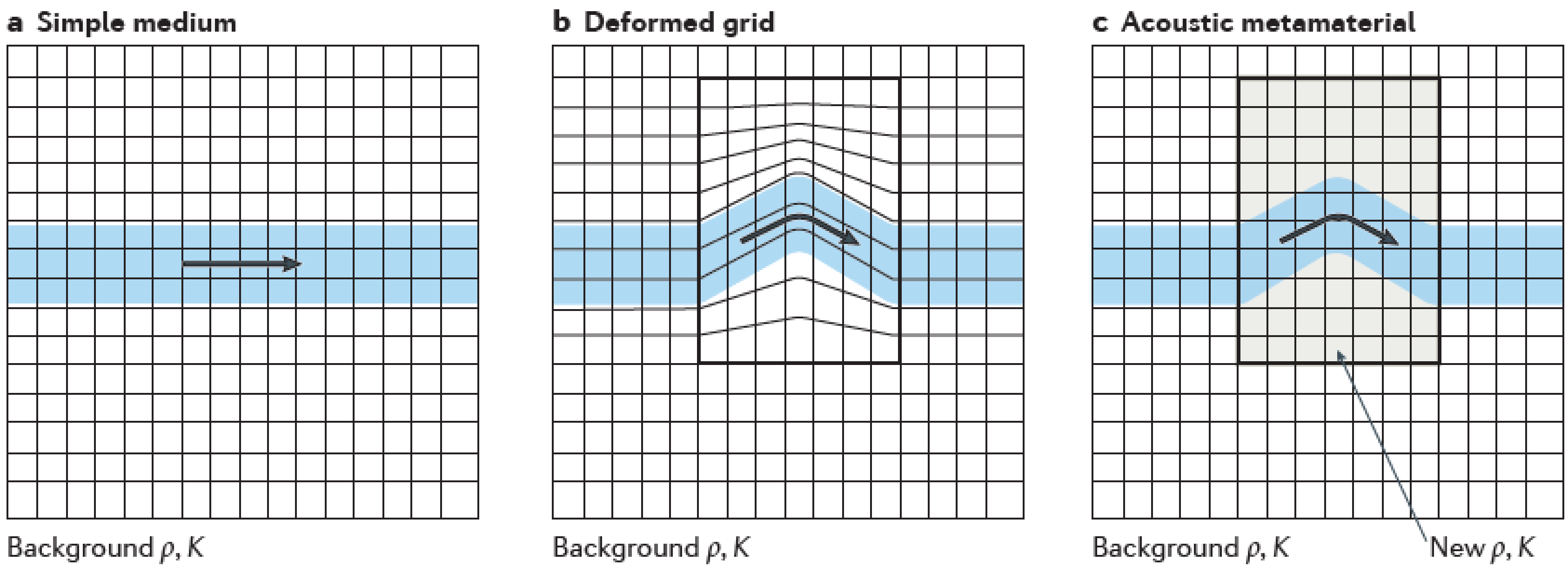

Figure 3 | **Conceptual illustration of transformation acoustics. a** | An acoustic wave propagates through a simple medium with known acoustic material properties. **b** | The acoustic wave is deformed in a finite region via a coordinate transformation that stretches or twists the underlying coordinate grid. This is what we want the acoustic wave to do. **c** | Through the mechanics of transformation acoustics, one can determine the acoustic material properties that will deform the acoustic wave in precisely the way that the coordinate transformation did. These material parameters will be, in general, difficult to obtain; to implement them into a physical medium, metamaterials are required.

S. A. Cummer, J. Christensen and A. Alu, Nature Materials (review), 1, 1 (2016)

Coordinate transformation

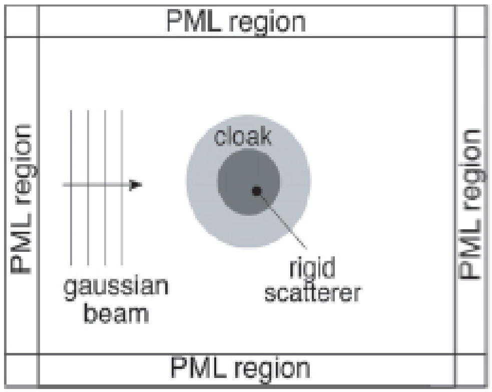

$$\rho_r = \frac{r}{r - R_1}, \qquad \rho_\phi = \frac{r - R_1}{r}, \qquad \lambda^{-1} = \left(\frac{R_2}{R_2 - R_1}\right)^2 \frac{r - R_1}{r}$$

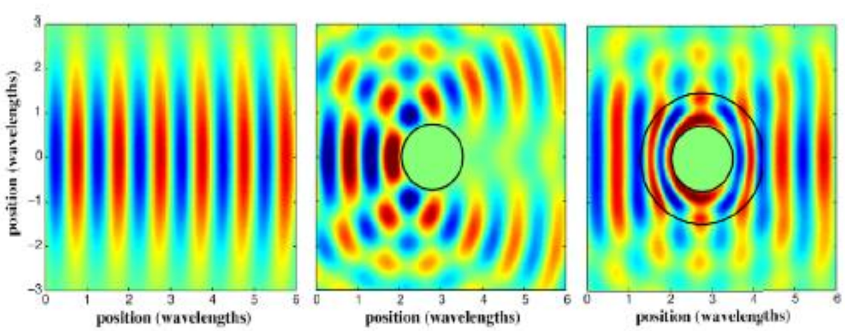

S.A. Cummer and D. Shurig, N.J. Phys. 9, 45 (2007)

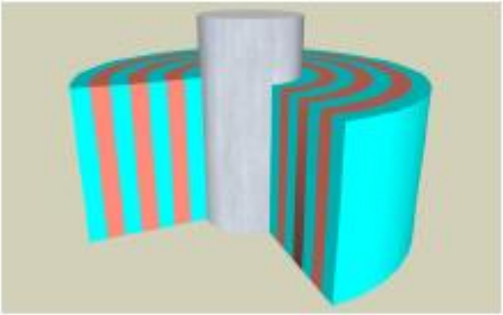

Cloak constituted by a multilayer structure

Each layer is constituted by a sonic crystal with appropriate effective parameters

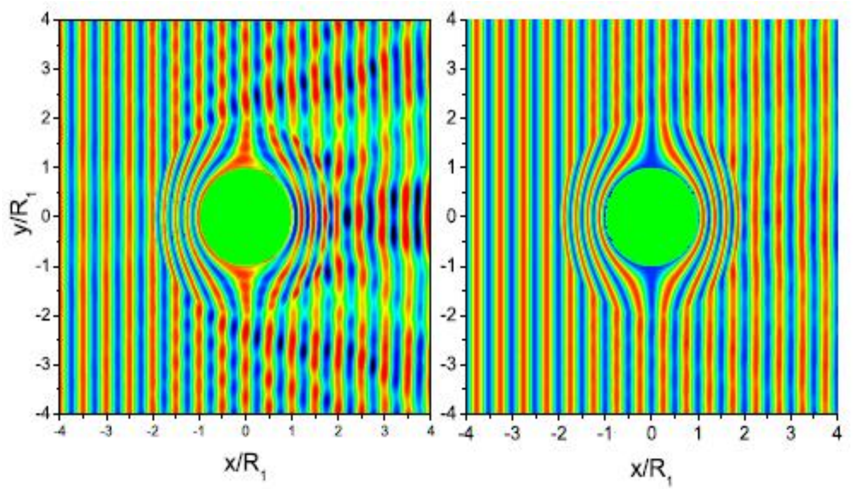

D. Torrent and J. Sanchez-Dehesa, N. J. Phys. 10, 063015 (2008)

Ultrabroadband Elastic Cloaking in Thin Plates

Cloaking

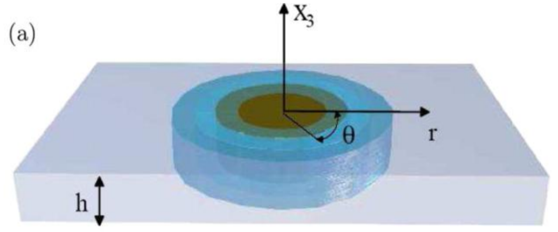

A0 Lamb mode obeys a biharmonic equation:

$$\langle\lambda\rangle\nabla\cdot\{\underline{\zeta}^{-1}\nabla[\langle\lambda\rangle\nabla\cdot(\underline{\zeta}^{-1}\nabla U)]\}-\beta_0^4U=0,$$

Homogeneization process

$$\frac{1}{E_r}=\frac{1}{1+\eta}\left(\frac{1}{E_A}+\frac{\eta}{E_B}\right),\qquad E_\theta=\frac{E_A+\eta E_B}{1+\eta}$$

$$\rho=\frac{\rho_A+\eta\rho_B}{1+\eta},$$

Transformation acoustic

$$E_r'=\left(\frac{R_2}{R_2-R_1}\right)^4\left(\frac{r-R_1}{r}\right)^4,\quad E_\theta'=\left(\frac{R_2}{R_2-R_1}\right)^4,\quad \rho'=1$$

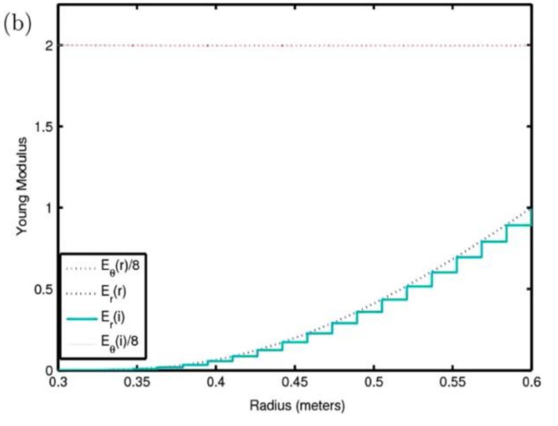

Geometry of the thin metamaterial plate of thickness h=1cm

The cloak is constituted by NM isotropic layers:
- M anisotropic homogeneous concentric layers
- Each of the M layers is composed by N thin isotropic layers through the homogenization process

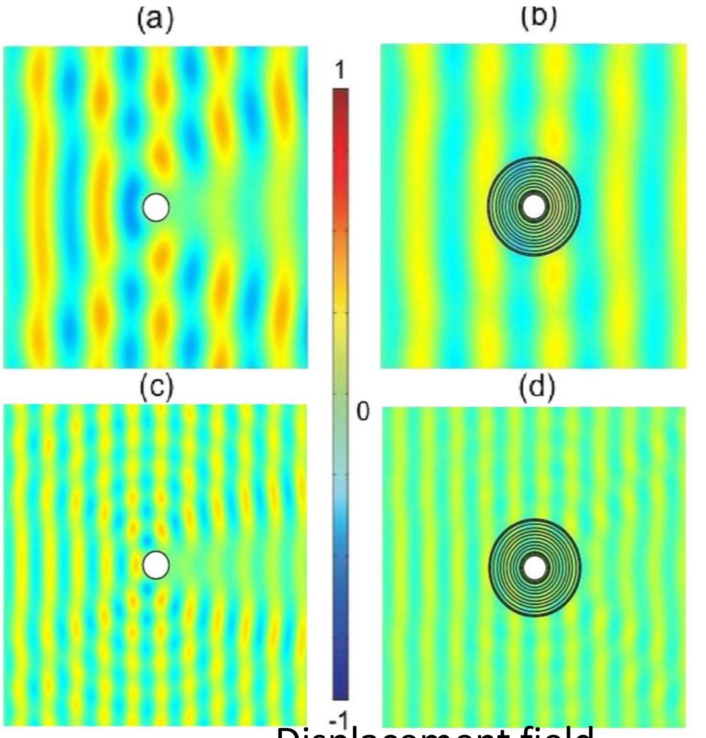

Displacement field

Scattering object of radius 17 cm

f=60 Hz (upper figure) and 150 Hz (lower figure)

M. Farhat, S. Guenneau and S. Enoch, Phys. Rev. Lett. 103, 024301 (2009)

Underwater Broadband Acoustic Cloak for Ultrasound Waves

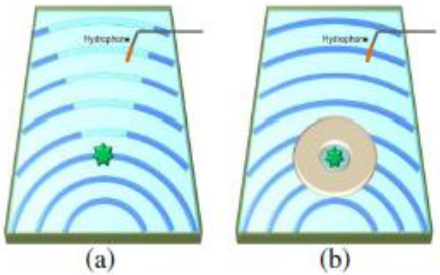

Schematic and details of the set-up

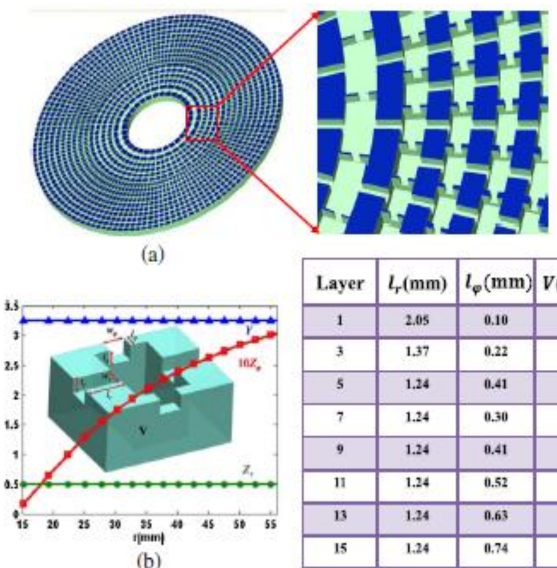

Layer	l_r(mm)	l_φ(mm)	V(mm^3)
1	2.05	0.10	3.00
3	1.37	0.22	2.29
5	1.24	0.41	2.06
7	1.24	0.30	2.06
9	1.24	0.41	2.06
11	1.24	0.52	2.06
13	1.24	0.63	2.06
15	1.24	0.74	2.06

(c)

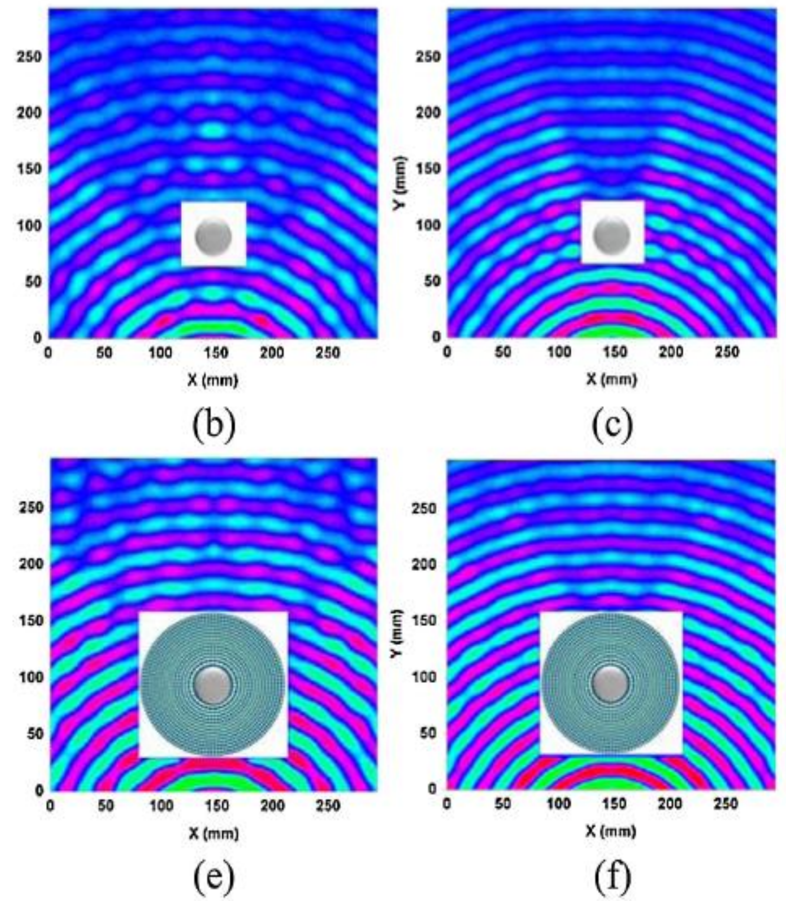

Pressure field with or without the cloak at two frequencies (52 and 64 kHz)

Shu Zhang, Chunguang Xia, and Nicholas Fang, Phys. Rev. Lett.106, 024301 (2011)

Axisymmetric Cloak Based on the Cancellation of Acoustic Scattering from a Sphere

Cloaking

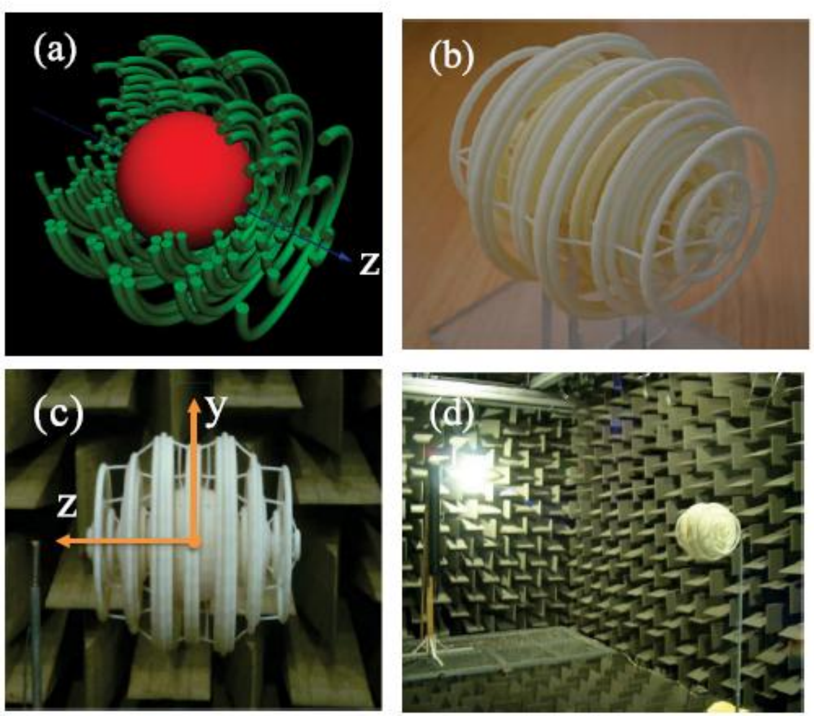

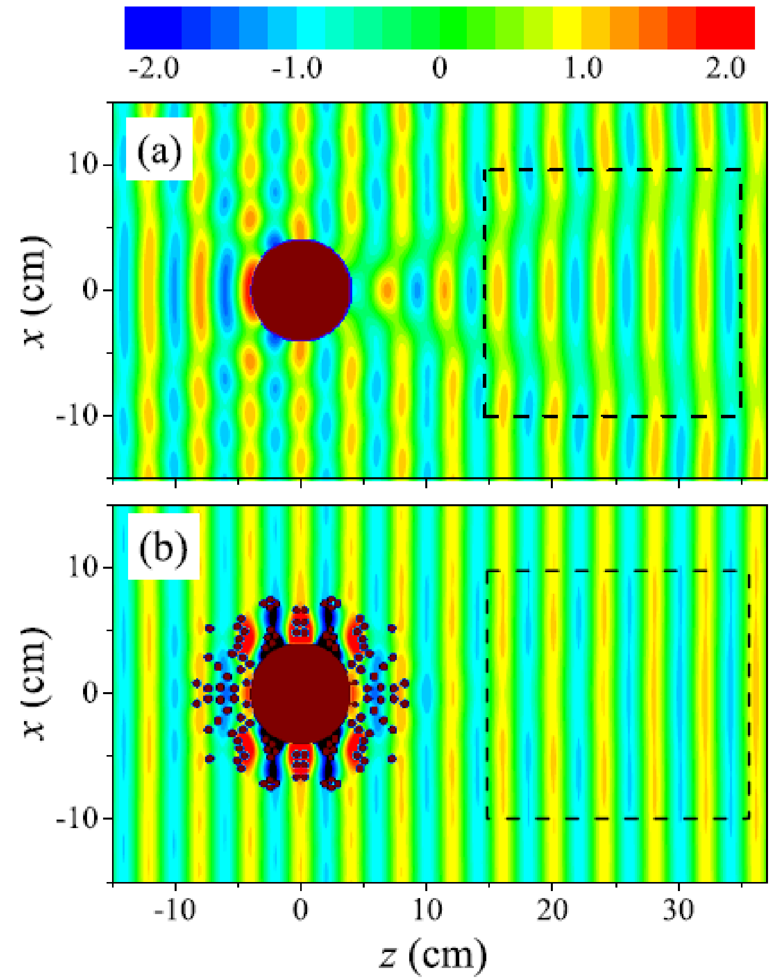

The cloak consists of 60 concentric acoustically rigid tori surrounding the cloaked object, a sphere of radius 4 cm. The major radii and positions of the tori along the symmetry axis are determined using the condition of complete cancellation of the acoustic field scattered from the sphere

Sphere radius=4cm, frequency=8.62 kHz

L. Sanchis, V. M. Garcia-Chocano,2R. Llopis-Pontiveros, A. Climente, J. Martinez-Pastor, F. Cervera, and J. Sanchez-Dehesa, PRL 110, 124301 (2013)

Acoustic Magnifying Hyperlens

Sub-wavelength imaging

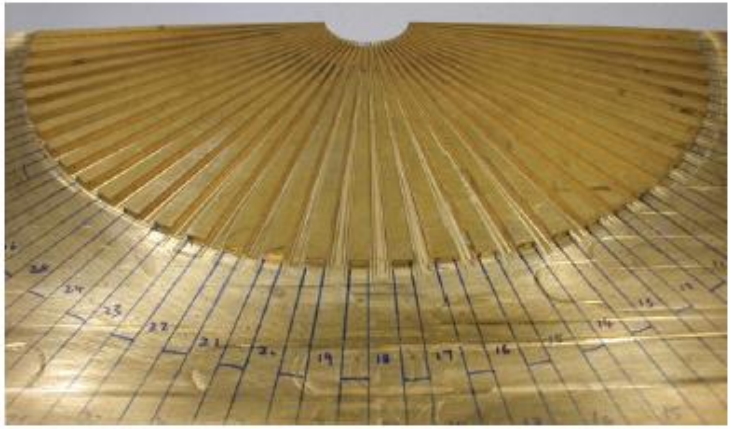

Lens made of 36 brass fins
(running radially from 2.7 to 21.9 cm)
embedded in air on a brass substrate

Imaging at the outer edge
without lens
with lens

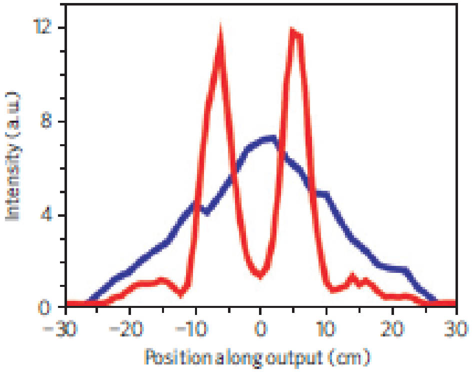

Pressure field (at 6.6 kHz)
The sources are separated by 1.2 cm,i.e. λ/4

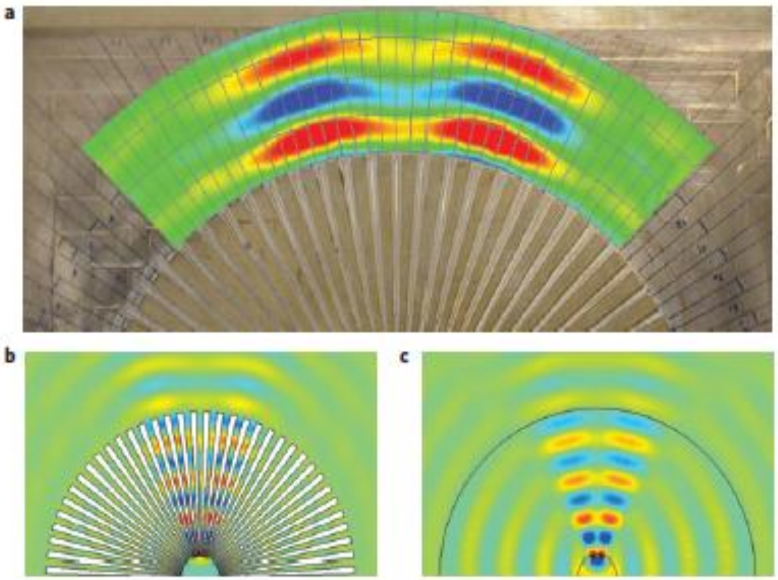

3D simulation

2D simulation
(with effective parameters)

Magnifying subwavelength objects by gradually converting evanescent components into propagating waves

J. Li, L. Fok, X. Yin, G. Bartal and X. Zhang, Nature Materials, 8, 931 (2009)

Acoustic Sub-wavelength Imaging

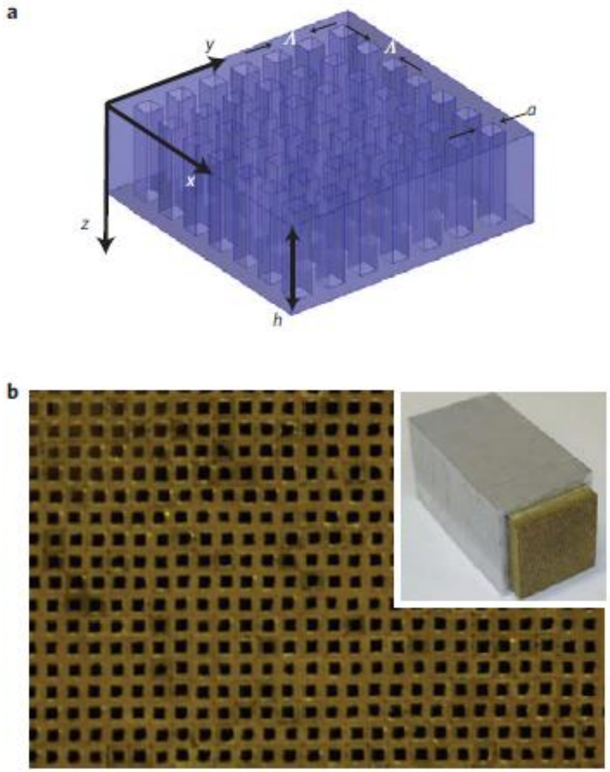

Holey-structured mametamaterial
a= 0.79 mm,, Λ= 1.58mm, h=158mm

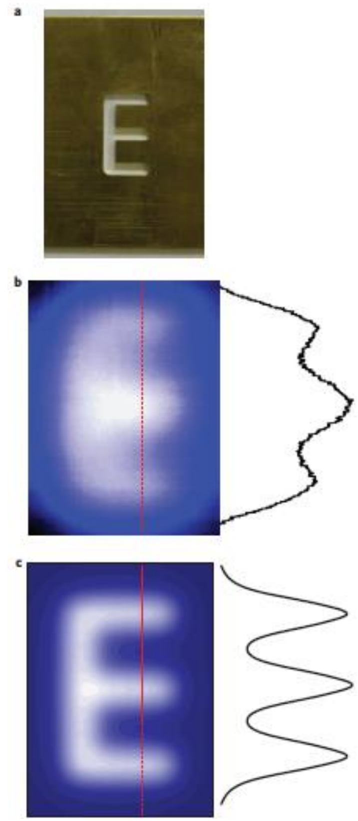

Linewidth of 3.18mm

Imaging at:
f=2.18kHz or λ=158mm
Linewidth= λ/50

The evanescent field components of the sub-wavelength object are efficiently transmitted due to their strong coupling to the Fabry-Pérot resonances inside the holey plate

J. Zhu, J. Christensen, J. Jung, L. Martin-Moreno, X. Yin, L. Fok, X. Zhang and F.J. Garcia-Vidal, Nature Physics, 7, 53 (2011)

Figure 4 | Simulation and experimental imaging of deep-subwavelength-sized letter E. a, Imaging object: letter 'E' with a linewidth 3.18 mm perforated in an ultrathin brass plate. **b**, Measured image of letter 'E', obtained at a distance $\Lambda = 1.58$ mm from the output plane, and the acoustic field distribution along the cross-section indicated by the red dashed line. The operating frequency is 2.18 kHz ($\lambda = 158$ mm). A $\lambda/50$ linewidth of the object can still be observed. **c**, Simulated image of letter 'E', obtained at a distance $\Lambda = 1.58$ mm from the output plane, and the acoustic field distribution along the cross-section indicated by the red dashed line.

Gradient-index phononic crystals

Refraction

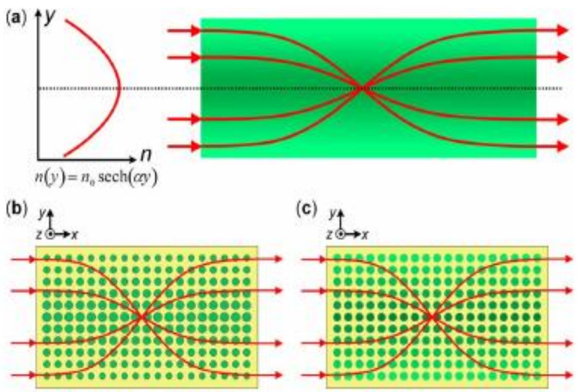

$$n(y) = n_0 \operatorname{sech}(\alpha y)$$

Schematic of graded PC: Change of the properties along the transverse direction:

- Left: adjusting the radii of the cylinders
- Right: change of elastic properties

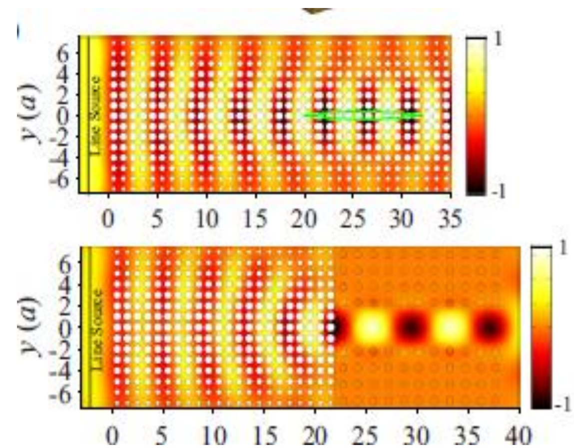

Illustrations of focusing in a PC plate and injection into a waveguide

T.T. Wu, et al, Appl. Phys. Lett.. 98, 171911 (2011)

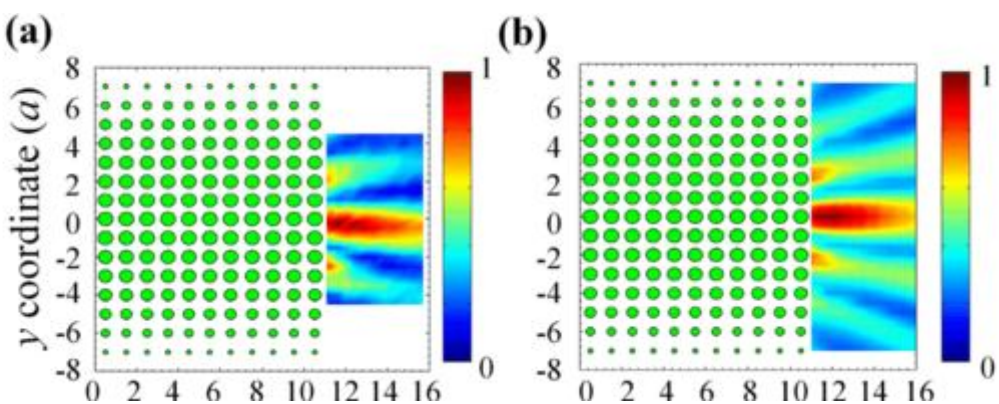

Experiment   Simulation

J. Zhao, et al. PRB. 93. 174306 (2016)

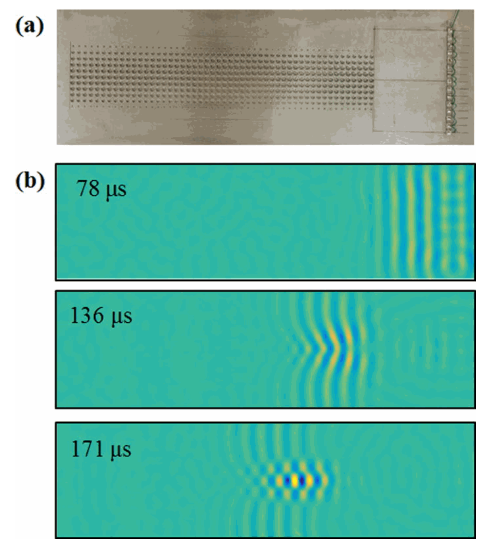

Focusing effect in time

S. Tol, et al. APL. 109. 063902 (2016)

Graded index devices in phononic plates for the full control of the three fundamental Lamb waves

- Homgeneization method to obtain the elastic constants of a 2D phononic crystal and then a plate

SH_0 mode $\rho^*\omega^2 = C_{66}^* k_{SH}^2$ $n_{SH} = \frac{k_{SH}^{II}}{k_{SH}^{I}}$

S_0 mode $\rho^*\omega^2 = C_{11}^*\left(1 - \frac{C_{13}^{*2}}{C_{11}^* C_{33}^*}\right) k_S^2$ $n_S = \frac{k_S^{II}}{k_S^{I}}$

A_0 mode $\rho^*\omega^2 = C_{11}^*\left(1 - \frac{C_{13}^{*2}}{C_{11}^* C_{33}^*}\right)\frac{h^2}{12} k_A^4$ $n_A^2 = n_S \frac{h^I}{h^{II}}$

Al-Gold-Hole unit cell
$R_b = 0.4a$, $R_a = 0.2a$

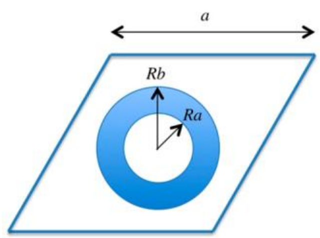

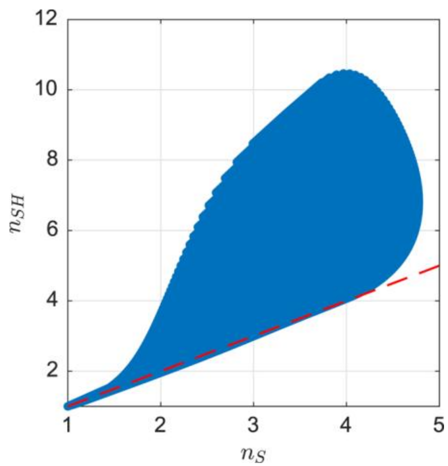

make a sweep of $R_b \in (0, 0.5a)$
and $R_a \in (0, R_b)$,

Full control

Choose proper R_b and R_a to control S_0 and SH_0 modes
+
Design proper thickness variation to control A_0 mode

Y. Jin et al, J. Appl. Phys., 117, 244904 (2015)
Y. Jin et al, Sci. Rep. 6, 24437 (2016)

Numerical examples

GRIN flat lens: $n(y) = n_0 \ \text{sech}(\alpha y)$

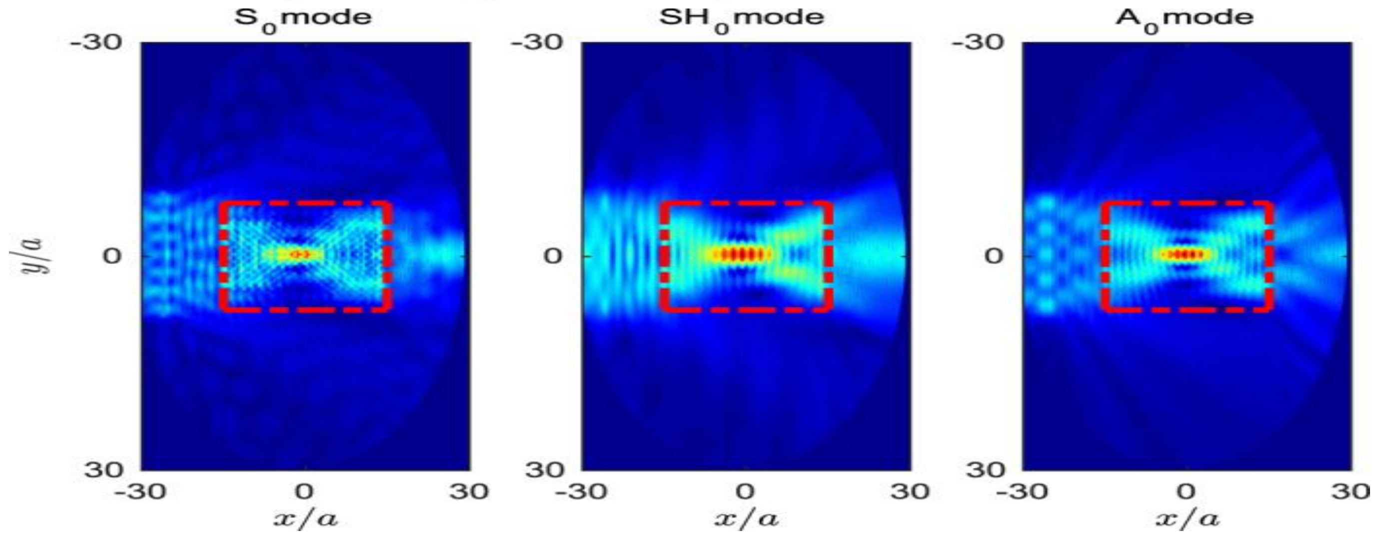

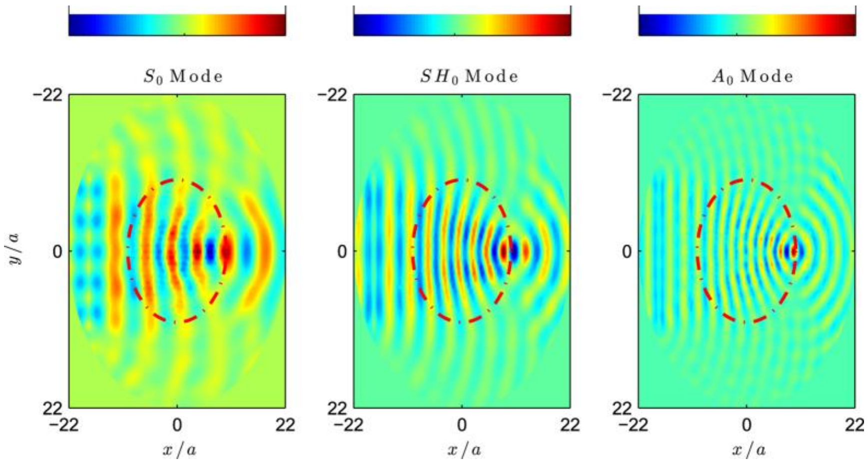

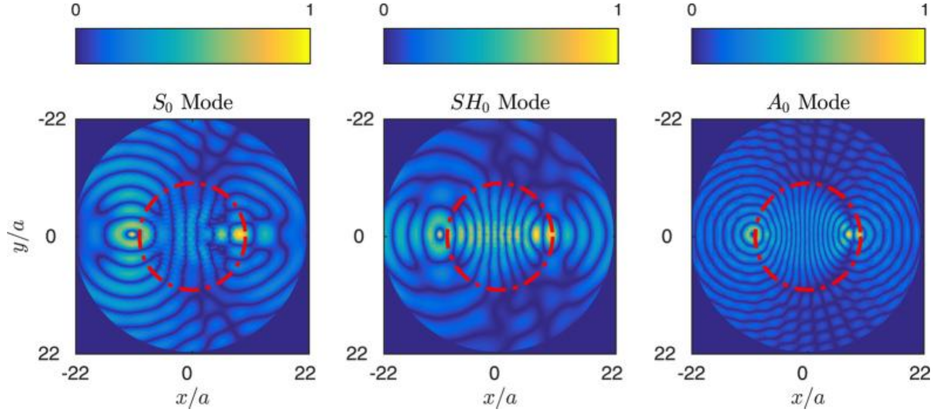

Luneburg lens: $n(r) = \sqrt{2 - (r/R_c)^2}$

Maxwell lens: $n(r) = 2/(1 + (r/R_c)^2)$

Acoustic Metamaterial by Coiling Up Space

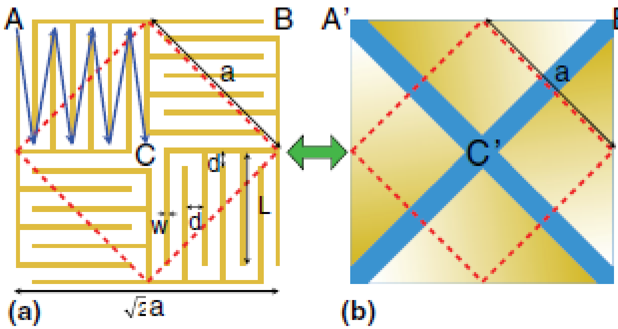

thickness w= 0.02a, length L =0.61a, fluid channels width d =0.81a

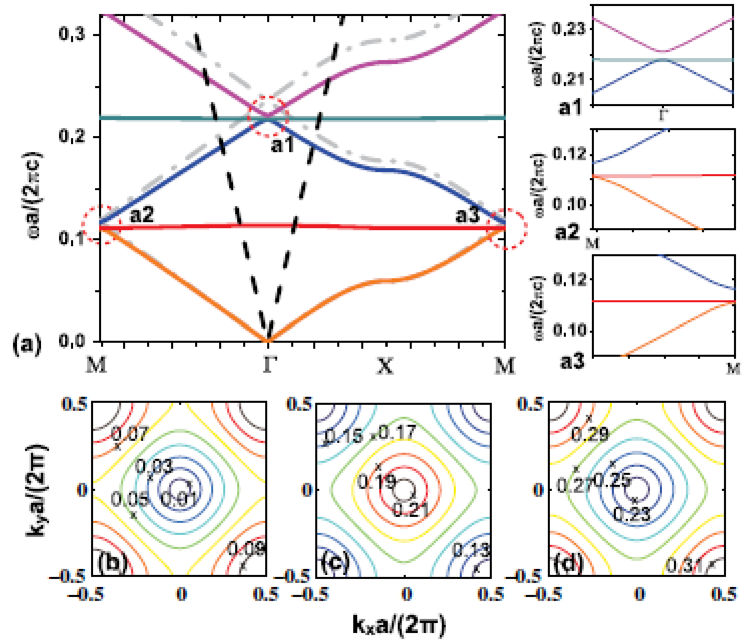

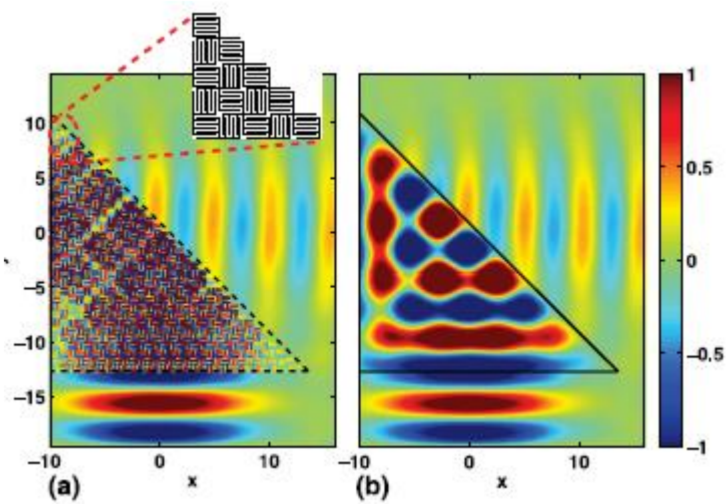

Frequency 0.191 in the background fluid. The corresponding relative effective index is n_r=-1

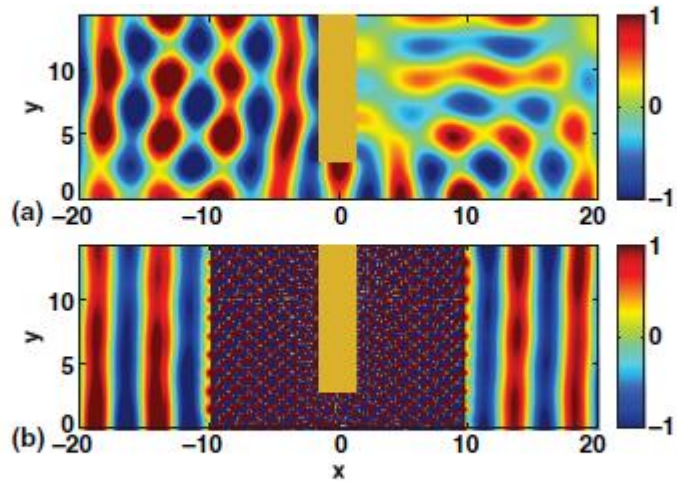

Zero index at frequency 0.214

Zixian Liang and Jensen Li, PRL 108, 114301 (2012)

Zero Index Metamaterial

$$v=\sqrt{\frac{\kappa}{\rho}} \qquad n\approx\frac{v_0}{v}$$

$$Z=\rho v=\sqrt{\kappa\rho}$$

Assume

$$n\to 0 \quad (or \quad v\to\infty) \quad but \quad \rho\to 0$$

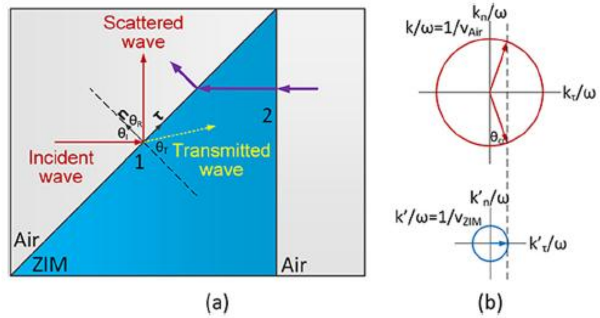

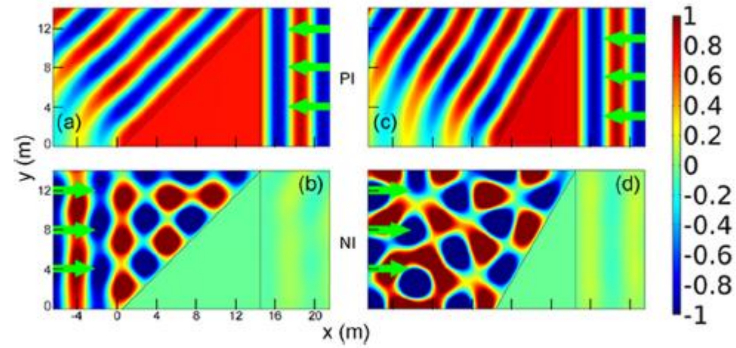

Idealized Ppisms (inclinations of 45° and 60°)

Unidirectional acoustic transmision through a prism

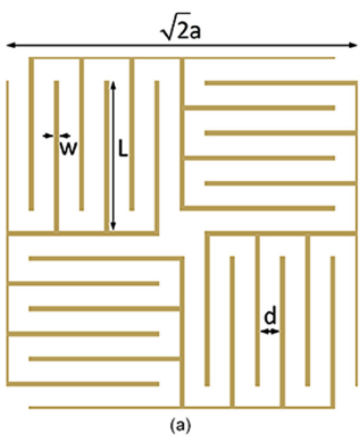

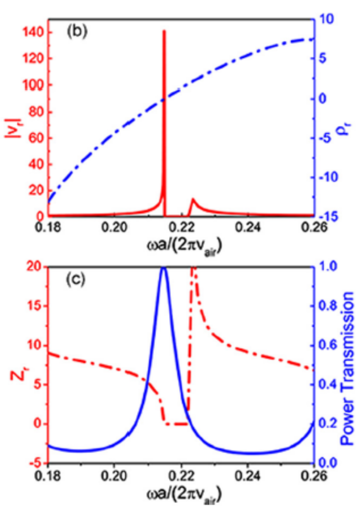

L=0.606 a, d=0.081 a, w=0.02 a

Coiling up structure to make a ZIM prism

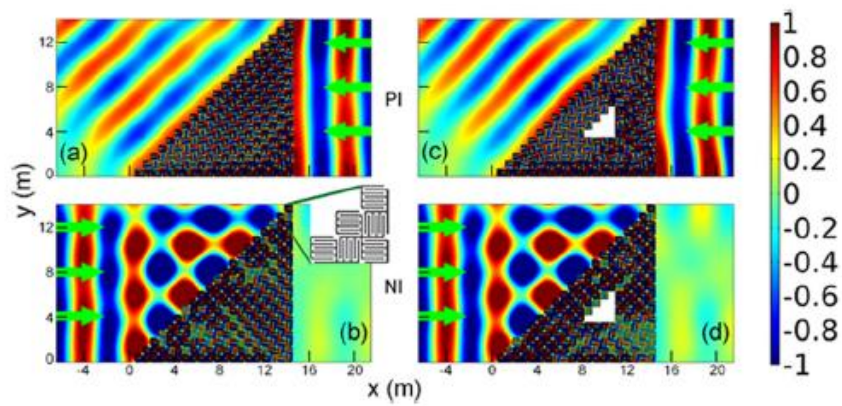

$$v=v(air)x140 \qquad \rho=\rho(air)/140$$

Ppism constituted by the coiling-up structure

Y. Li, B. Liang, , Z. Gu, X. Zou, and J. Cheng, Appl. Phys. Lett. 103, 053505 (2013)

Acoustic diodes and acoustic rectification

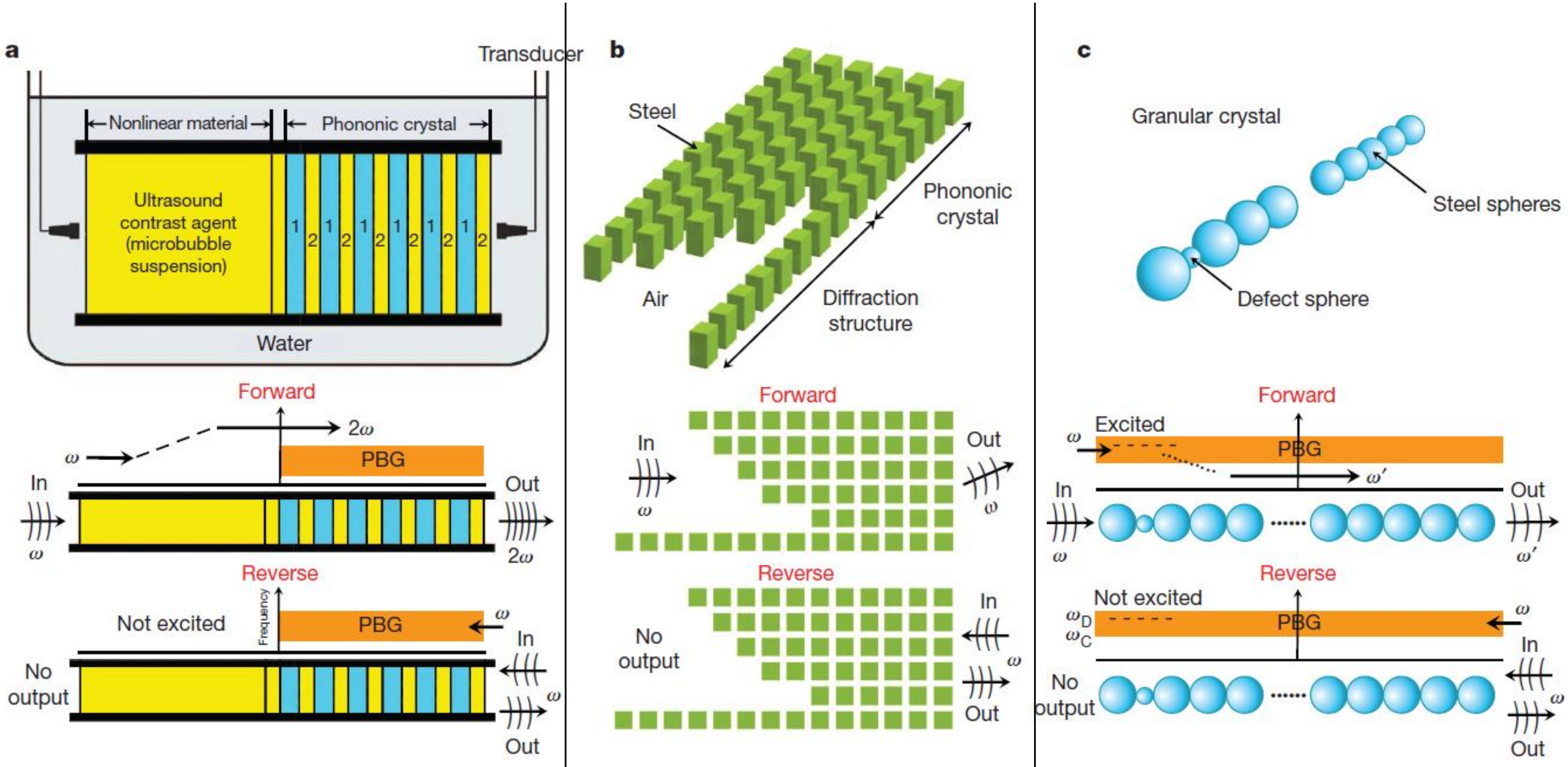

B. Liang et al, Nature Mater., 9, 989 (2010)

X.F. Li et al, Phys. Rev. Lett. 106, 084301 (2011)

N. Boechler et al, Nature Mater. 10, 665(2011)

From M. Maldovan in Nature 503, 209 (2013)

Acoustic Metamaterial by Coiling Up Space

Focusing by a GRIN lens based on coiling space units

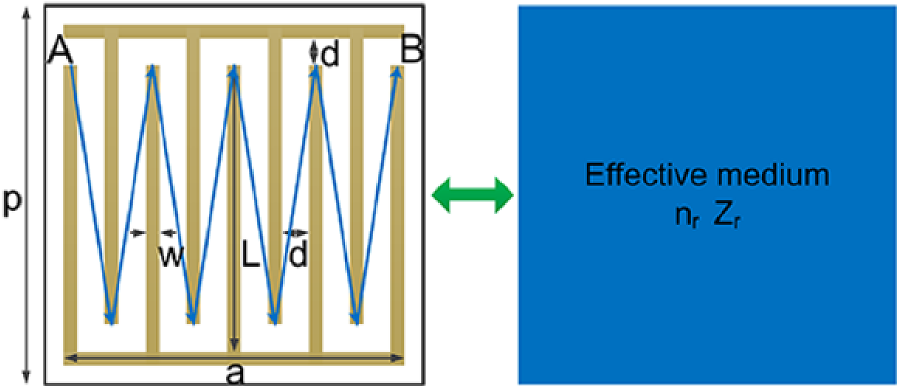

L=0.85 a, w=0.03 a, p=1cm

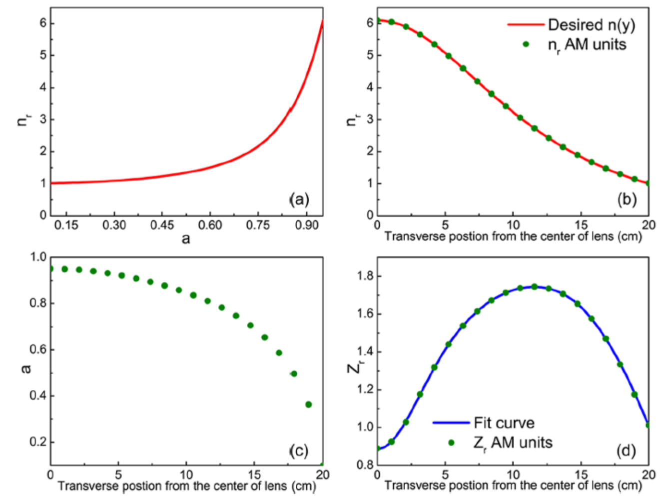

Designed lens

$$n(y) = n_0 \, \mathrm{sech}\,(\alpha y)$$

Free space

Idealized lens

Designed lens

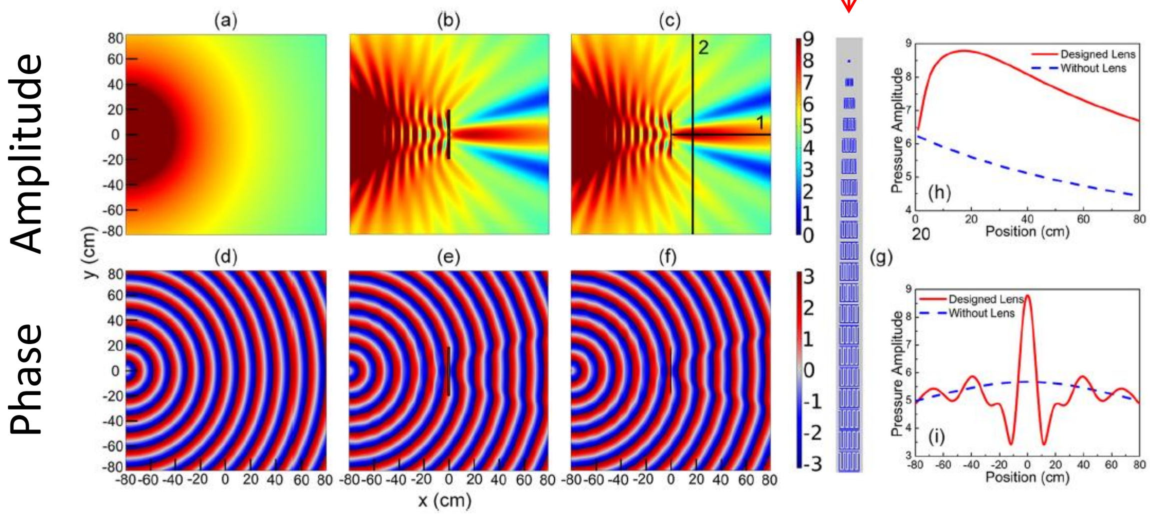

Frequency: 2500 Hz

Y. Li, B. Liang, X. Tao, X. Zhu, X. Zou, and J. chun Cheng, Appl. Phys. Lett. **101, 233508 (2012)**

Convert Acoustic Resonances to Orbital Angular Momentum

Xue Jiang,[1] Yong Li,[2] Bin Liang,[1,*] Jian-chun Cheng,[1,†] and Likun Zhang[3,‡]

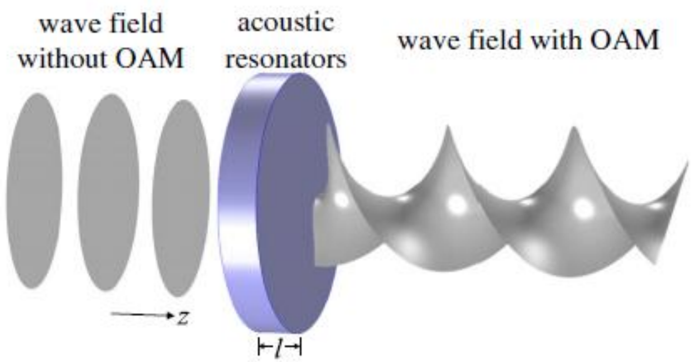

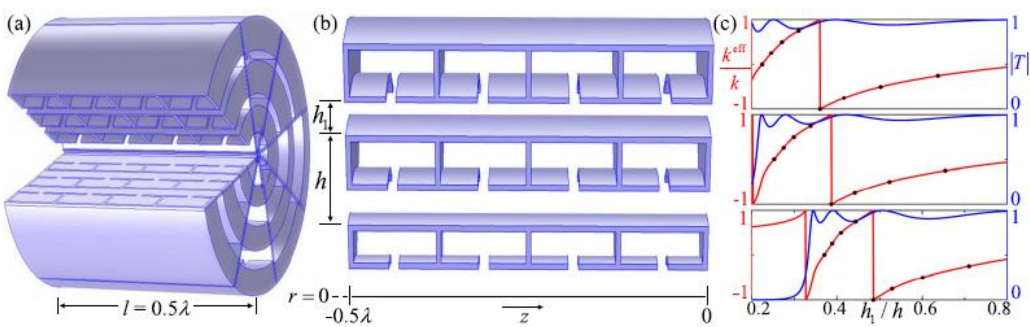

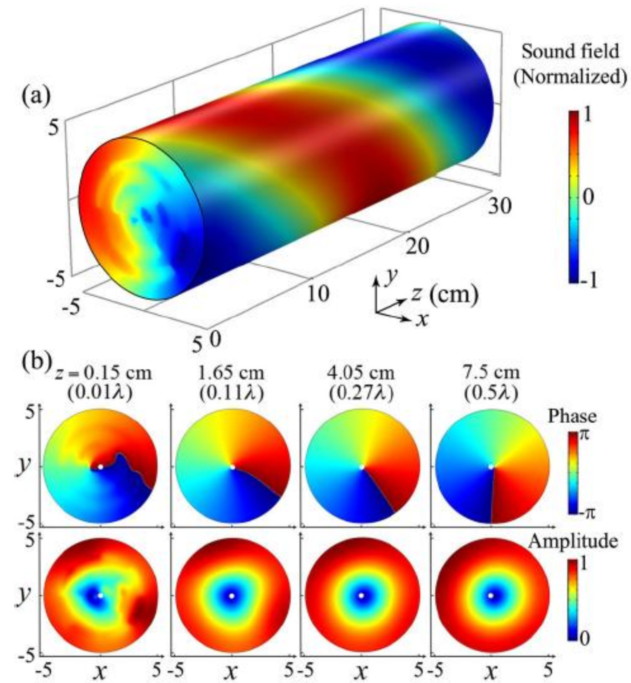

f= 2287 Hz, λ=15 cm in air

Twisted wave front with a screw dislocation along the propagation axis

Acoustic Metasurfaces for Wave Manipulation

Metasurface: Sub-wavelength thin metamaterial able to produce:

- Local phase shift over 2π span to control the transmitted (or reflected) wavefront.
- Impedance matching to ensure the penetration of wave energy.

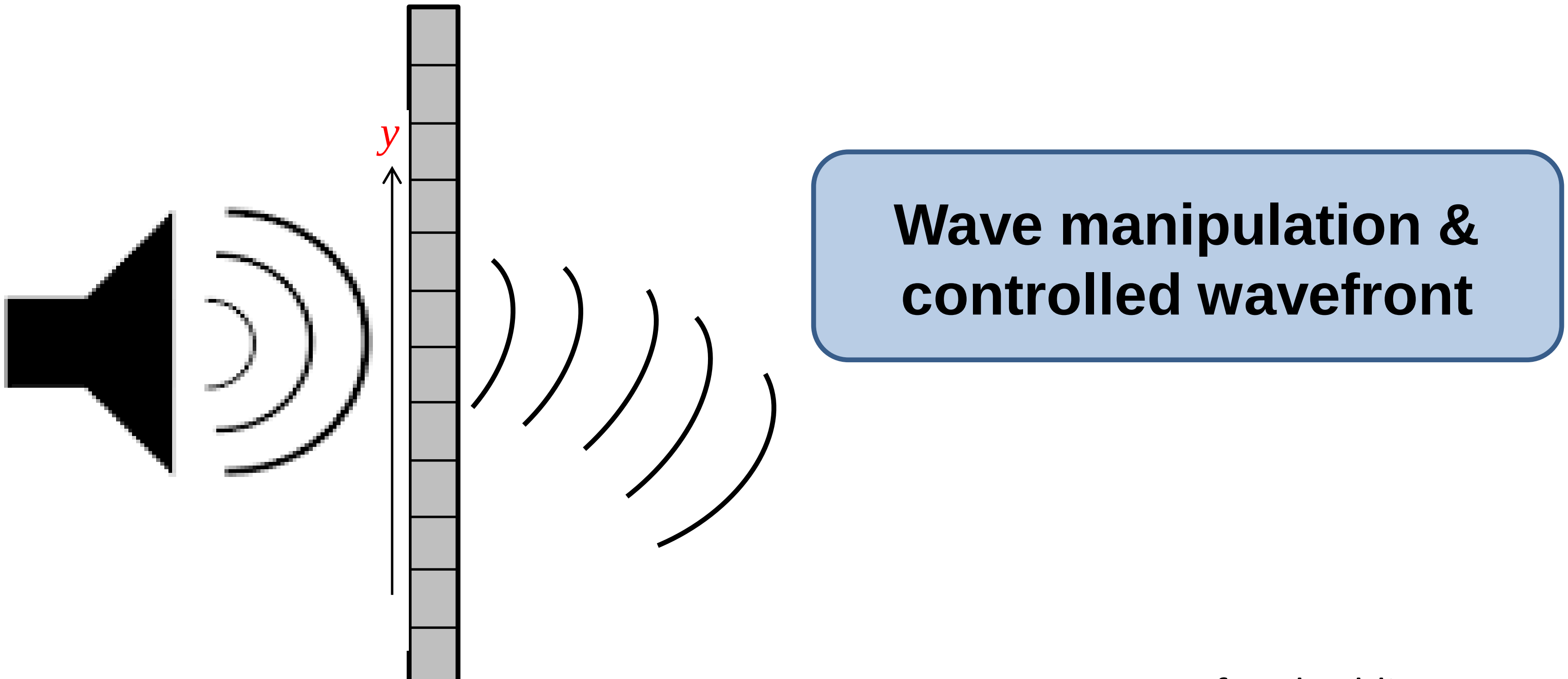

Courtesy of Badreddine Assouar

Wavefront modulation and subwavelength diffractive acoustics with an acoustic metasurface

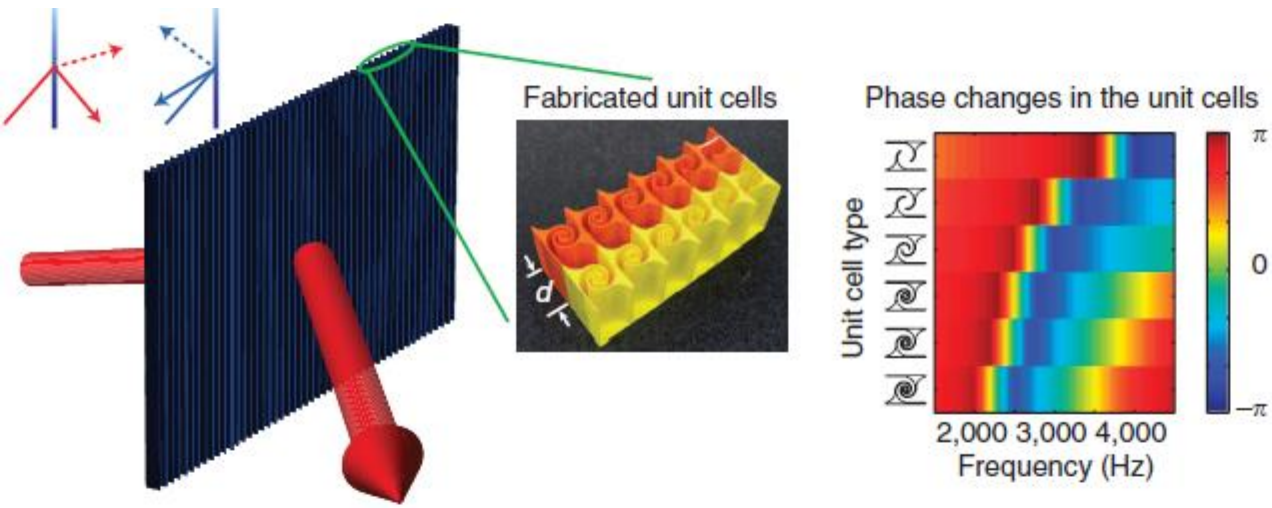

Acoustic metasurface based on tapered labyrinthine metamaterials.

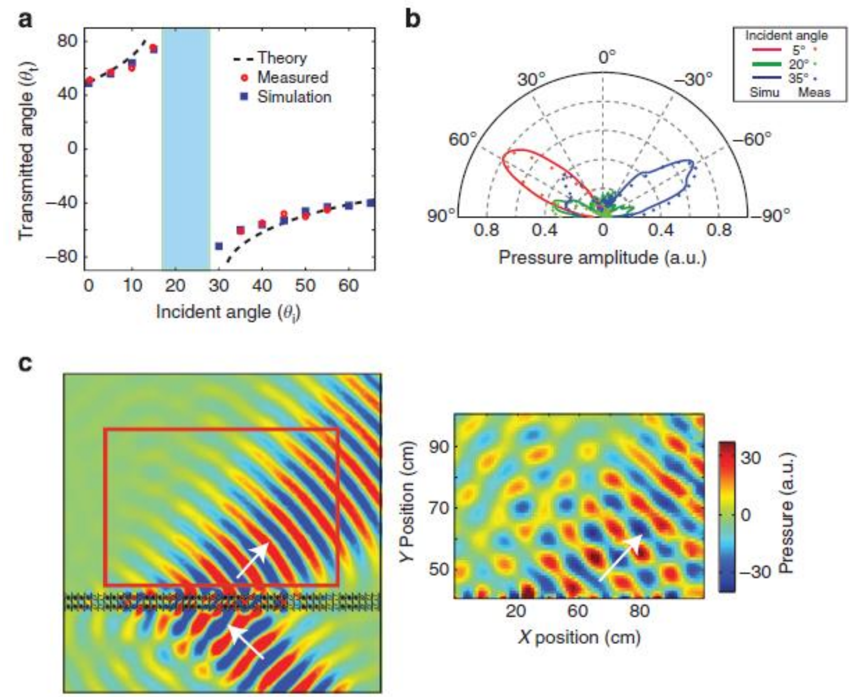

Snell law: $(\sin\theta_t - \sin\theta_i)k_0 = \xi$ (Instead of 0)

where $\xi = \mathrm{d}\phi_s/\mathrm{d}x$

More generally: $(\sin\theta_t - \sin\theta_i)k_0 = \xi + n_G G$

Y. Xie, W. Wang, H. Chen, A. Konneker, B. Popa & S. A. Cummer, Nat. Commun. 5, 6553 (2014)

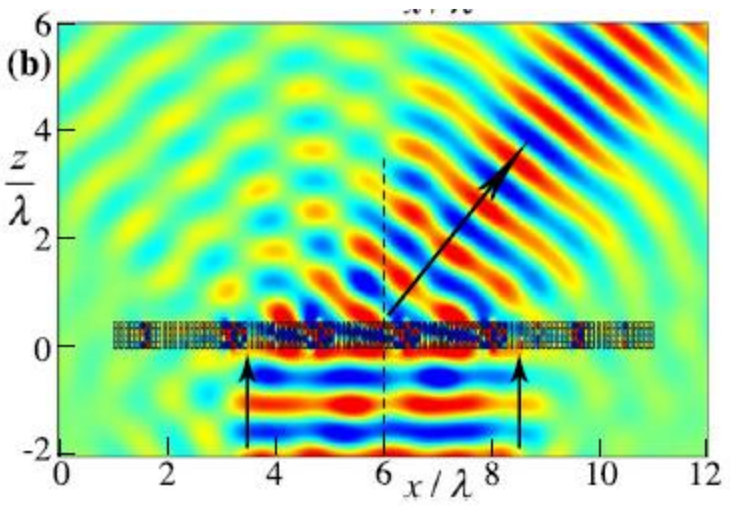

Anomalous refraction

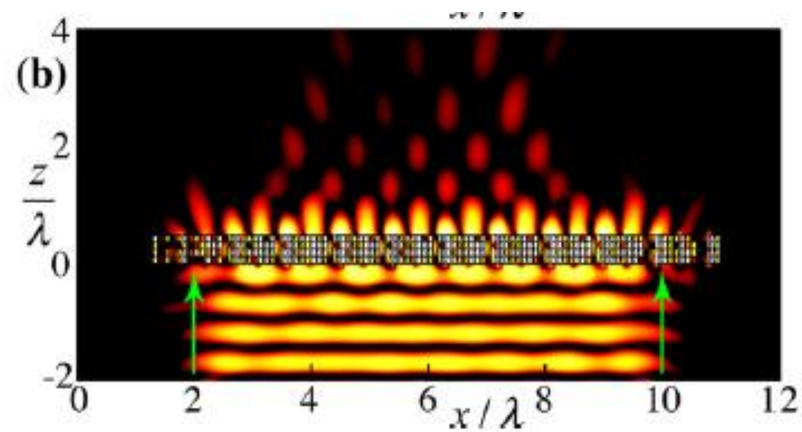

Conversion of a propagating wave into an evanescent wave

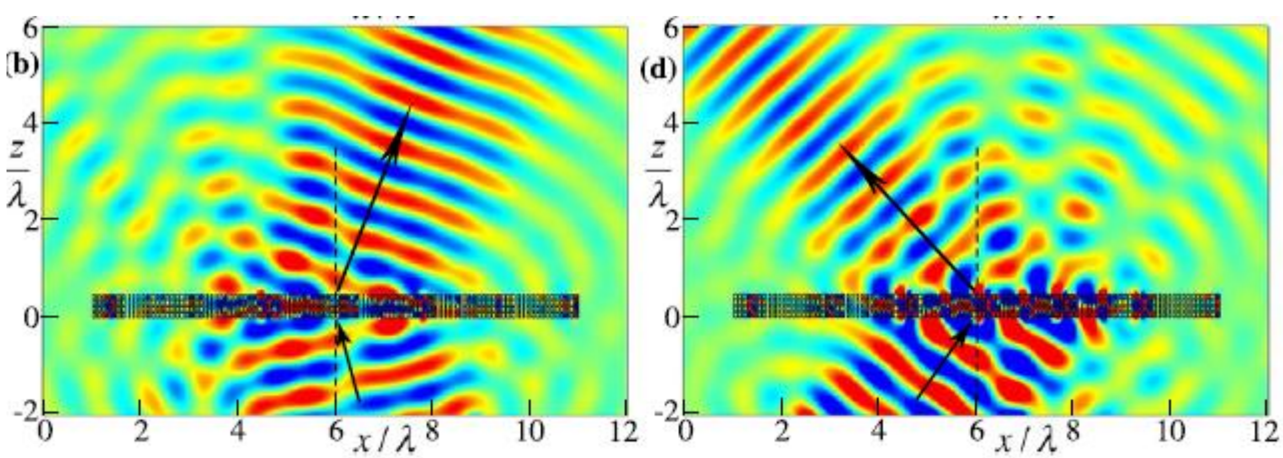

Negative refraction

Y. Li, S. Qi & M. B. Assouar, New J. Phys. 18 (2016) 043024

Metascreen-based acoustic passive phased array

Example of design: an element of a hybrid structure

The metasurface is stacked up by an array of elements

- ✓ A full 2π range
- ✓ A high transmission
- ✓ A fine resolution

A Helmholtz resonator acts as a lumped element providing an **effective acoustic reactance** to shift the phase of the incident acoustic field.

A series of Helmholtz resonators

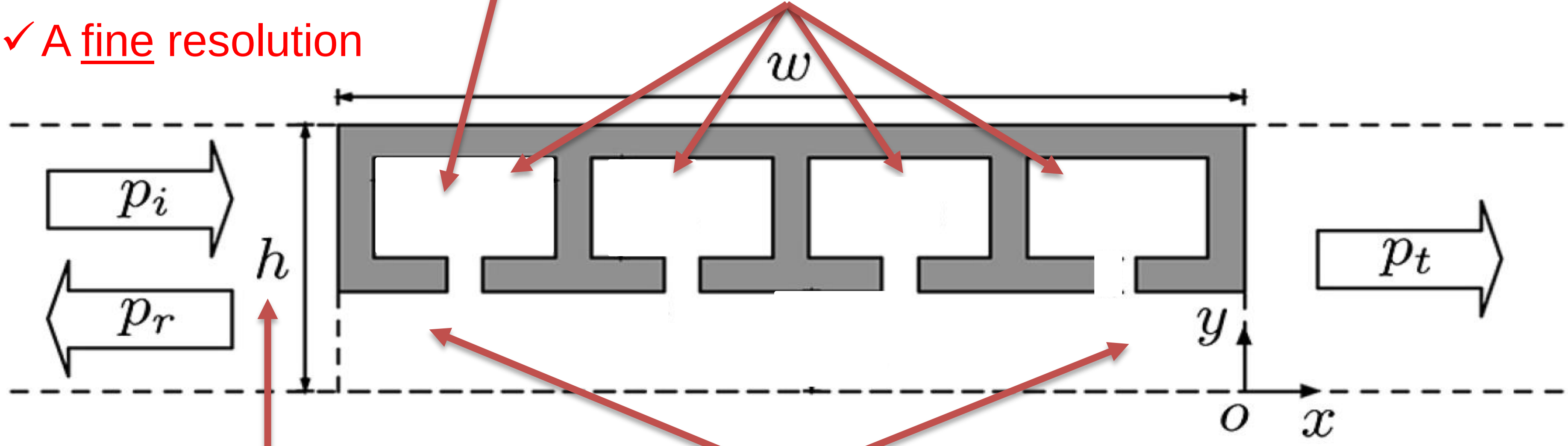

Fine dimension along the screen: $h = \lambda/10$

A straight pipe (for high transmission)

Fabry-Perot resonance: $w = \lambda/2$

Courtesy of Badreddine Assouar

Acoustic Metasurfaces for Wave Manipulation

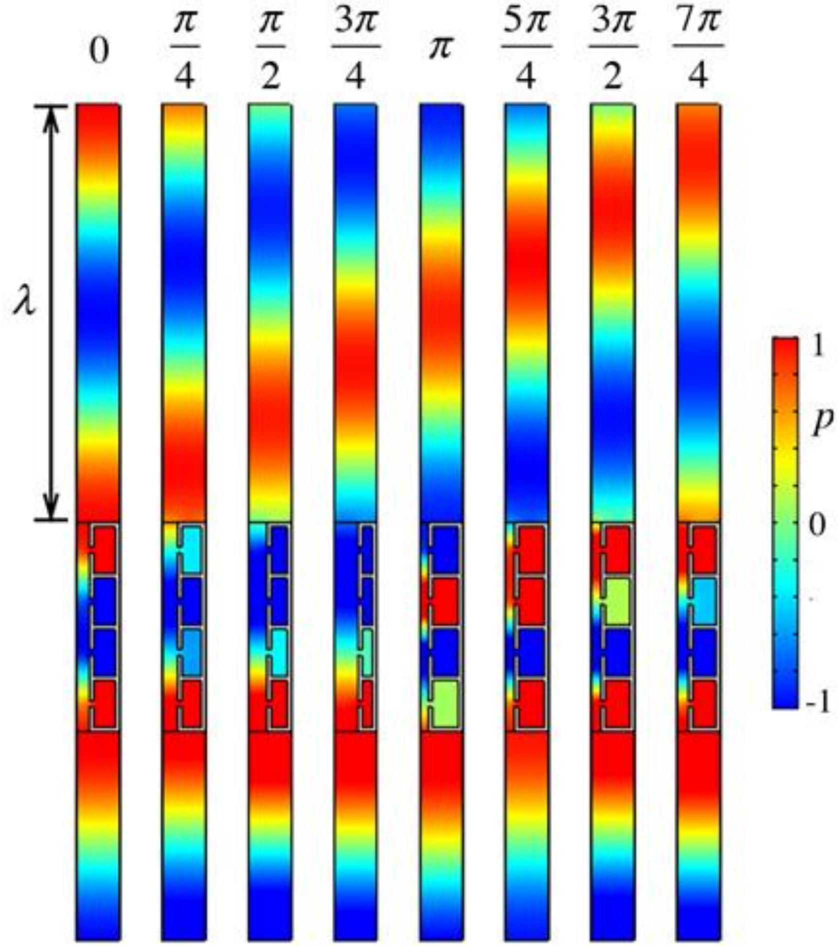

Y. Li, S. Qi & M. B. Assouar, New J. Phys. 18 (2016) 043024

Courtesy of Badreddine Assouar

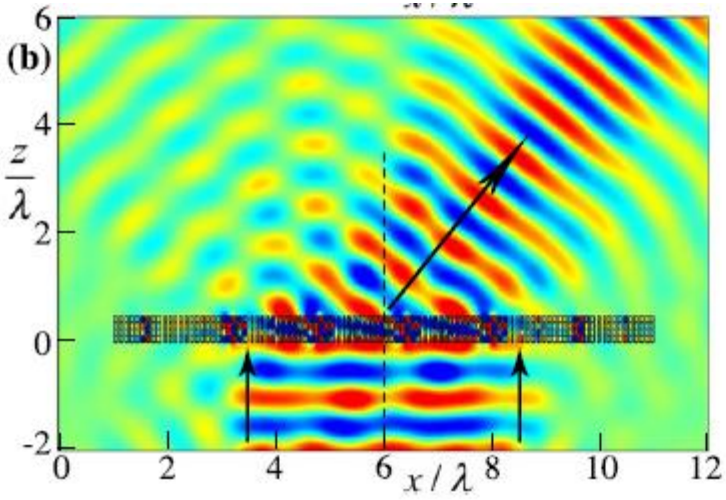

Anomalous refraction

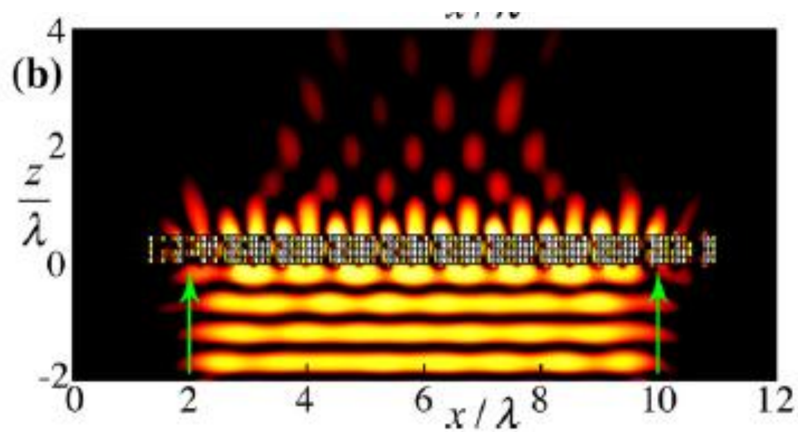

Conversion of a propagating wave into an evanescent wave

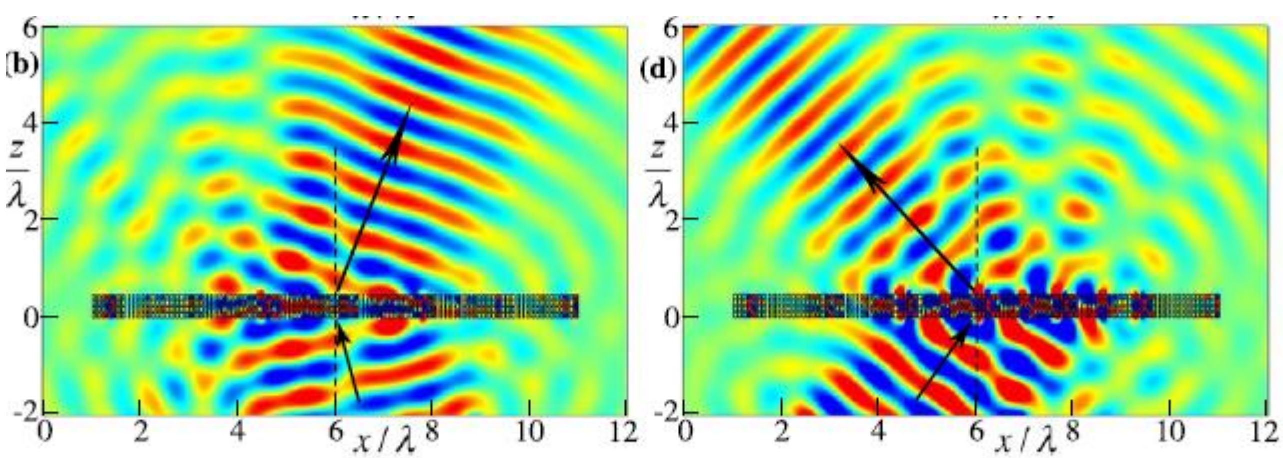

Negative refraction

Y. Li, S. Qi & M. B. Assouar, New J. Phys. 18 (2016) 043024

Acoustic Focusing and Energy Confinement Based on Multilateral Metasurfaces

The coiling-up space is used to control the effective acoustic paths, which can ensure the predefined phase lead or lag for desired wavefront tailoring.

- Metasurface based on a labyrinthine structures to induce a 2π phase shift.
- Adjusting the geometrical parameters of a labyrinthine unit cell to cover 2π span.

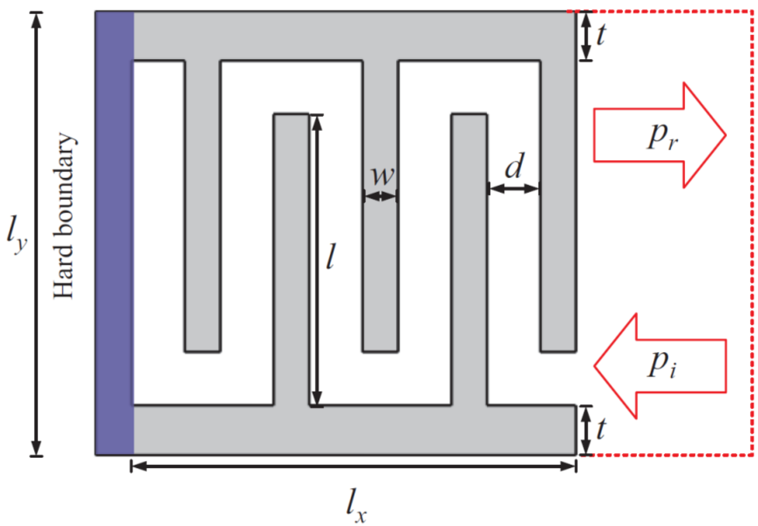

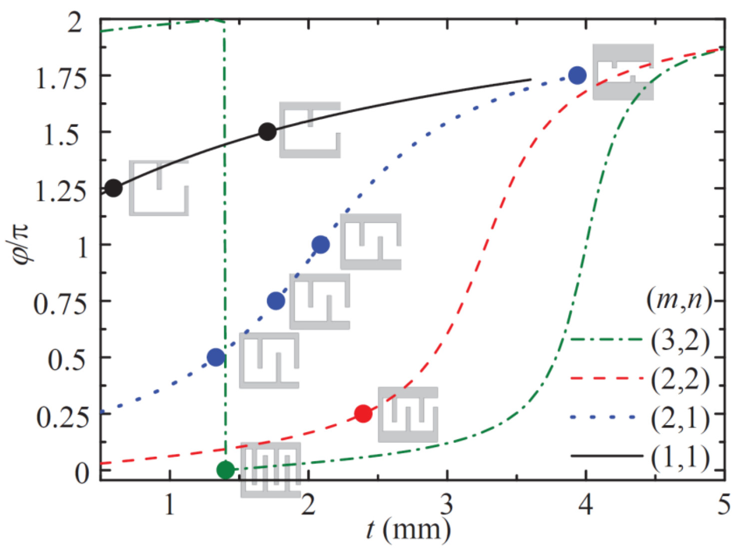

S. Qi, Y. Li & M. B. Assouar, Phys. Rev. Applied 7 (2017) 054006.

Courtesy of Badreddine Assouar

Multilateral metasurface for energy confinement

Multilateral metasurfaces (2 sided)

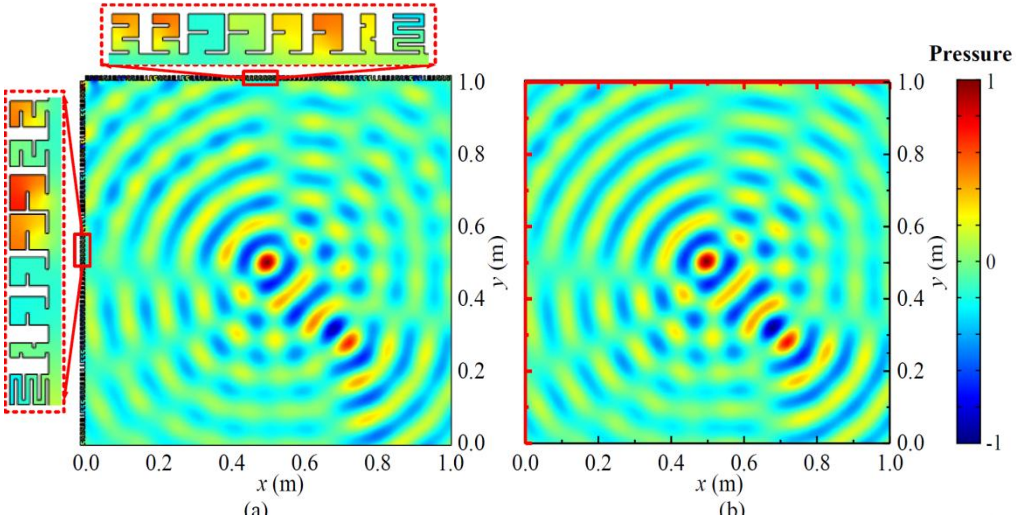

Normalized sound pressure field (Num & Theo)

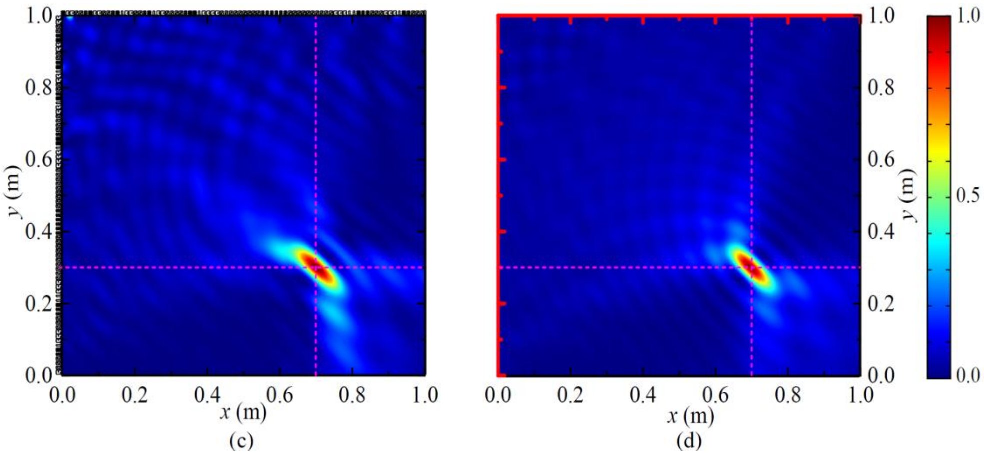

Normalized reflected sound intensity field $|p|^2$ (Num & Theo)

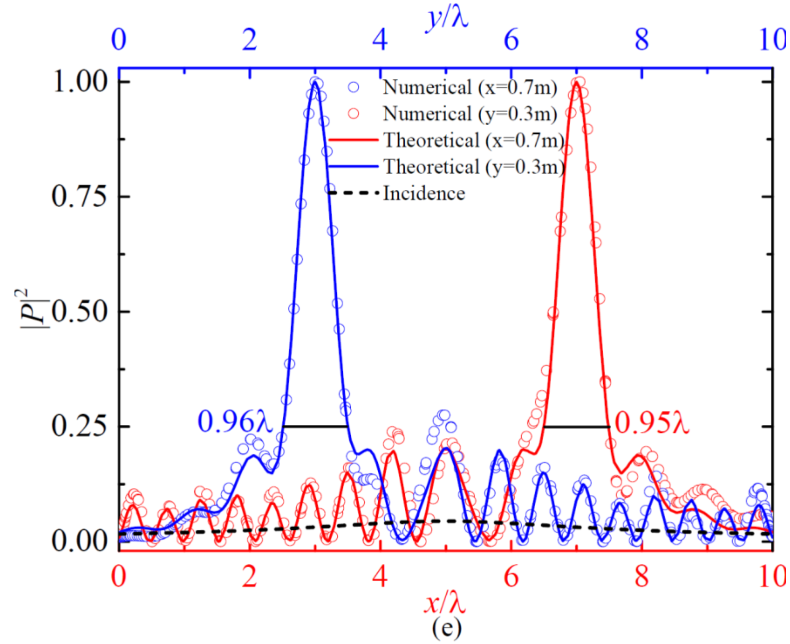

Numerical and theoretical sound intensities of the cross section lines

Courtesy of Badreddine Assouar

Outline

5. Brief overview of refractive properties

- Negative refraction and focusing
- Self-collimation and beam splitting

6. Subwavelength structures and applications of metamaterials

- Effective properties (positive and negative dynamic parameters)
- Focusing and imaging. Superlens and heperlens
- Cloaking
- GRIN devices
- Metasurfaces. Resonating units and space coiling. Absorption. Phase manipulation

7. Active materials and some emerging topics

Non reciprocal behaviors . Time-space periodicity. PT symmetry. Topological phononics.

8. Dual phononic-photonic crystals (phoXonic) and Optomechanics

- Simultaneous phononic-photonic band gaps.
- Waveguide modes. Slow and fast modes
- Enhanced phonon-photon interaction in a cavity. Comparison of photoelastic and optomechanic effects
- Phononic and Phoxonic sensors

Bragg band gaps tunability in an homogeneous piezoelectric rod with periodic electrical boundary conditions

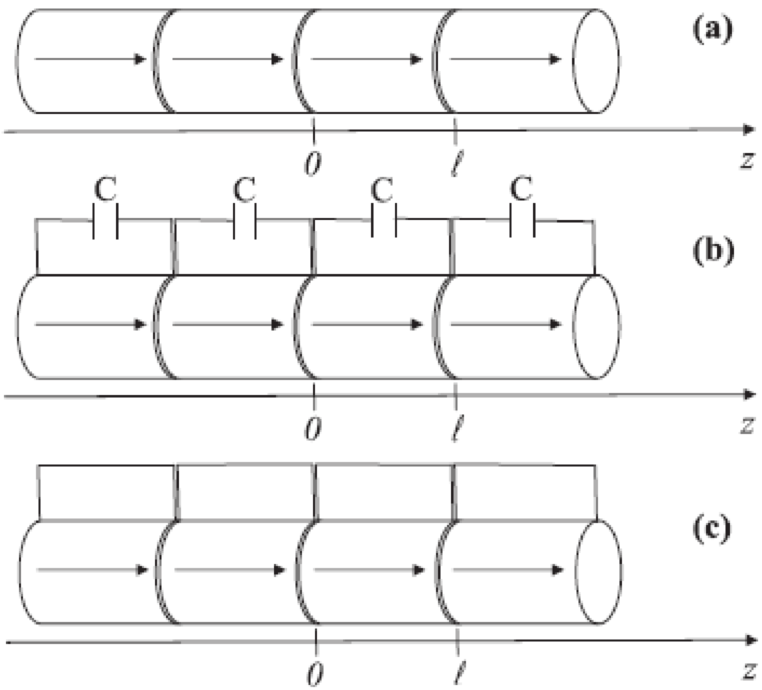

(a) Open circuit
(b) Short circuit via capacitance C
(c) Short circuit

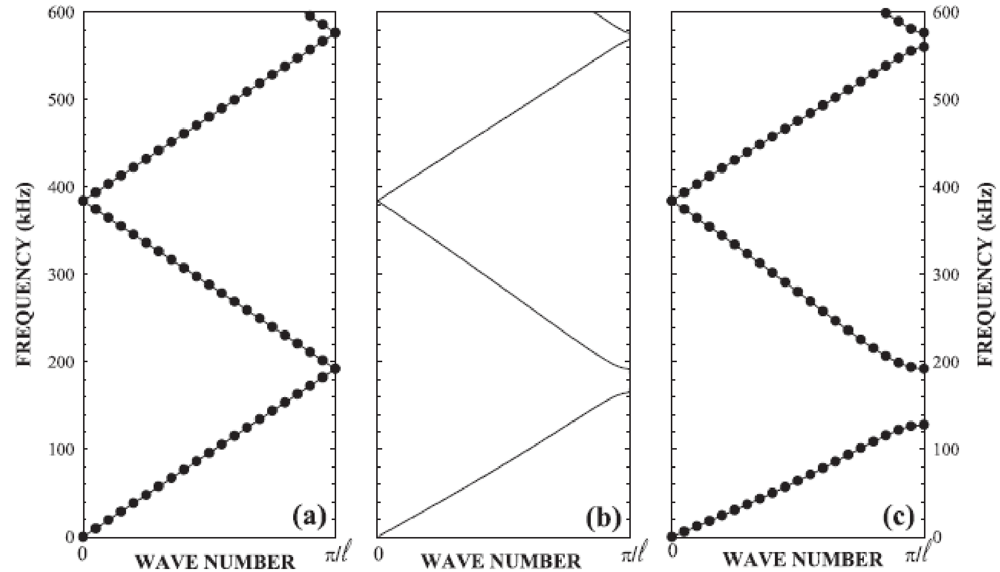

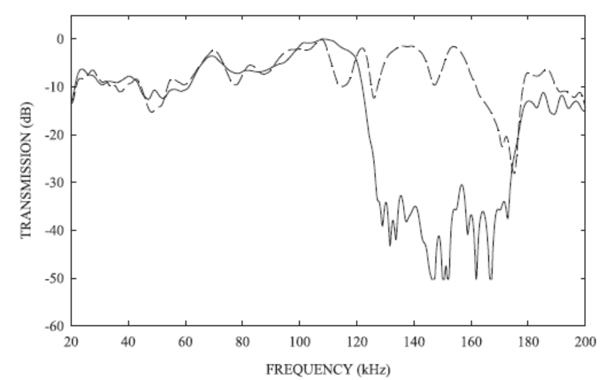

Experimental transmission

S. Degraeve, C. Granger, B. Dubus, J. O. Vasseur, M. Pham Thi, and A.-C. Hladky-Hennion, J. Appl. Phys. 115, 194508 (2014)

Tunable magnetoelastic phononic crystals

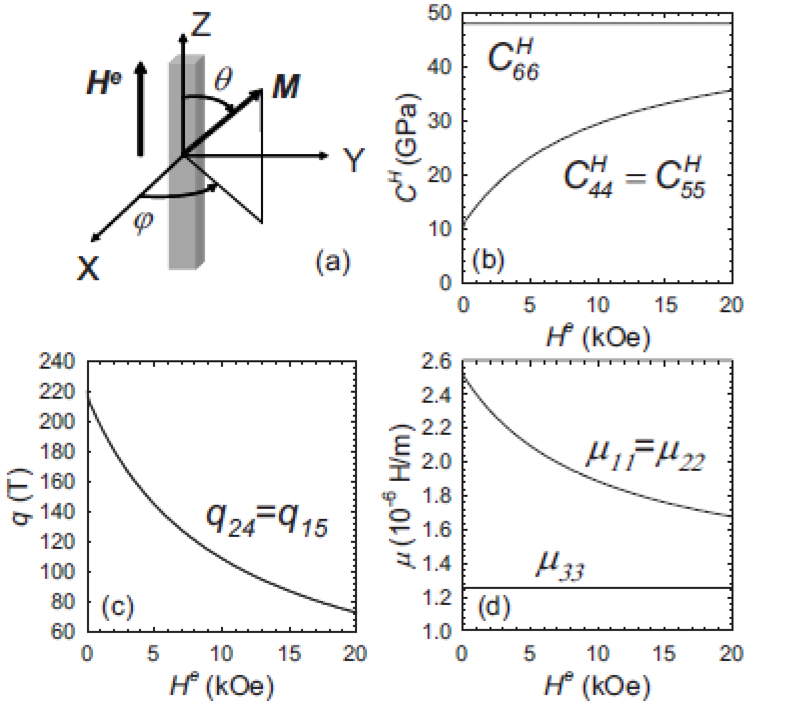

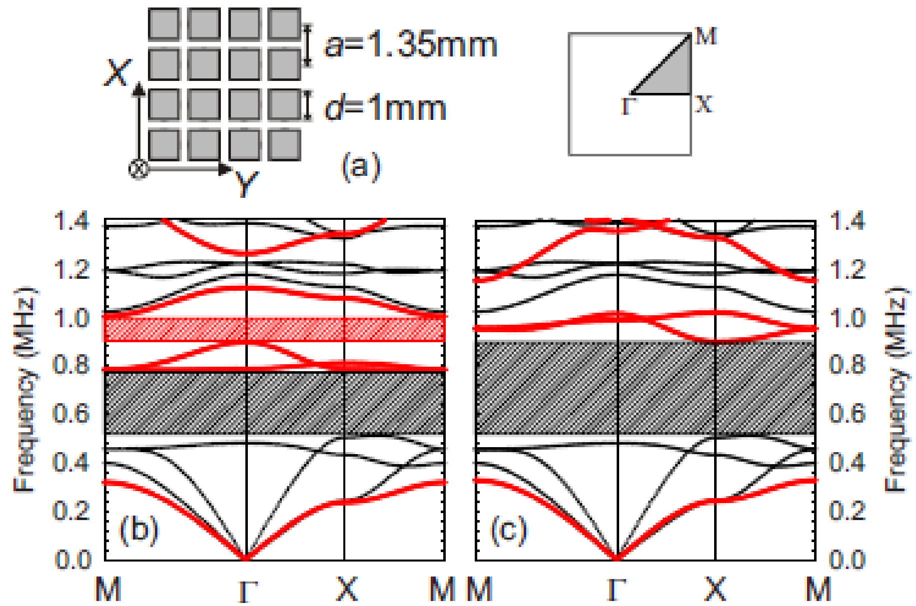

H_{ext}=0

H_{ext}=13 kOe

Magnetorestrictive materails (Terfenol D) submitted to an external magnetic field

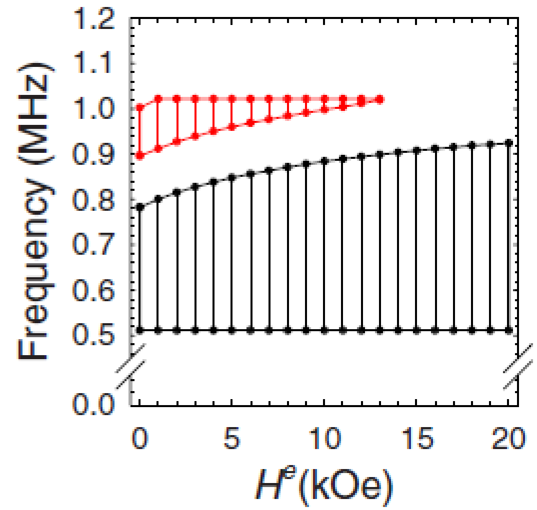

Band gaps versus H_{ext}

J.-F. Robillard,O. Bou Matar, J. O. Vasseur, P. A. Deymier, M. Stippinger, A.-C. Hladky-Hennion, Y. Pennec and B. Djafari-Rouhani, Appl. Phys. Lett. 95,124104 (2009)

Harnessing Buckling to Design Tunable Locally Resonant Acoustic Metamaterials

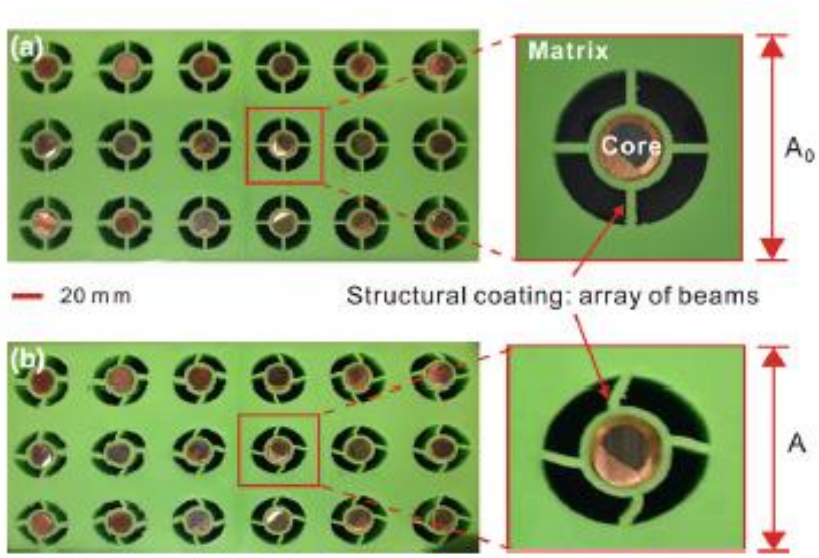

Resonating units dispersed in an elastomeric matrix
Each resonator consists of a metallic core connected to the matrix through elastic beams

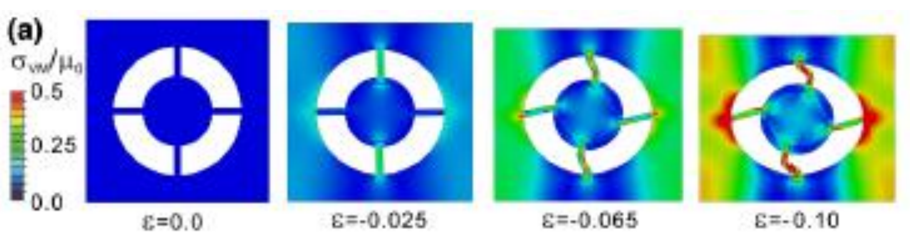

Compressibve strain applied to the vertical direction
The effective stifness is significantly aletred by the buckling Which in turn changes the dispersion curves

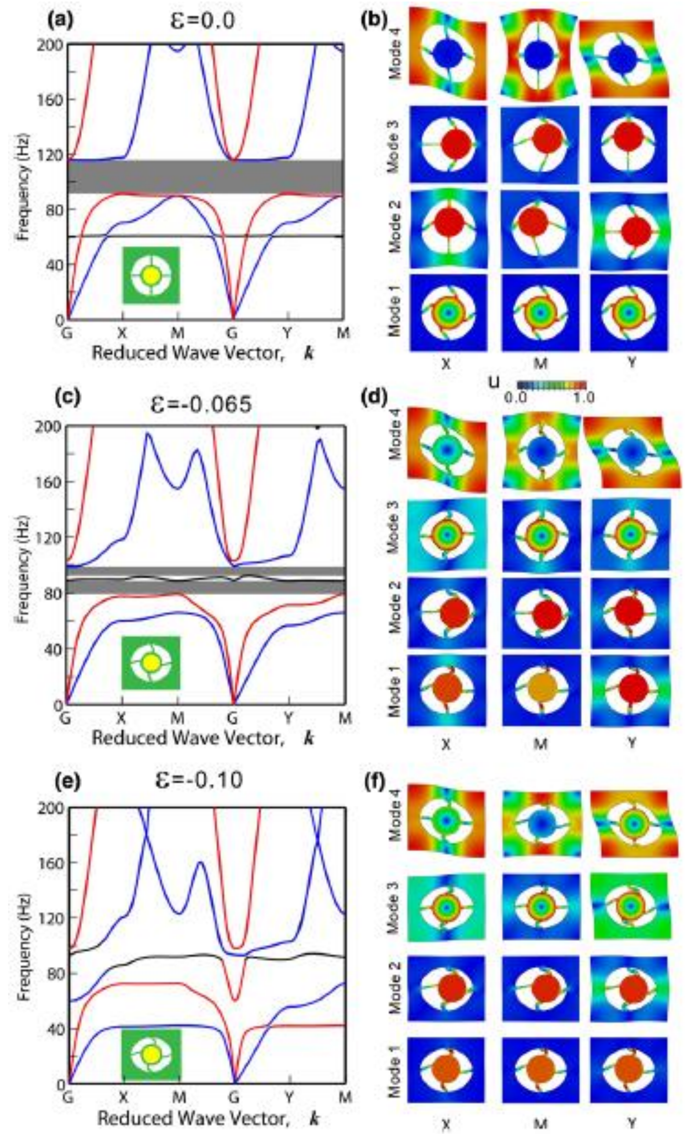

P. Wang, F. Casadei, S. Shan, J.C. Weaver and K. Bertoldi, PRL 113, 014301 (2014)

Non-reciprocal and highly nonlinear active acoustic metamaterials

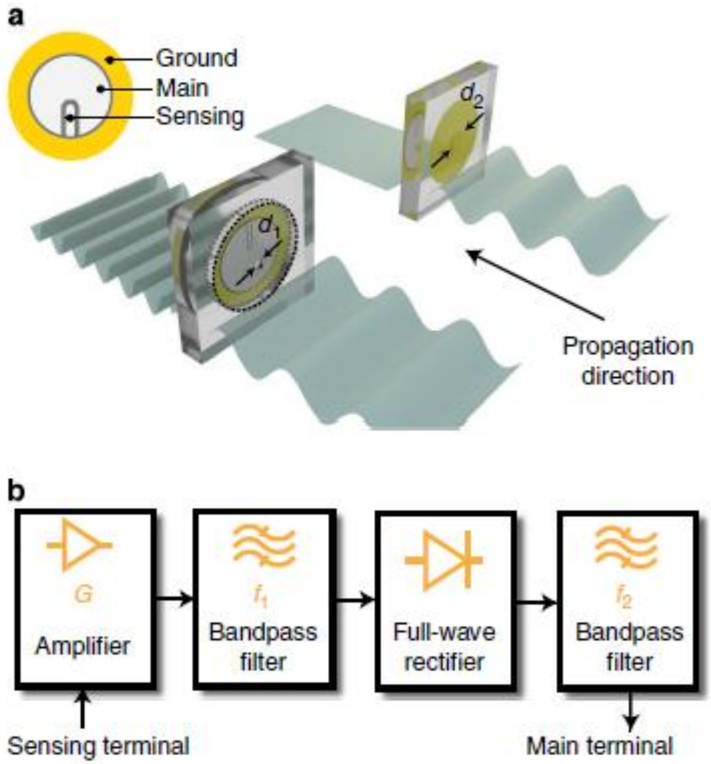

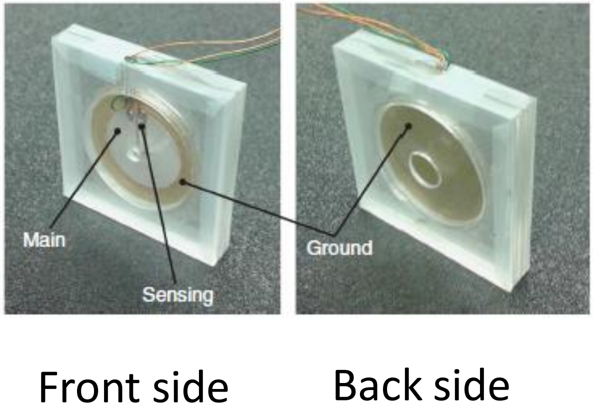

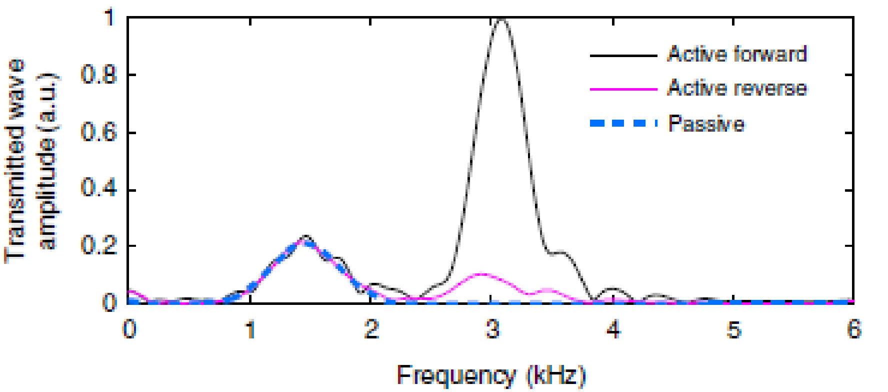

-Two highly subwavelength Helmholtz cavities tuned on different frequencies (1500 and 3000 Hz) to create the asymmetry needed for the non-reciprocal behavior.

-The cavities share a common wall consisting of a piezoelectric membrane (PZM) augmented by a nonlinear electronic circuit that sets the behavior of the membrane.

B. Popa & S.A. Cummer, Nat. Commun. 5, 4398 (2014)

Acoustic diodes and acoustic rectification

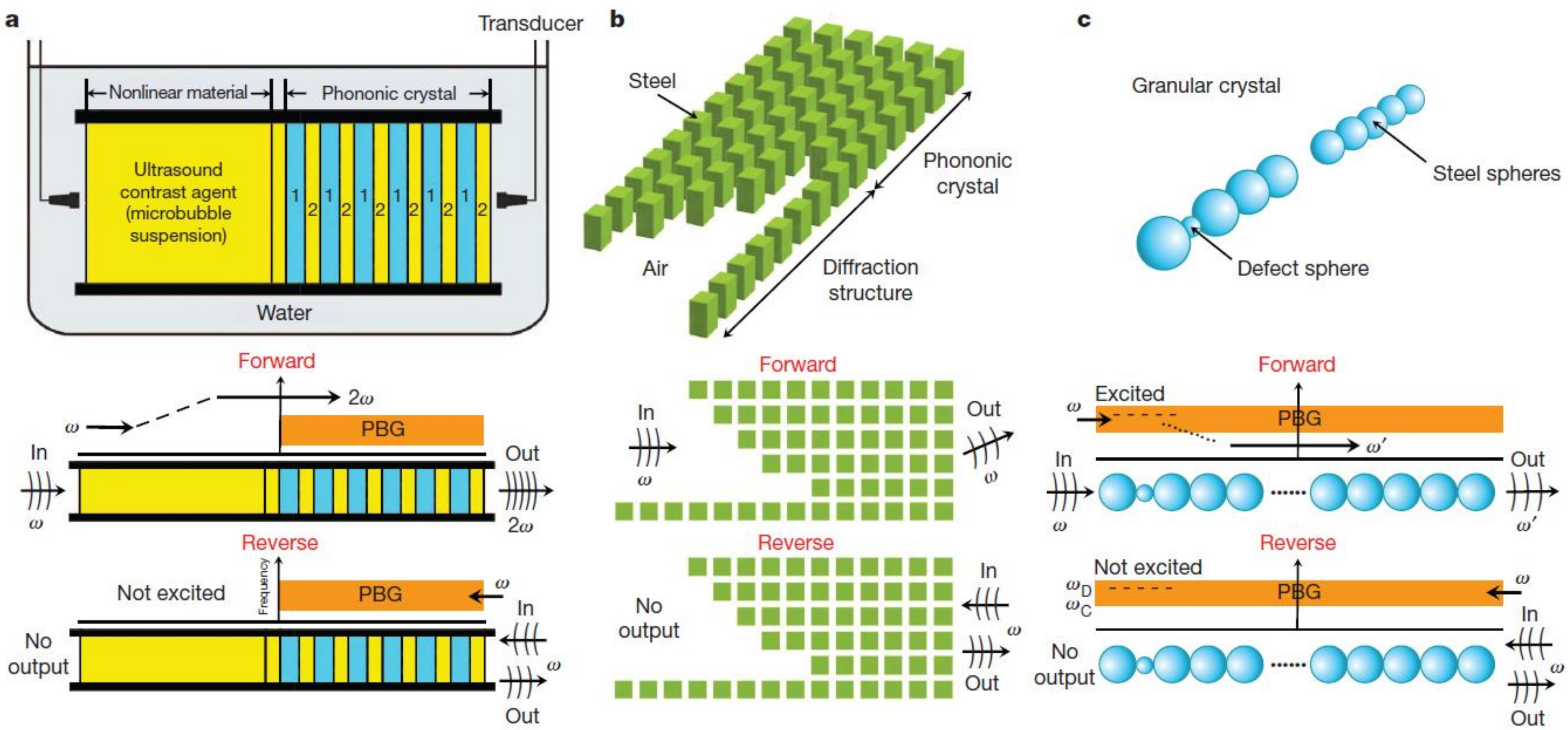

B. Liang et al, Nature Mater., 9, 989 (2010)

X.F. Li et al, Phys. Rev. Lett. 106, 084301 (2011)

N. Boechler et al, Nature Mater. 10, 665(2011)

From M. Maldovan in Nature 503, 209 (2013)

Temporal modulation of a 1D phononic crystal

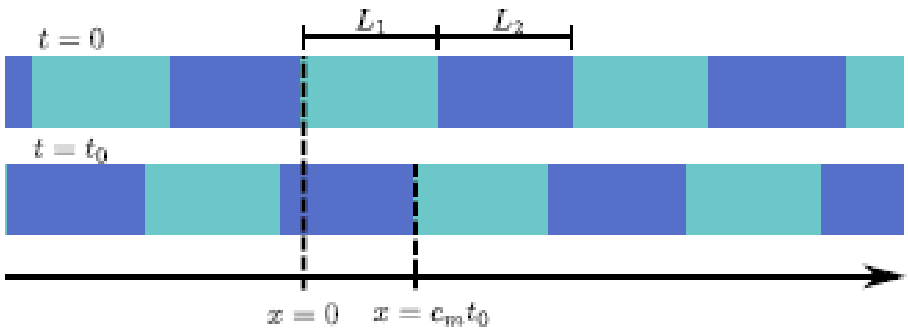

Modulated phononic crystals: Non-reciprocal wave propagation and Willis materials
H. Nassar , X.C. Xu , A.N. Norris , G.L. Huang, , J. Mech. Phys. Sol. 101, 10 (2017)

-Piezoelectric aresonator arrays for tunable acoustic waveguides and metamaterials
F. Casadei, T. Delpero, A. Bergamini, P. Ermanni and M. Ruzzene, J. Appl. Phys. 112, 064902 (2012)

- Bulk elastic waves with unidirectional backscattering-immune topological states in a time-dependent superlattice
N. Swinteck, , S. Matsuo, K. Runge, J. O. Vasseur, P. Lucas, and P. A. Deymier,, J. Appl. Phs. 118, 063103 (2015)

- Brillouin scattering-like effect and non-reciprocal propagation of elastic waves due to spatio-temporal modulation of electrical boundary conditions in piezoelectric media
C. Croënne, J. O. Vasseur, O. Bou Matar, M.-F. Ponge, P. A. Deymier, A.-C. Hladky-Hennion, and B. Dubus Appl. Phys. Lett. 110, 061901 (2017)

- Non-reciprocal elastic wave propagation in spatiotemporal periodic structures
G. Trainiti and M. Ruzzene, New J. Phys. 18 083047 (2016)

Modulated phononic crystals: Non-reciprocal wave propagation and Willis materials

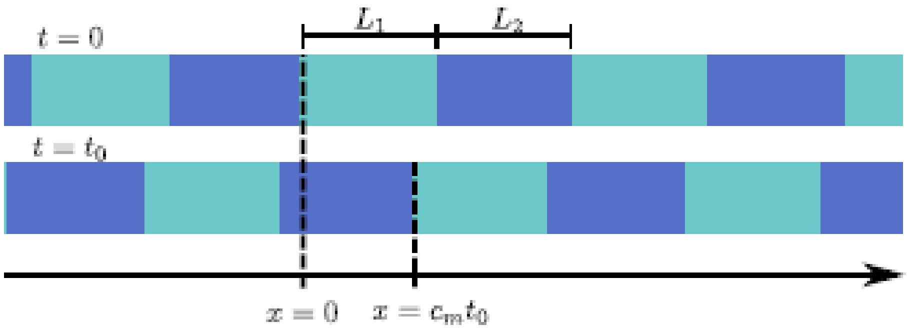

A 1D phononic crystal modulated both in space and time

- Without time modulation

$$\cos(kL) = \cos\left(\frac{\omega}{c_1}L_1\right)\cos\left(\frac{\omega}{c_2}L_2\right) - \frac{1}{2}\left(\frac{z_1}{z_2}+\frac{z_2}{z_1}\right)\sin\left(\frac{\omega}{c_1}L_1\right)\sin\left(\frac{\omega}{c_2}L_2\right)$$

- With time modulation

$$\cos\left[kL - c_m(\omega - c_m k)\left(\frac{L_1}{c_1^2 - c_m^2} + \frac{L_2}{c_2^2 - c_m^2}\right)\right]$$
$$= \cos\left(\frac{\omega - c_m k}{c_1^2 - c_m^2}c_1 L_1\right)\cos\left(\frac{\omega - c_m k}{c_2^2 - c_m^2}c_2 L_2\right) - \frac{1}{2}\left(\frac{z_1}{z_2}+\frac{z_2}{z_1}\right)\sin\left(\frac{\omega - c_m k}{c_1^2 - c_m^2}c_1 L_1\right)\sin\left(\frac{\omega - c_m k}{c_2^2 - c_m^2}c_2 L_2\right)$$

The following transformation applies between the moving and reference frame:

$$kx - \omega t = K\xi - \Omega t$$

or

$$k = K, \quad \omega = \Omega + c_m k$$

H. Nassar , X.C. Xu , A.N. Norris , G.L. Huang, J. Mech. Phys. Sol. 101, 10 (2017)

Modulated phononic crystals: Non-reciprocal wave propagation and Willis materials

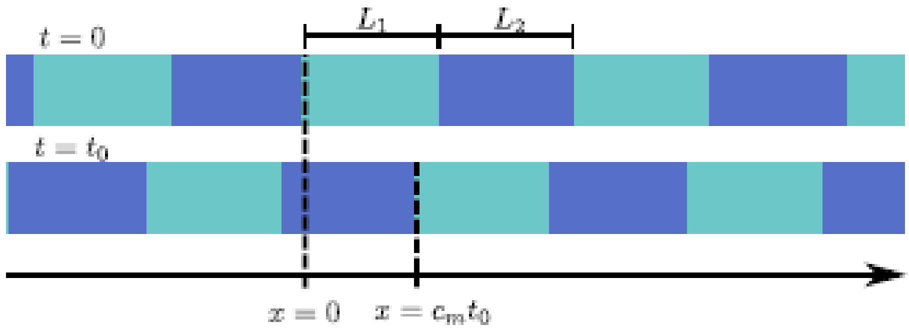

A 1D phononic crystal modulated both in space and time

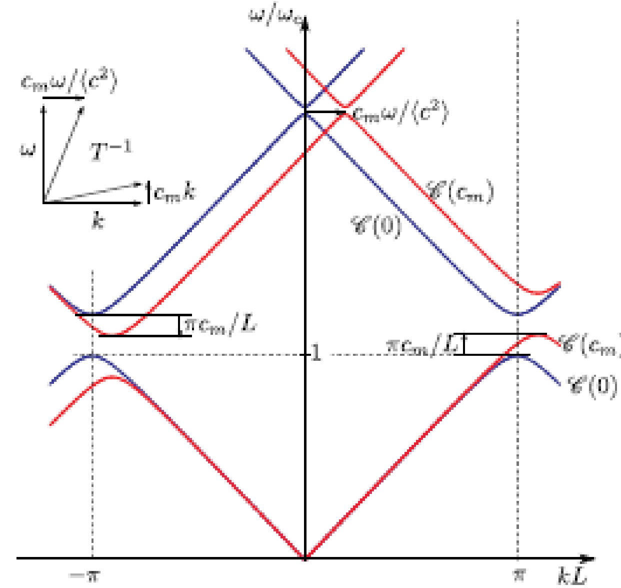

Small modulation

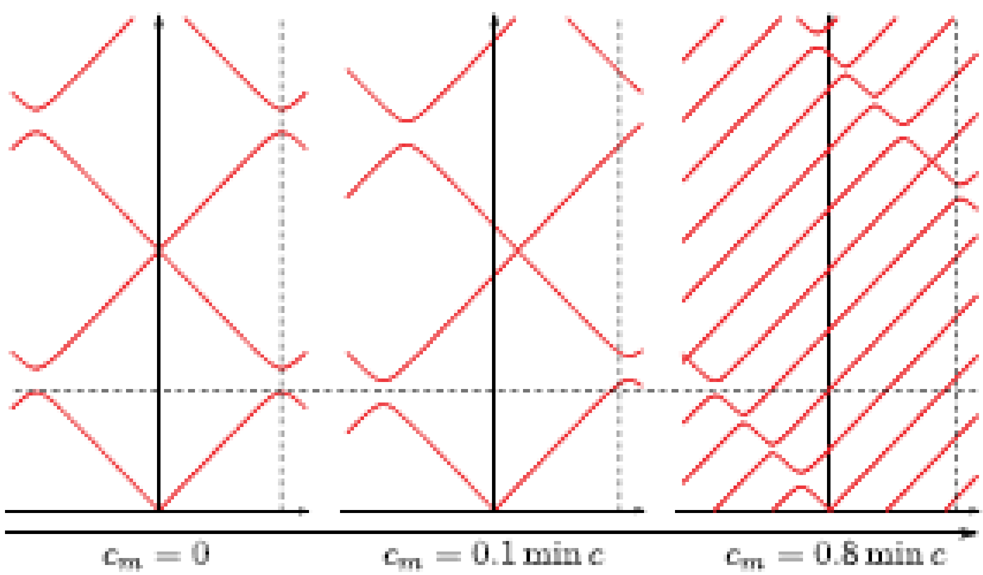

Increasing modulation

H. Nassar , X.C. Xu , A.N. Norris , G.L. Huang,
J. Mech. Phys. Sol. 101, 10 (2017)

Non-reciprocal (topological) edge states in a phononic crystal with circulating fluid

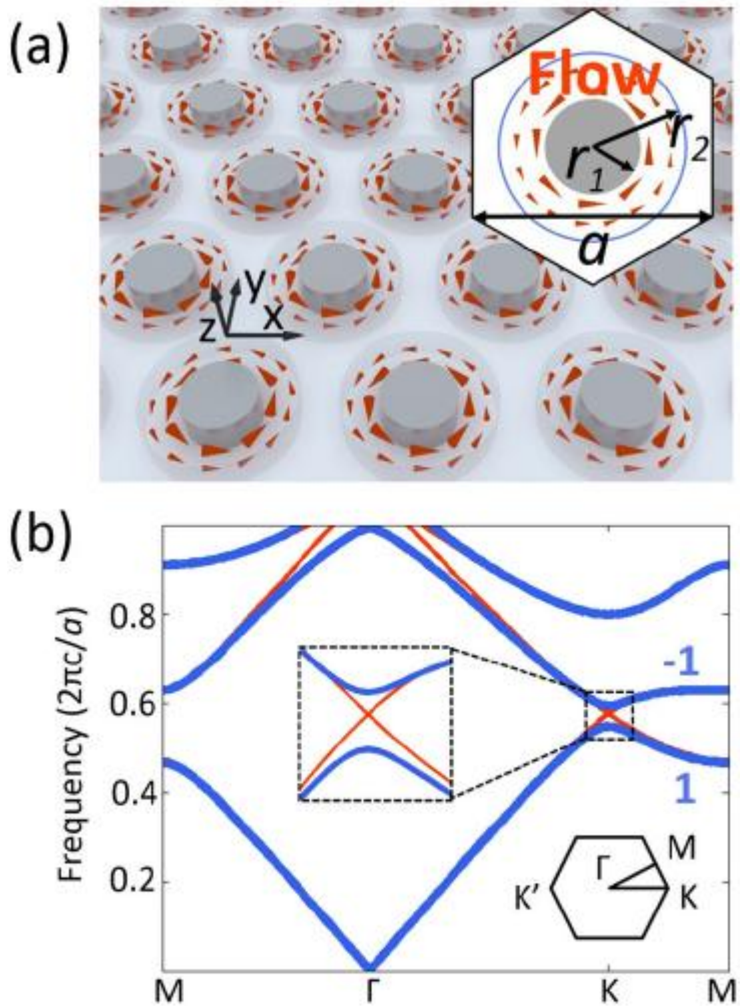

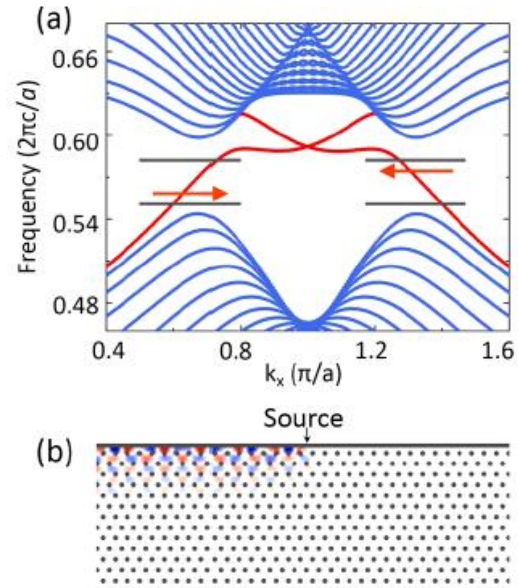

← Left propagating wave

$$\frac{1}{\rho}\nabla\cdot\rho\nabla\phi-(\partial_t+\vec{v}_0\cdot\nabla)\frac{1}{c^2}(\partial_t+\vec{v}_0\cdot\nabla)\phi=0,$$

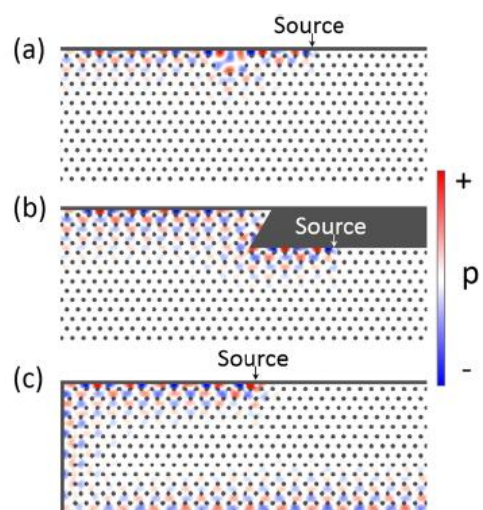

Robustness with respect to:

← Disorder

← Zigzag shape

← travel along the edge

Z. Yang, F. Gao, X. Shi, X. Lin, Z. Gao, Y. Chong, and B. Zhang, PRL 114, 114301 (2015)

Subwavelength ultrasonic circulator based on spatiotemporal modulation

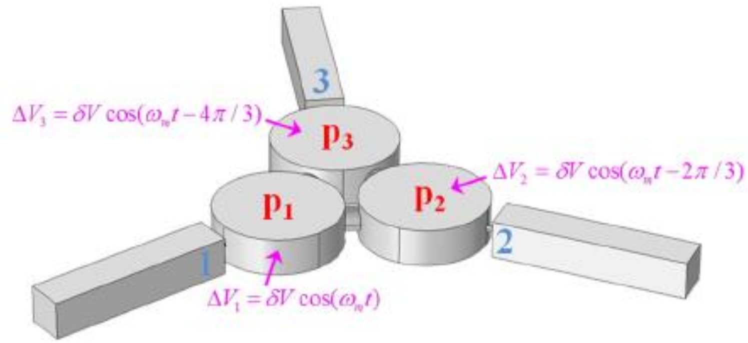

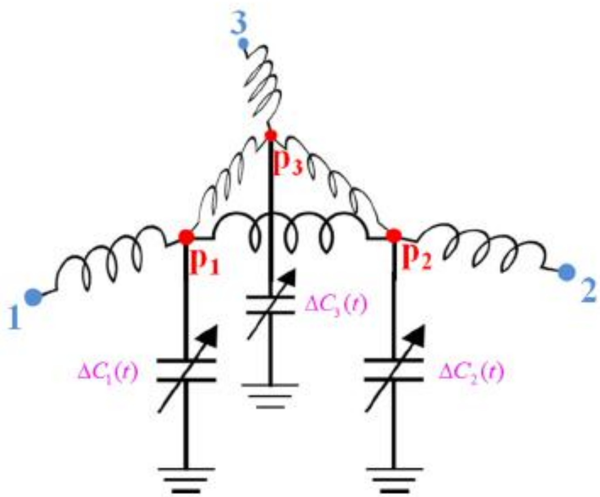

Geometry of the proposed three-port network: three acoustic cavities connected via small channels and coupled to three waveguides. The volumes *V of the cavities* are weakly modulated *in a rotating fashion, with amplitude δV and* frequency ω_m.

Acoustic isolation

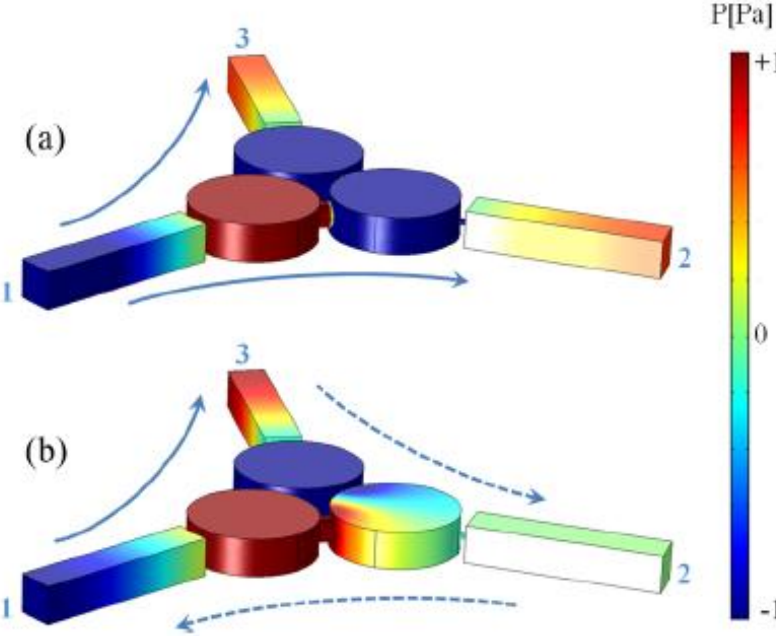

(a) Modulation turned off
(b) Modulation turned on

R. Fleury, D.L. Sounas, and A. Alu, Phys.Rev.B 91, 174306 (2015)

Parity-Time -Symmetric Acoustics: unidirectional transparency at given frequencies

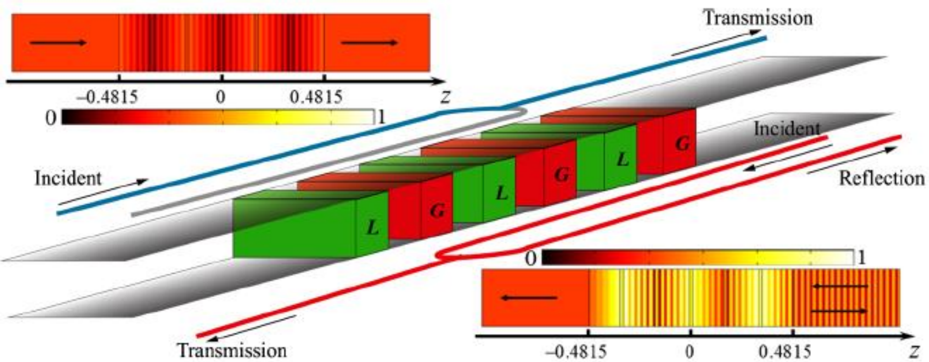

$$r_L r_R^* = 1 - |t|^2 \quad \text{or} \quad \sqrt{R_L R_R} = |T-1|$$

This PT -symmetric medium is designed to be reflectionless for acoustic waves incident from the left

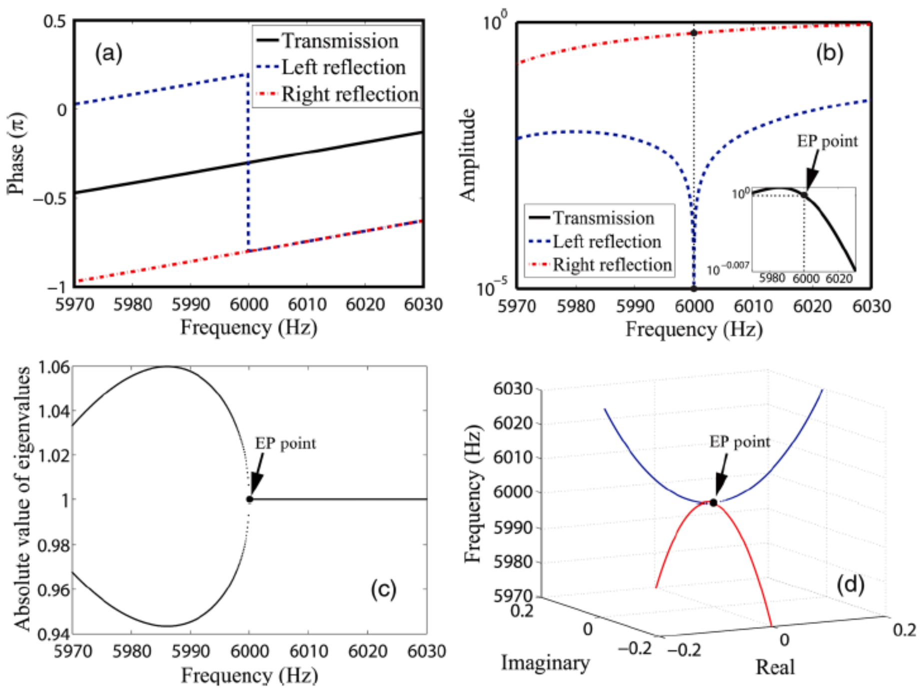

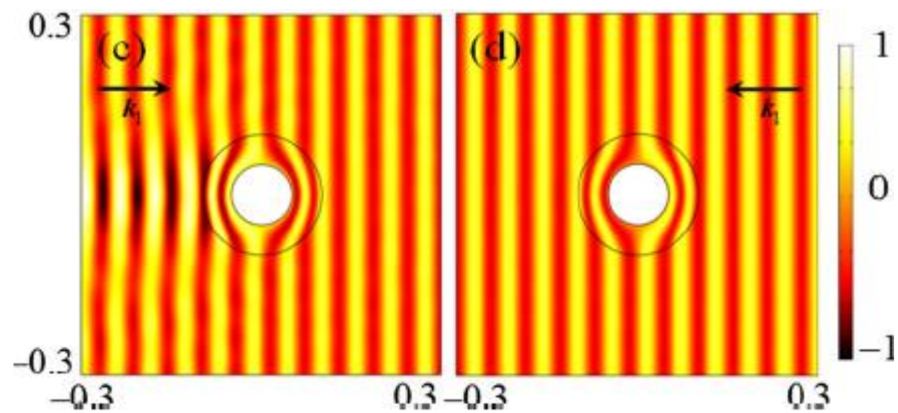

One way invisibility cloak

Based on PT medium
+
transformation acoustic method

X. Zhu, H. Ramezani, C. Shi, J. Zhu, and X. Zhang, Phys. Rev X 4, 031042 (2014)

Received 14 Sep 2015 | Accepted 18 Feb 2016 | Published 30 Mar 2016 DOI: 10.1038/ncomms11110 OPEN

Accessing the exceptional points of parity-time symmetric acoustics

Chengzhi Shi[1,*], Marc Dubois[1,*], Yun Chen[2], Lei Cheng[2], Hamidreza Ramezani[1], Yuan Wang[1] & Xiang Zhang[1,3,4]

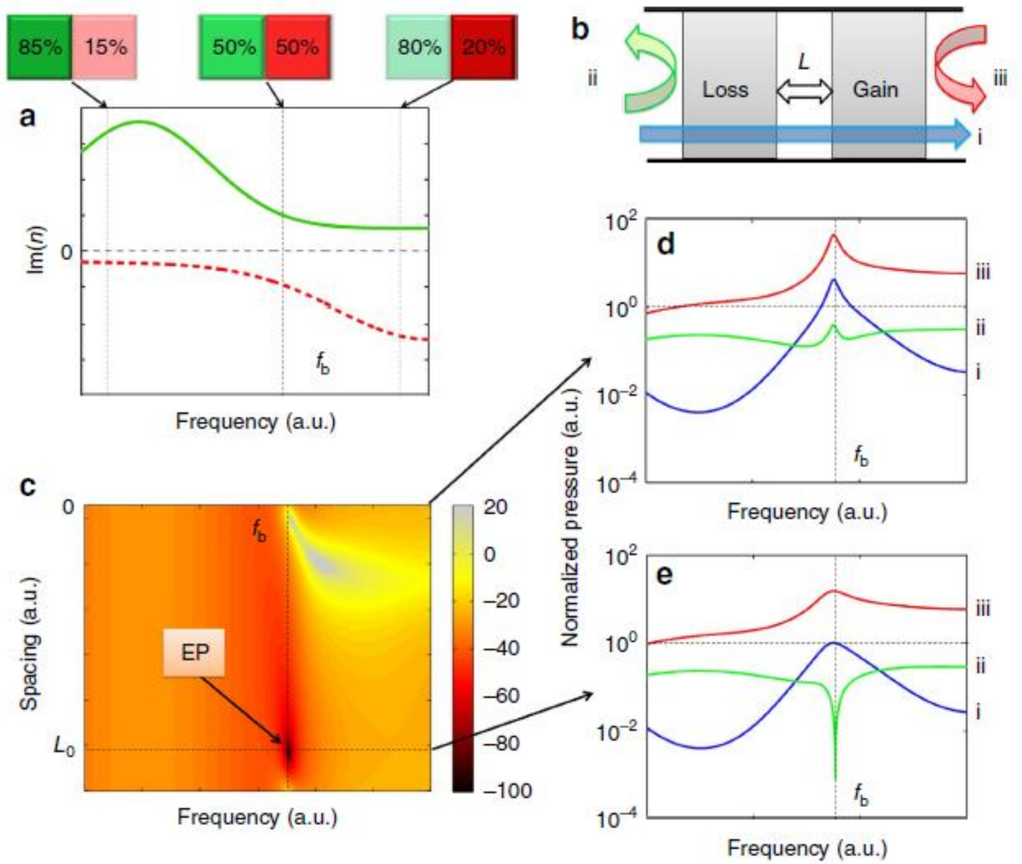

Figure 1 | Accessing the exceptional point of acoustic PT system by tuning the spacing between loss and gain materials. (**a**) Imaginary parts of the refractive indices of loss and gain materials are typically dispersive, thus the PT symmetric condition could only be satisfied at single frequency f_b where the loss and gain materials are exactly balanced. (**b**) Loss and gain materials assembled with spacing. (**c**) Amplitude of the reflection from the loss side as a function of frequency and the spacing between the loss and gain materials. Exceptional point (EP) occurs at frequency f_b and a specific spacing L_0 when the reflection vanishes. (**d**) The normalized transmissions (blue, i), reflections from the loss (green, ii), and from the gain (red, iii) in logarithmic scale without spacing, no exceptional point observed. (**e**) Similar representation to **d** with spacing L_0, an exceptional point observed at f_b.

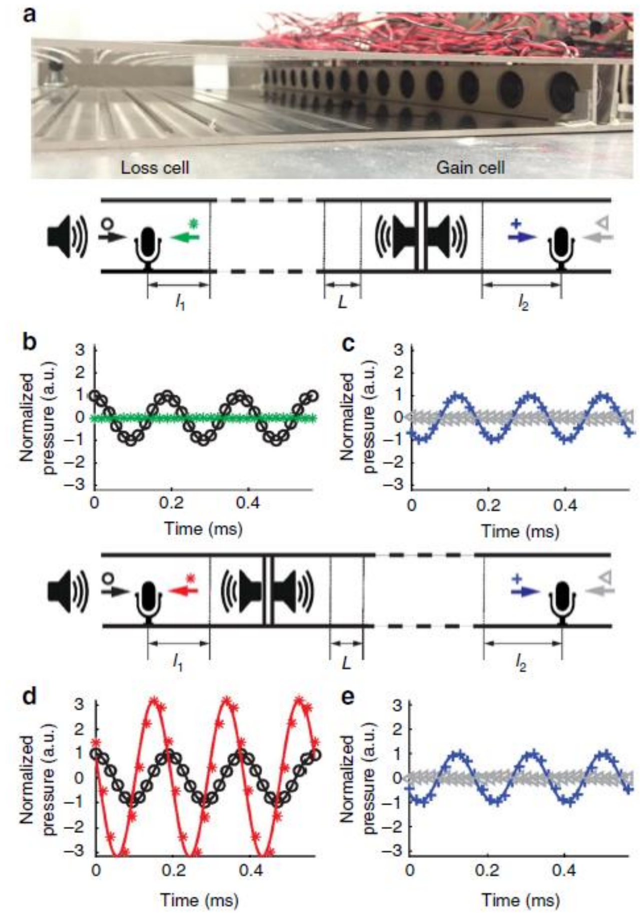

Figure 2 | Experiment demonstration of unidirectional transparency of the PT symmetric system at 5.3 kHz. (**a**) The photo of an experimental sample including loss and gain units. (**b**,**c**) The calculated (solid curves) and measured (marked dots) transmissions and reflections when the incident wave is coming from the loss side. (**d**,**e**) Similar representation to **b** and **c**) when the incident wave is from the gain side. Black, green, red, blue and grey colours denote the incidence, reflection from the loss side, the reflection from the gain side, the transmission and the reflection from the end of the waveguide, respectively. All results have been normalized with the amplitude of incidence. The two calibrated unidirectional microphones are mounted at $l_1 = 15.5$ cm and $l_2 = 13$ cm away from the boundaries of our PT symmetric materials. The spacing between the loss and gain materials is $L = 1.24$ cm. No reflection is observed from the loss side (green curve and dots in **b**), ∼330% reflection is observed from the gain side (red curve and dots in **d**), and total transmissions ($|t| = 1$) have been observed on both sides, resulting in unidirectional transparency from the loss side.

An invisible acoustic sensor based on parity-time symmetry

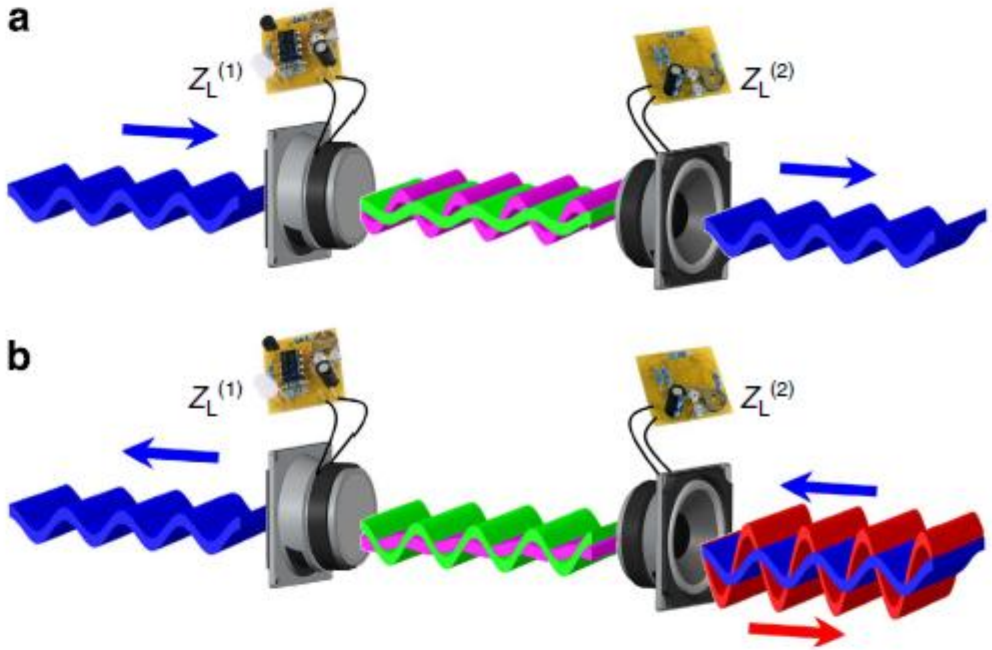

Figure 1 | A parity-time invisible acoustic sensor. A PT-symmetric acoustic system is realized by using a pair of electromechanical resonators(here loudspeakers) loaded with properly tailored electrical circuits. The left loudspeaker is operated as a sensor by loading it with an absorptive circuit, while the other forms an acoustic gain element. Their combination is a compact PT-symmetric unit cell that is transparent from the left (a), while it can at the same time extract the impinging signal. On the contrary, the system is highly reflective when excited from the right (b).

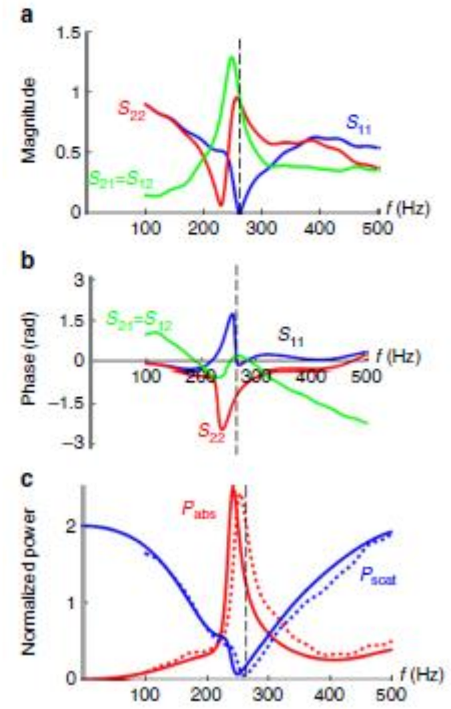

Experimental results. (a,b) Measured scattering parameters, magnitude (a) and (b) phase. The device is unidirectionally transparent at the design frequency (dashed vertical line in all panels). (c) Absorbed power at the passive loudspeaker, and total scattered power by the device, normalized by the incident power at port 1, theory (solid lines) and experiment (dashed lines).

R. Fleury, D.L. Sounas, and A. Alu, Nat. Commun. 6, 6905 (2015)

Acoustic topological insulator and robust one-way sound transport

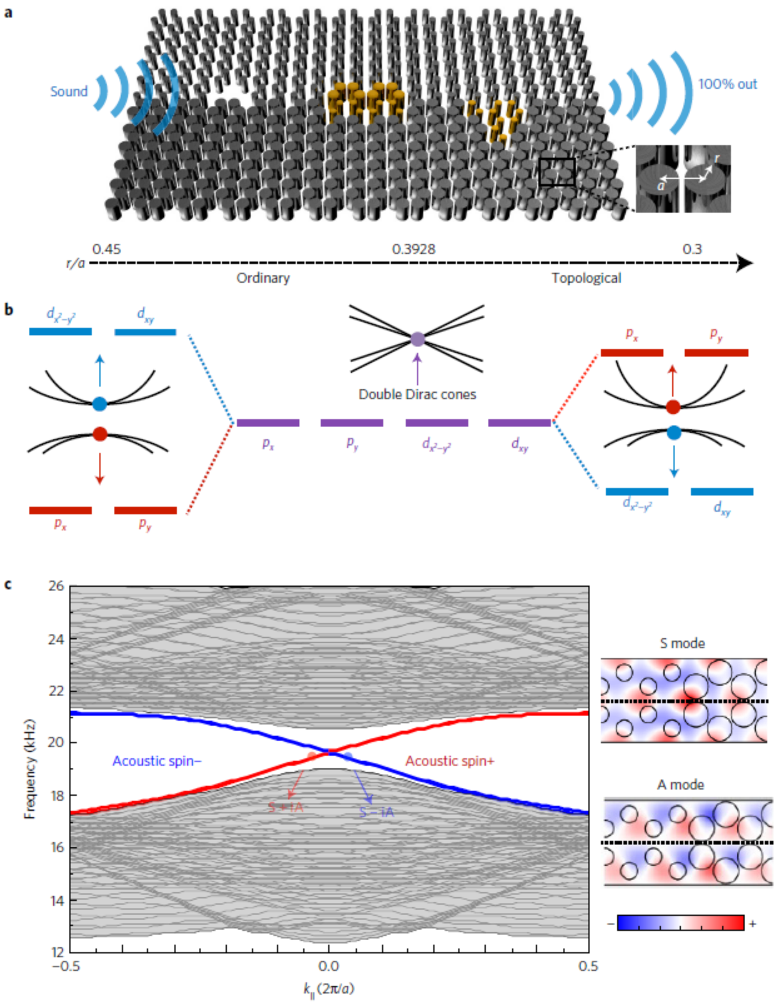

Acoustic insulator and band inversion mechanism

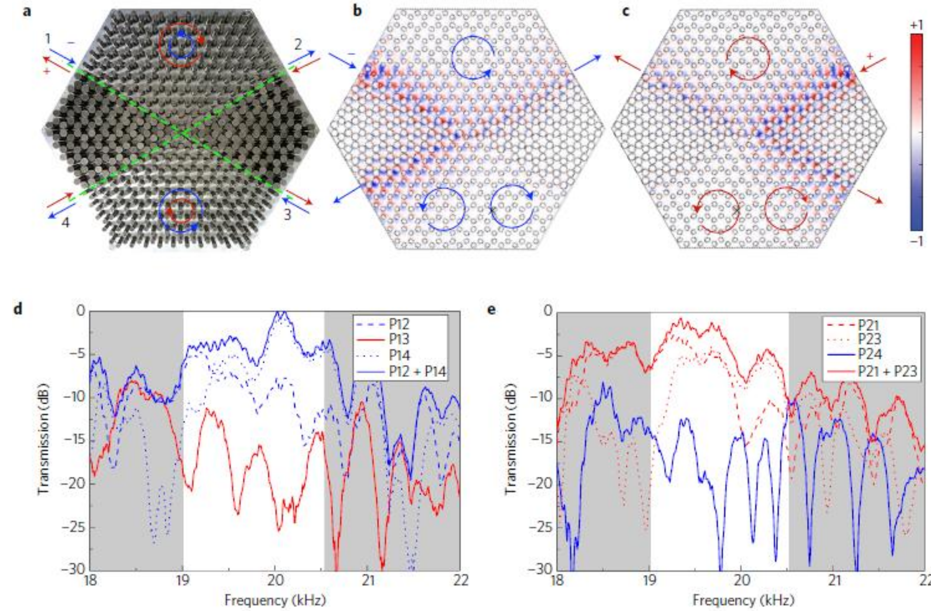

Acoustic one-way transport

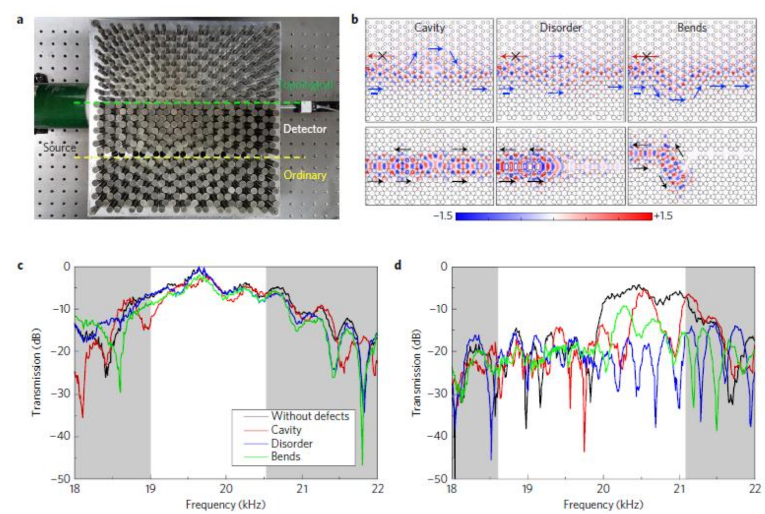

Robust one-way sound transport

C. He, X. Ni, H.Ge , X.Chen Sun, Y. Chen, M. Lu,
X. Liu and Y. Chen, Nat. Phys. 3867, 1124 (2016)

Topological phases and nonreciprocal propagation

Topological Creation of Acoustic Pseudospin Multipoles in a Flow-Free Symmetry-Broken Metamaterial Lattice

Z. Zhang, Q Wei, Y. Cheng, T. Zhang, D. Wu and X. Liu

Phys. Rev. Lett. 118,084303 (2017)

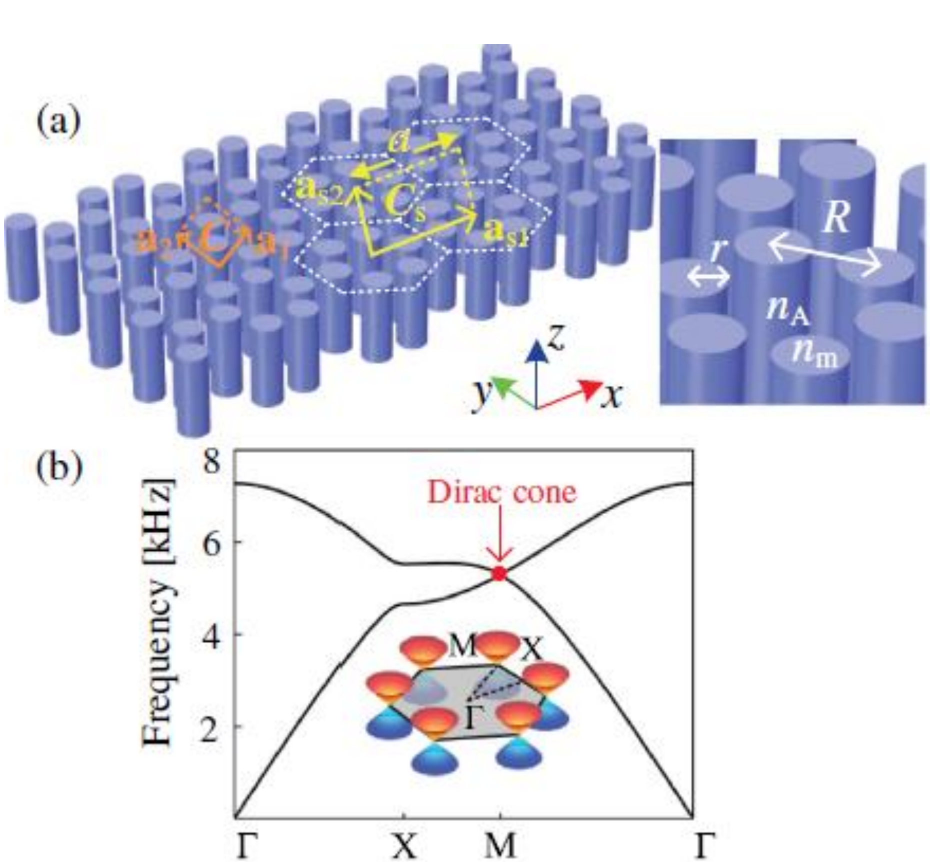

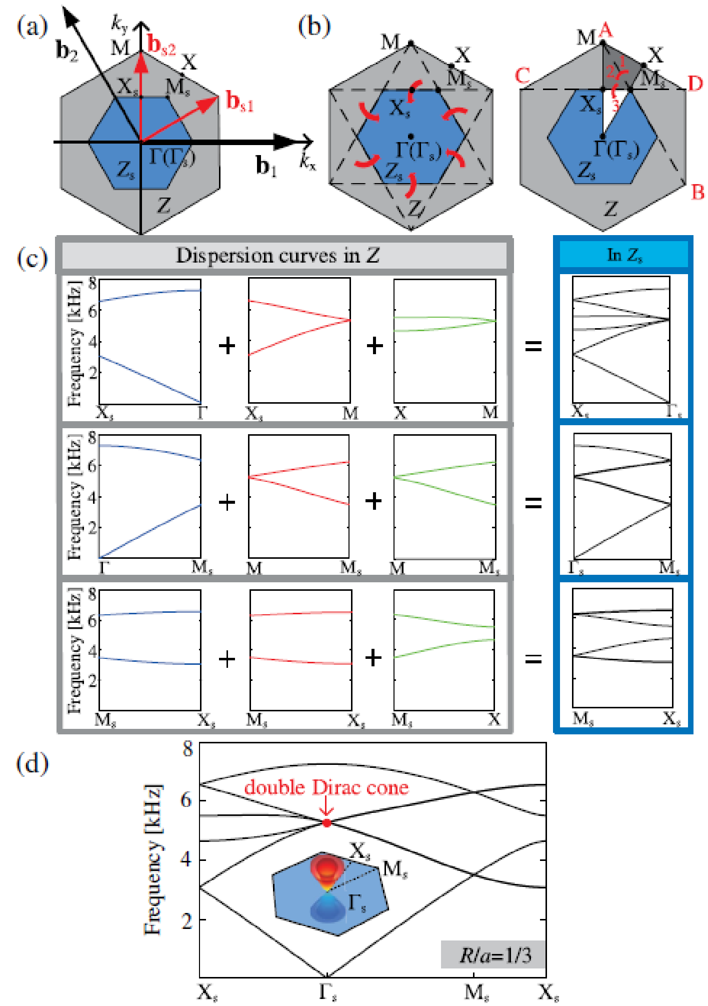

Topological phases and nonreciprocal propagation

Topological Creation of Acoustic Pseudospin Multipoles in a Flow-Free Symmetry-Broken Metamaterial Lattice

Z. Zhang, Q Wei, Y. Cheng, T. Zhang, D. Wu and X. Liu

Phys. Rev. Lett. 118,084303 (2017)

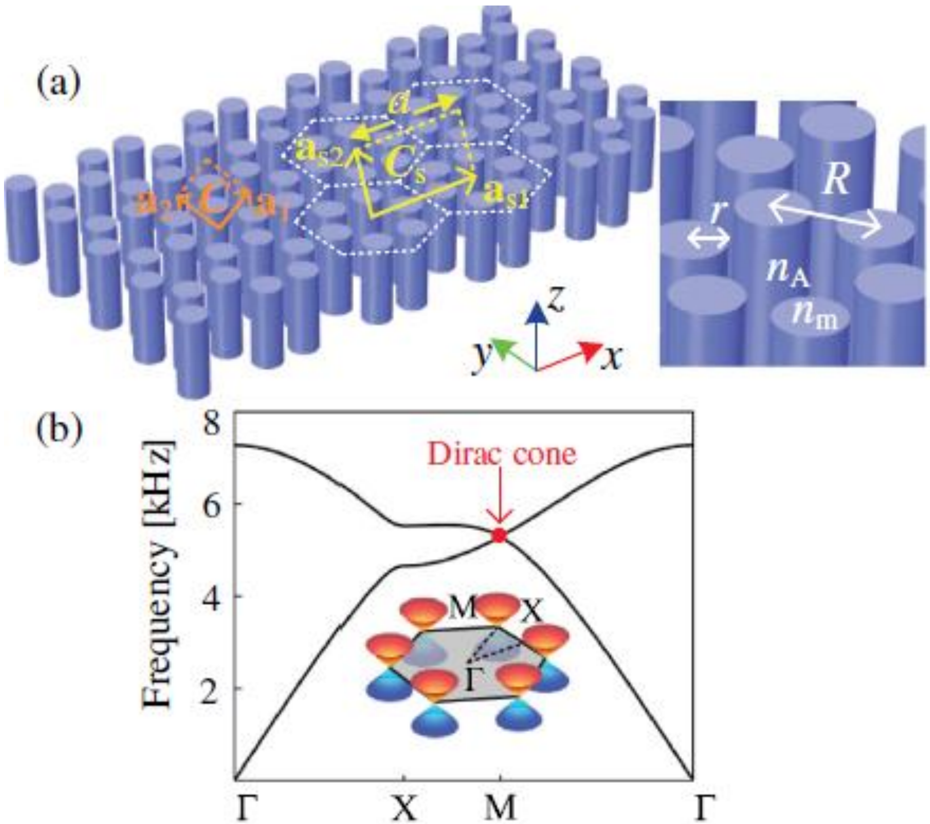

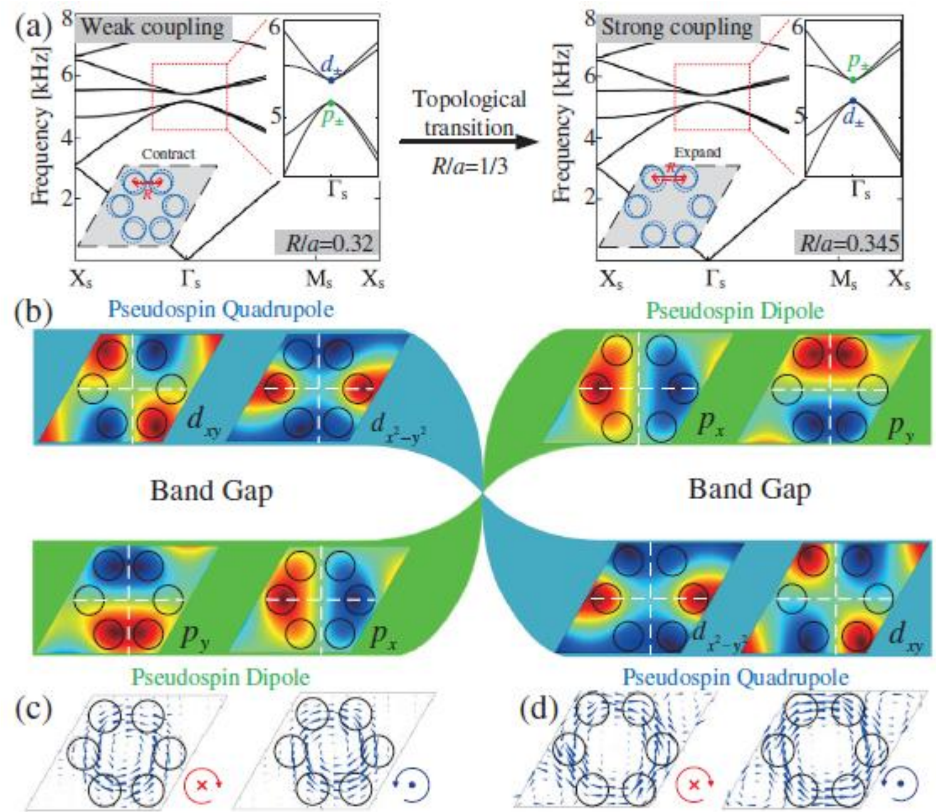

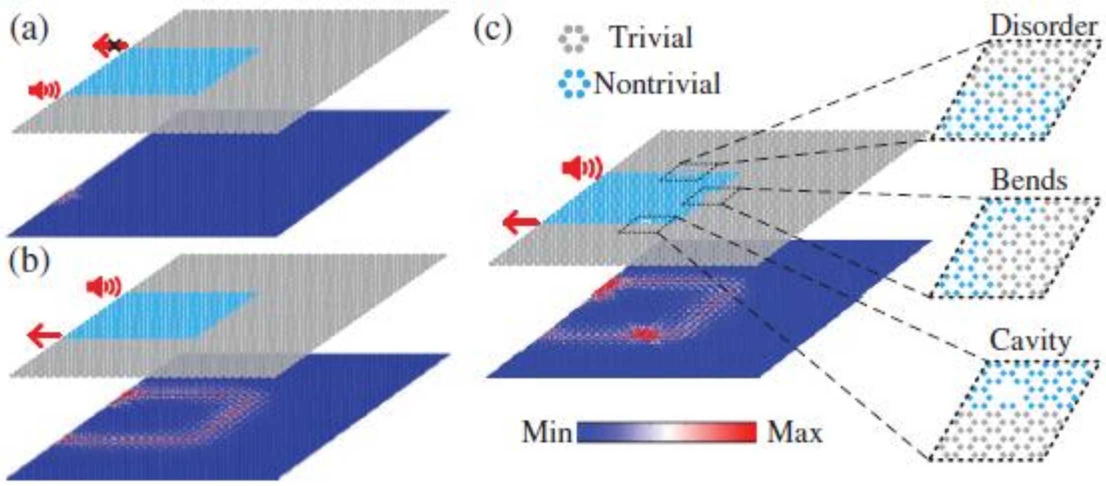

Topologically protected one-way edge waveguide for airborne sound and the robustness against defects.

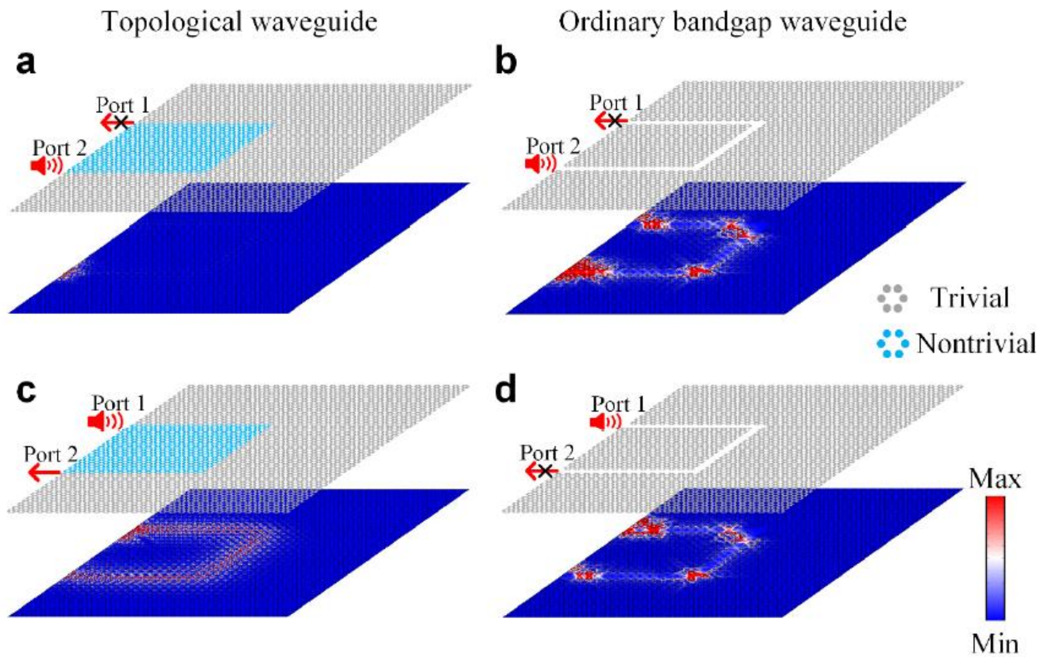

Comparison between topological waveguide and ordinary waveguide

Topological phases and nonreciprocal propagation

Topologically protected elastic waves in phononic metamaterials

S. Hossein Mousavi, Alexander B. Khanikaev & Zheng Wang

Nature Communications 6, 8682 (2015)

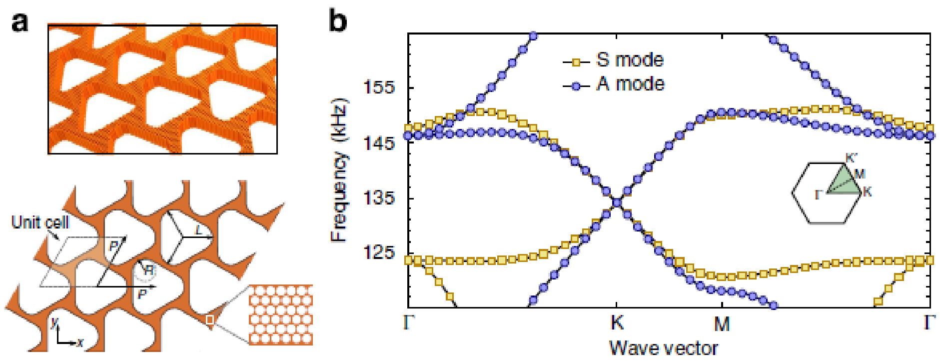

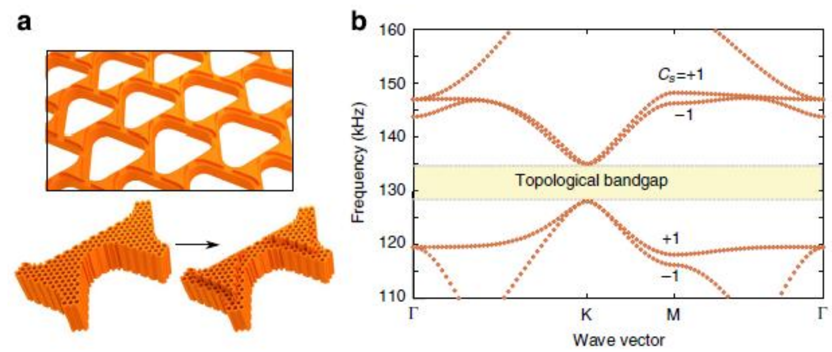

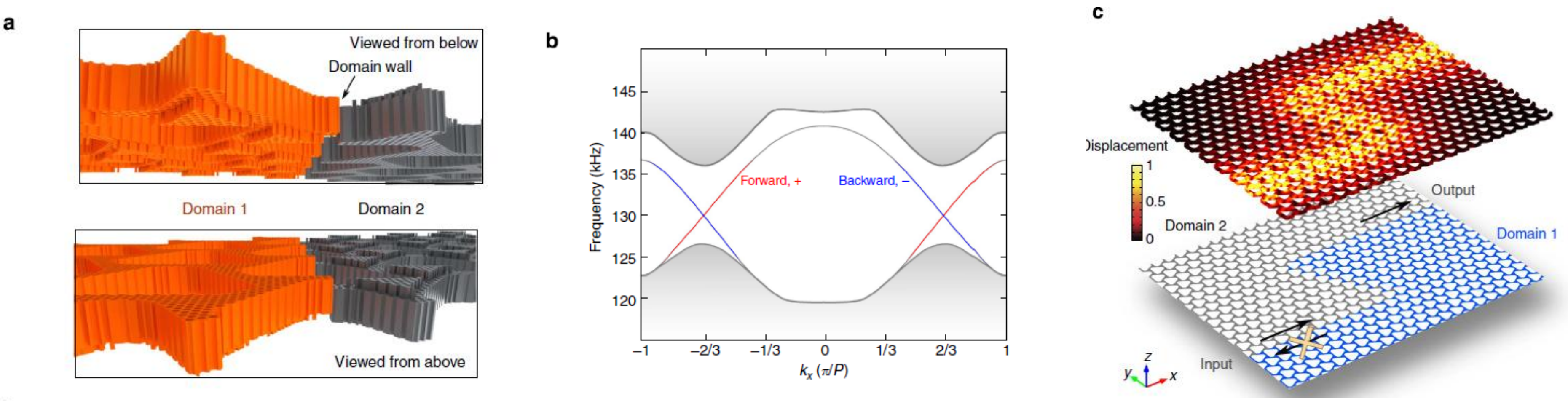

Topological phases and nonreciprocal propagation

Topologically protected elastic waves in phononic metamaterials
S. Hossein Mousavi, Alexander B. Khanikaev & Zheng Wang
Nature Communications 6, 8682 (2015)

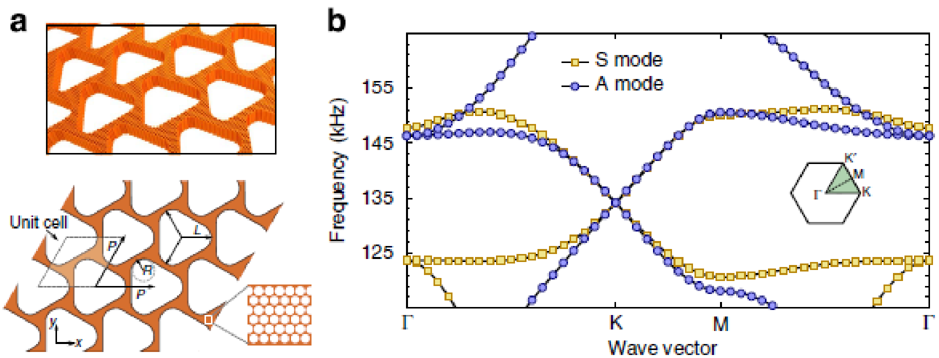

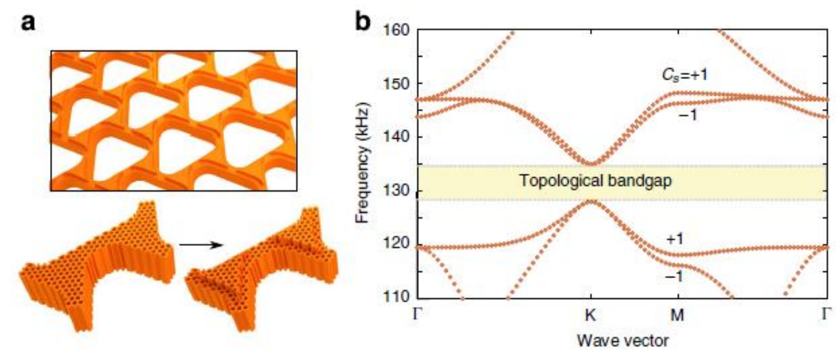

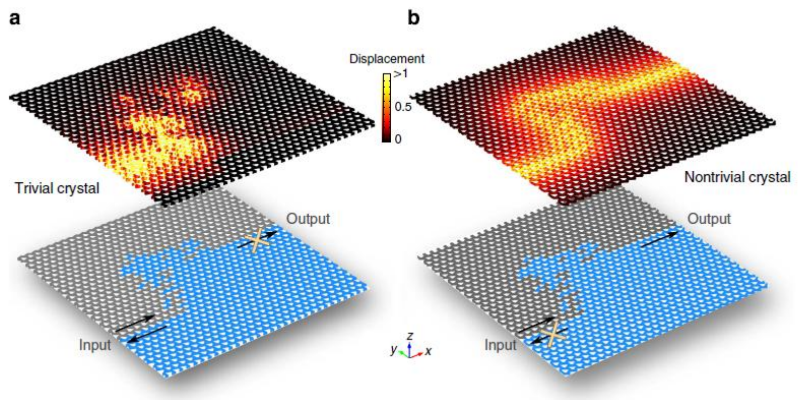

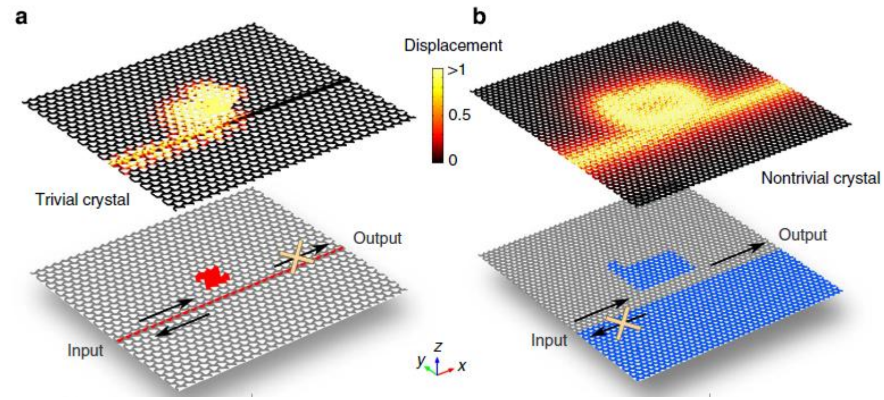

Outline

5. Brief overview of refractive properties

- Negative refraction and focusing
- Self-collimation and beam splitting

6. Subwavelength structures and applications of metamaterials

- Effective properties (positive and negative dynamic parameters)
- Focusing and imaging. Superlens and heperlens
- Cloaking
- GRIN devices
- Metasurfaces. Resonating units and space coiling. Absorption. Phase manipulation

7. Active materials and some emerging topics

Non reciprocal behaviors . Time-space periodicity. PT symmetry. Topological phononics.

8. Dual phononic-photonic crystals (phoXonic) and Optomechanics

- Simultaneous phononic-photonic band gaps.
- Waveguide modes. Slow and fast modes
- Enhanced phonon-photon interaction in a cavity. Comparison of photoelastic and optomechanic effects
- Phononic and Phoxonic sensors

Dual phononic-photonic band gaps

Si rods in air or holes in a Si matrix

PhoXonic crystals

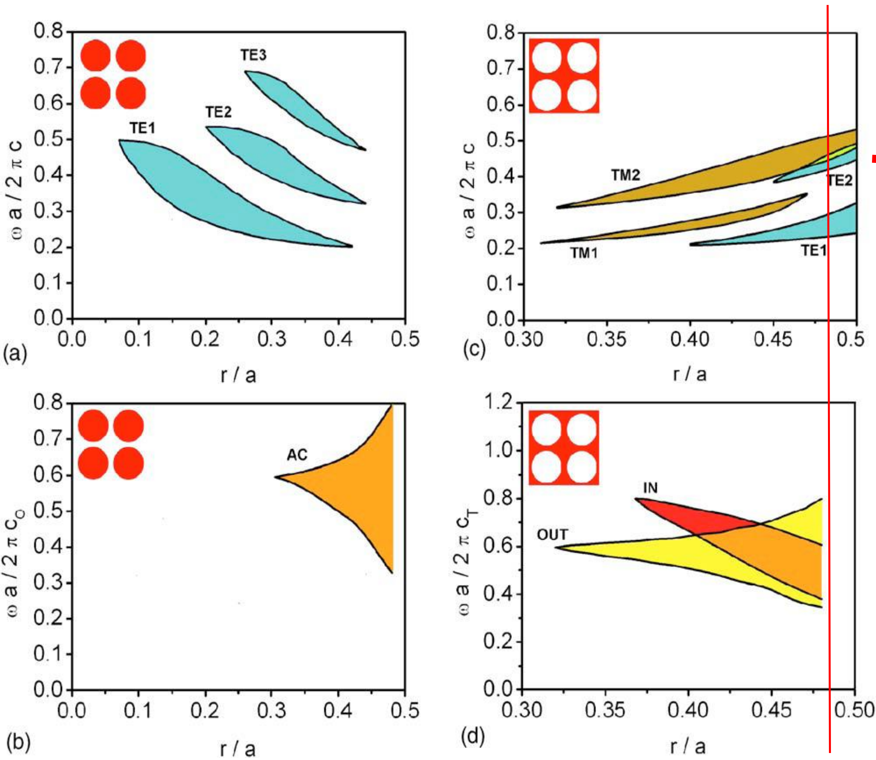

M. Maldovan and E.L. Thomas, Appl. Phys. Lett. 88, 251907 (2006)

Photonic band structure for TM modes

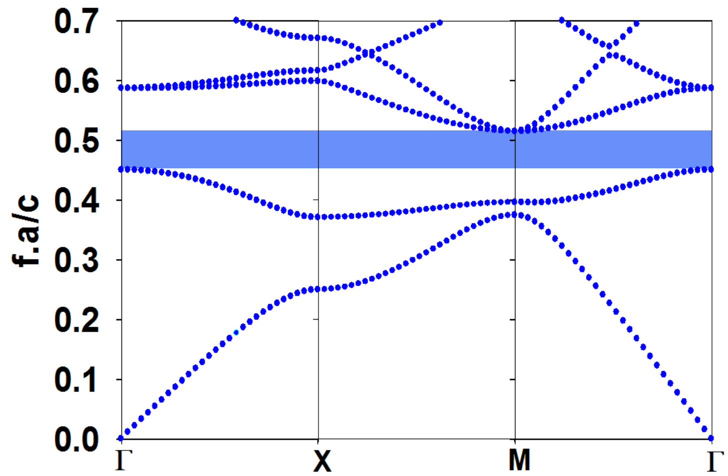

r/a=0.48

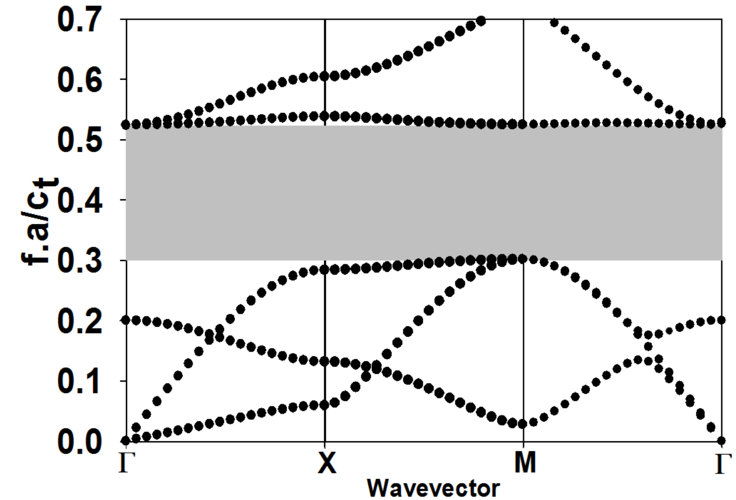

Phononic band structure for in-plane modes

a=700 nm

Photonic band gap:

f=2 10^{14} Hz λ=430nm in Si or **λ=1500nm** in vacuum

Phononic band gap:

f=3.5 GHz or λ=2400nm in Si

PhoXonic crystals

Localised photonic TM modes inside band gap

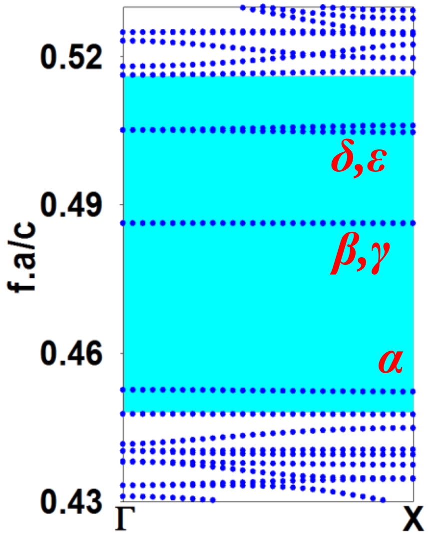

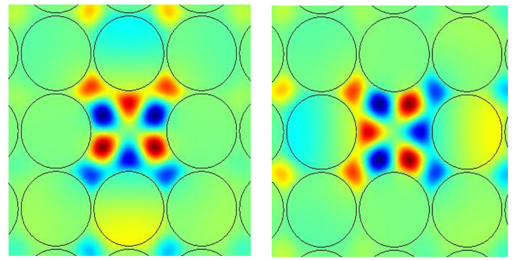

Optical modes β and γ

Photonic band structure for TM modes

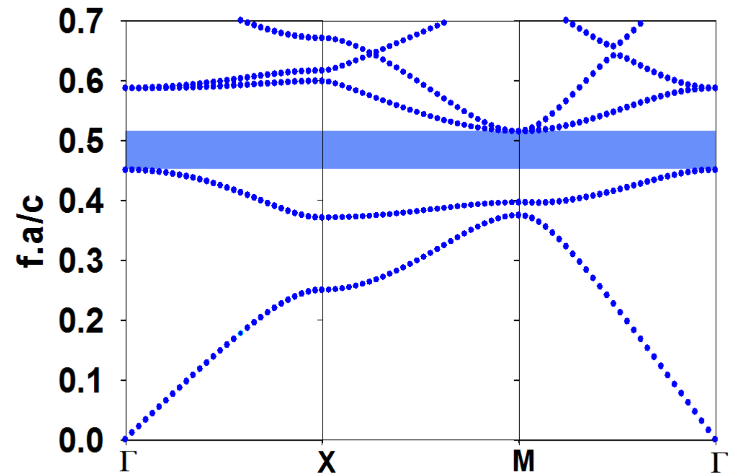

r/a=0.48

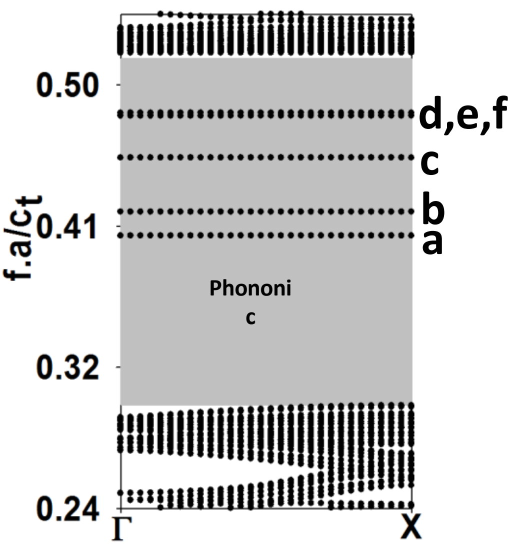

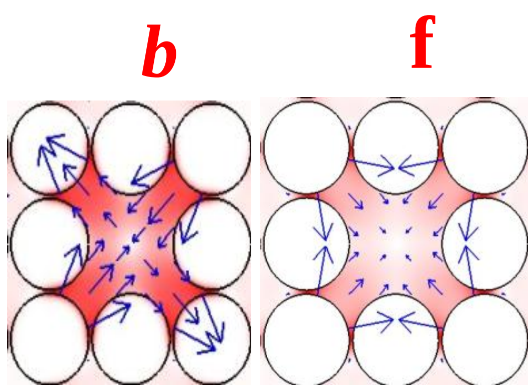

Acoustic modes b and f

Localised phononic modes inside band gap

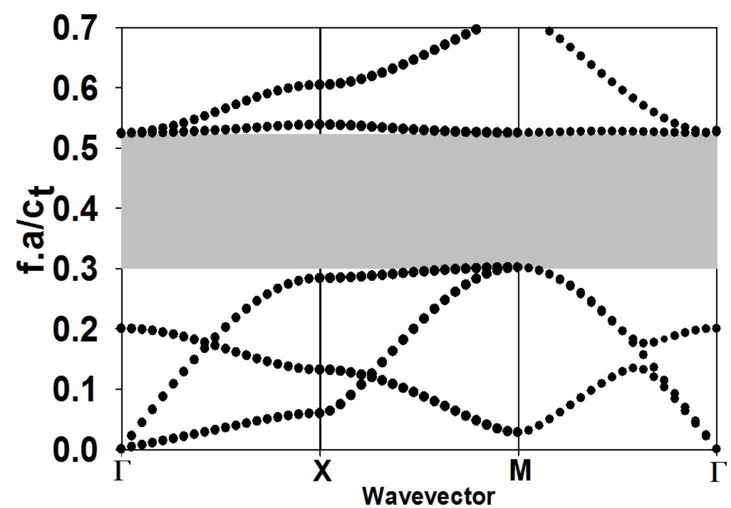

Phononic band structure for in-plane modes

Optomechanic interaction in:

- **Q. Rolland, et al, Appl. Phys. Lett. 101, 061109 (2012)**
- **S. El-Jallal et al, J.Phys.: Condensed Matter (2013, under press)**

(a)

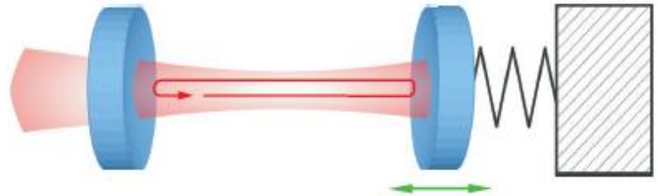

(b)

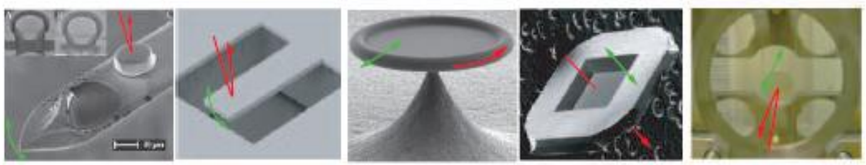

$\mathcal{F}$	200	30,000	22,000	15,000	4,000
$\Omega_m/2\pi$	12.5 kHz	814 kHz	57.8 MHz	134 kHz	12.7 Hz
Q_m	18,400	10,000	2,900	$1.1\cdot10^6$	19,950
m_{eff}	24 ng	190 µg	15 ng	40 ng	~1 g
Ref.	[34]	[26,27]	[22,28]	[30]	[29]

T.J. Kippenberg, K.J. Vahala, Opt. Exp. 15, 17172 (2007)

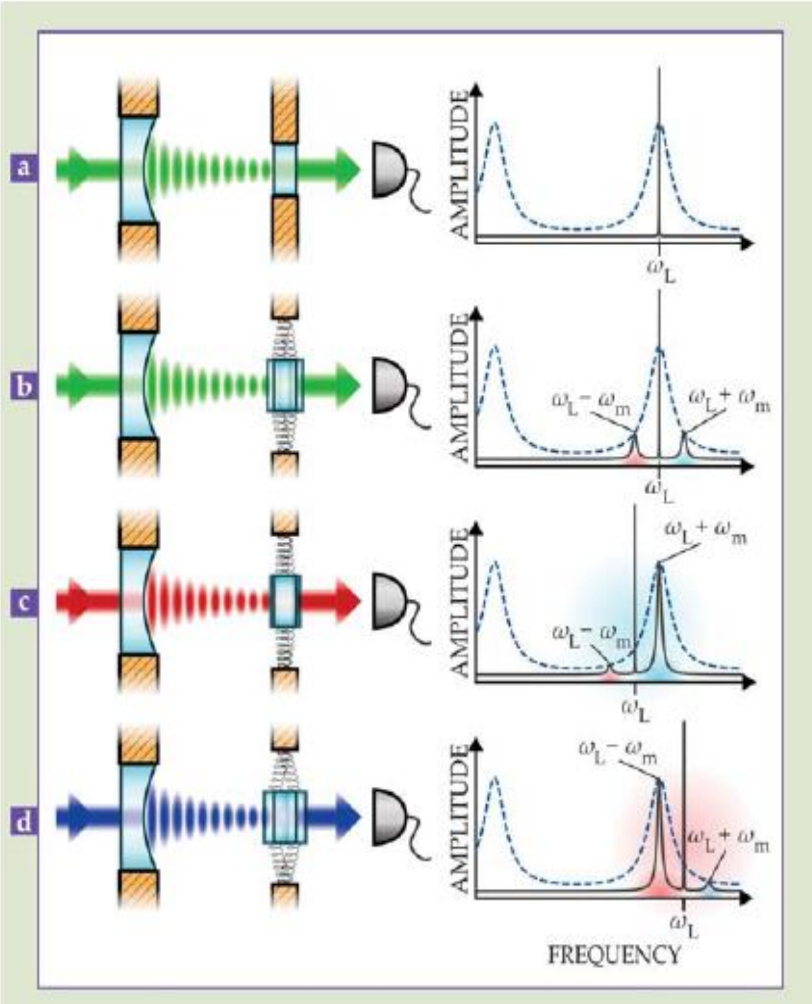

M. Aspelmeyer, P. Meystre, K. Schwab,
Physics Today 65, 29 (2012)

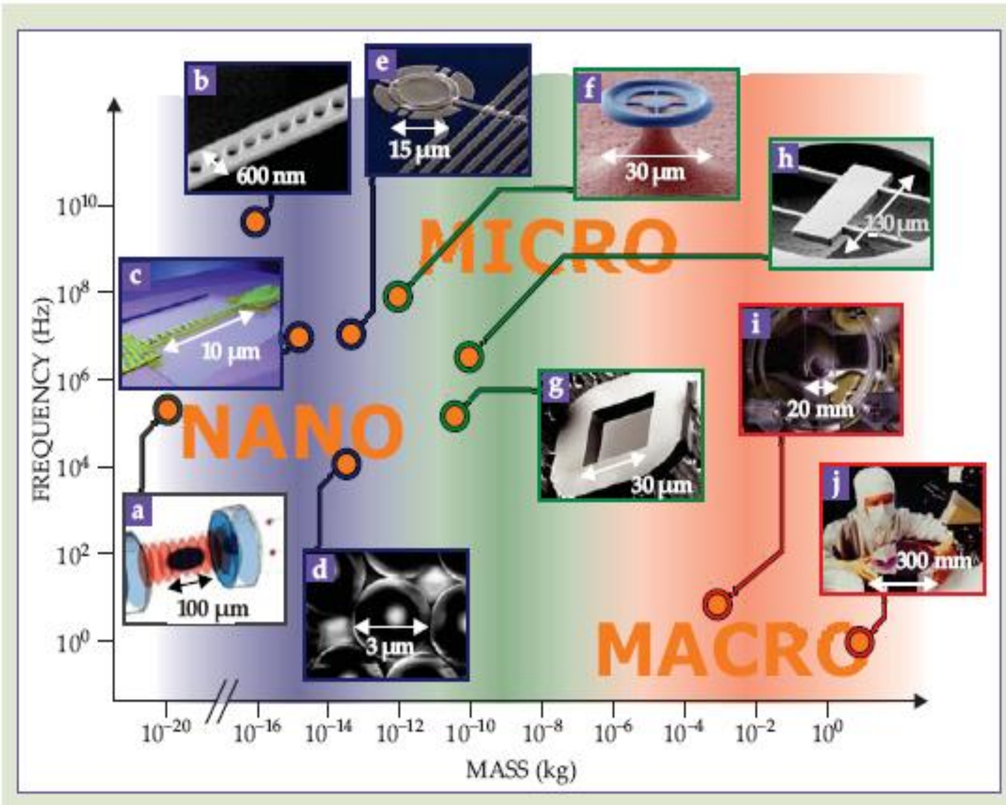

Cavity optomechanical devices ranging from nanometer sized structure (10^{-20} kg) to micromechanical structures (10^{-11} kg) to centimeter sized structures (kg)

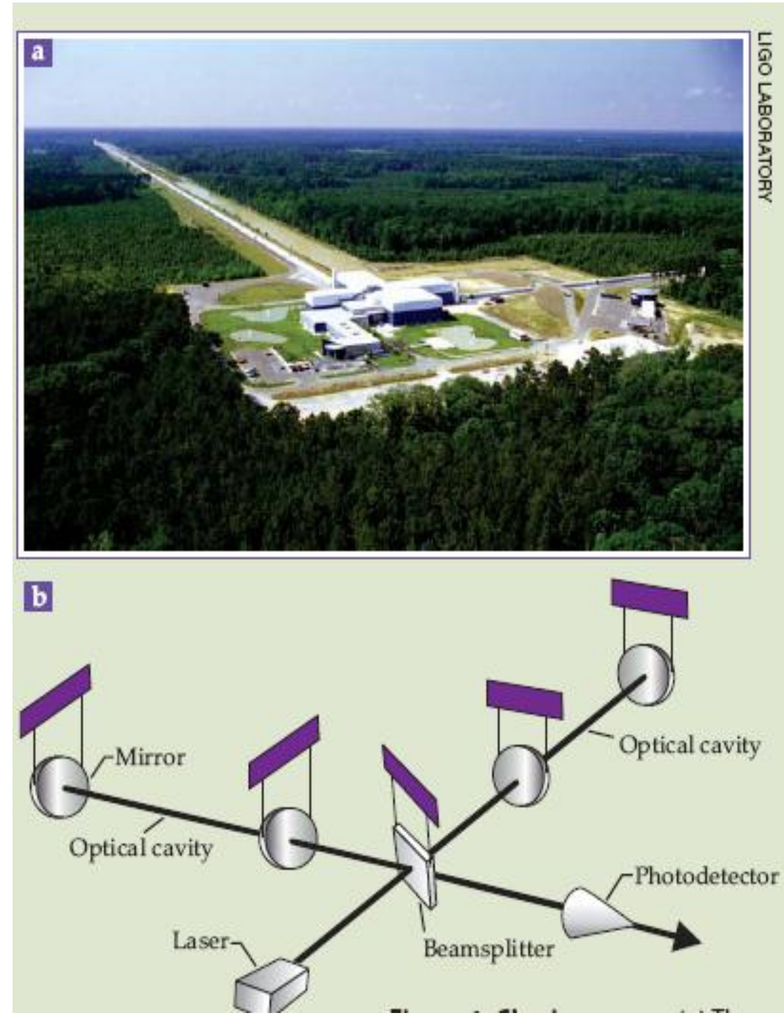

LIGO

(Laser Interferometer Gravitational-Wave Observatory)

M. Aspelmeyer, P. Meystre, K. Schwab, Physics Today 65, 29 (2012)

Interaction of optical and mechanical waves for optomechanical coupling

Eichenfield et al., Nature 462, 78 (2009)

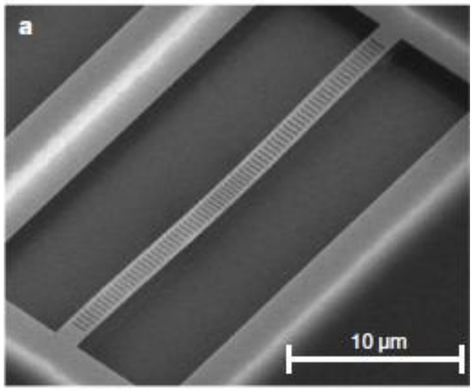

Silicon nanobeam with rectangular holes

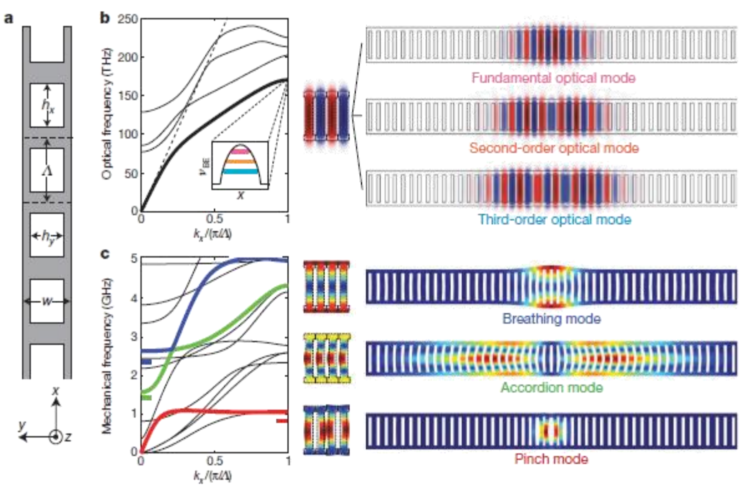

Suspended membrane

Gavertin et al., PRL 106, 203902, 2011

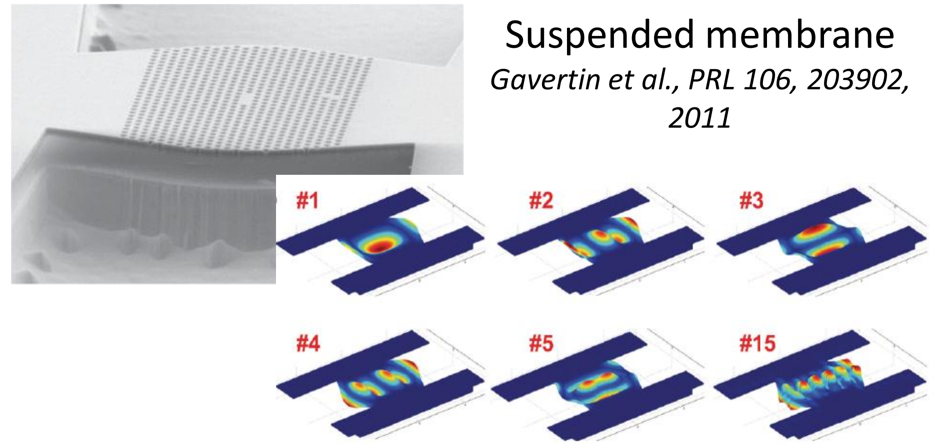

D. A. Fuhrmann, et al., Nature Photonics 5, 605 (2011)

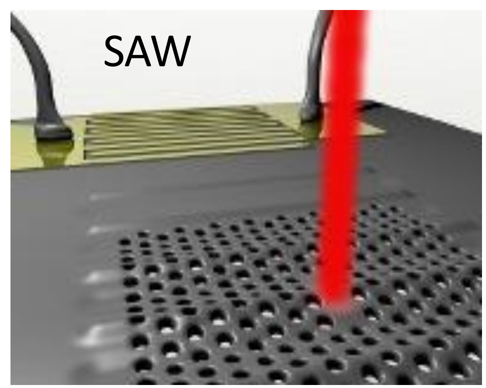

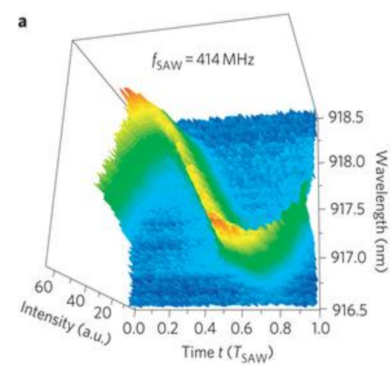

Optomechanical crystal design

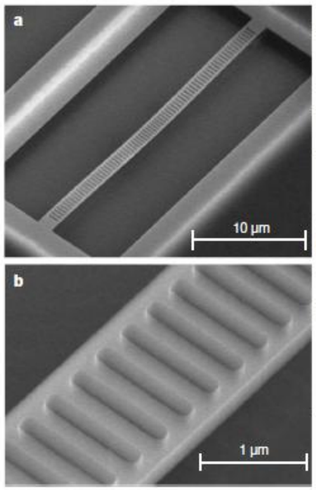

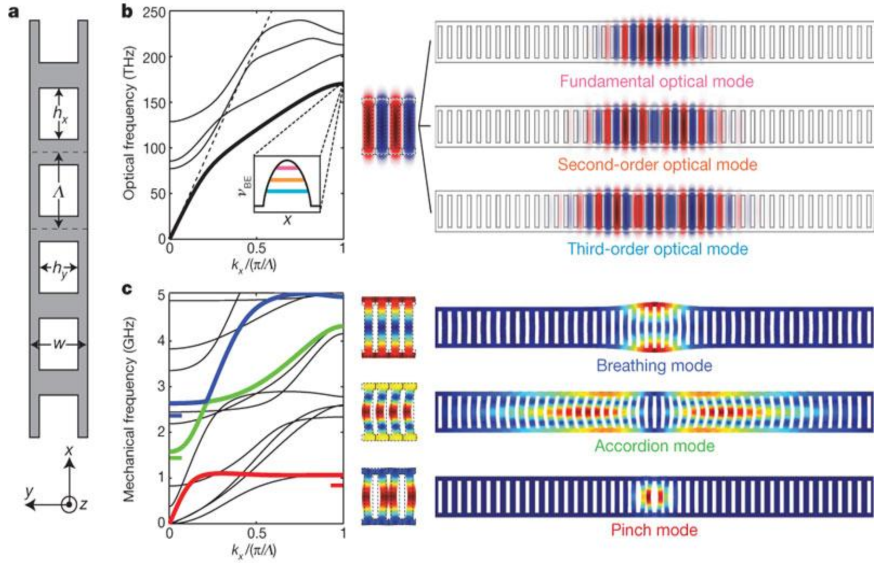

← Optical modes

← Vibrational modes

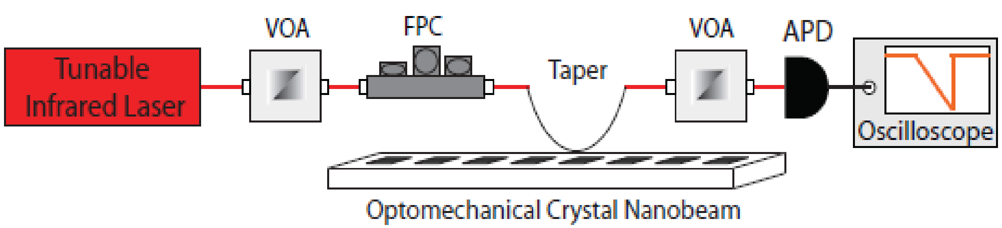

FIG. 4: Experimental setup used to measure optical, mechanical, and optomechanical properties of silicon optomechanical crystal nanobeam.

M. Eichenfield, J. Chan, R.M. Camacho, K.J. Vahala and O. Painter, Nature 462, 78 (2009)

Optomechanical crystal design

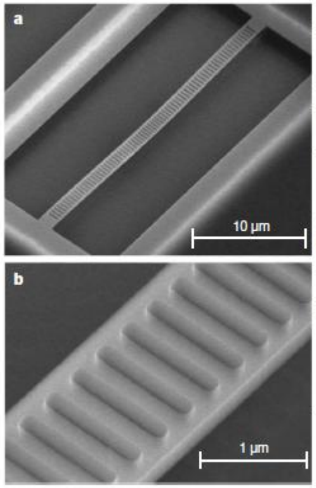

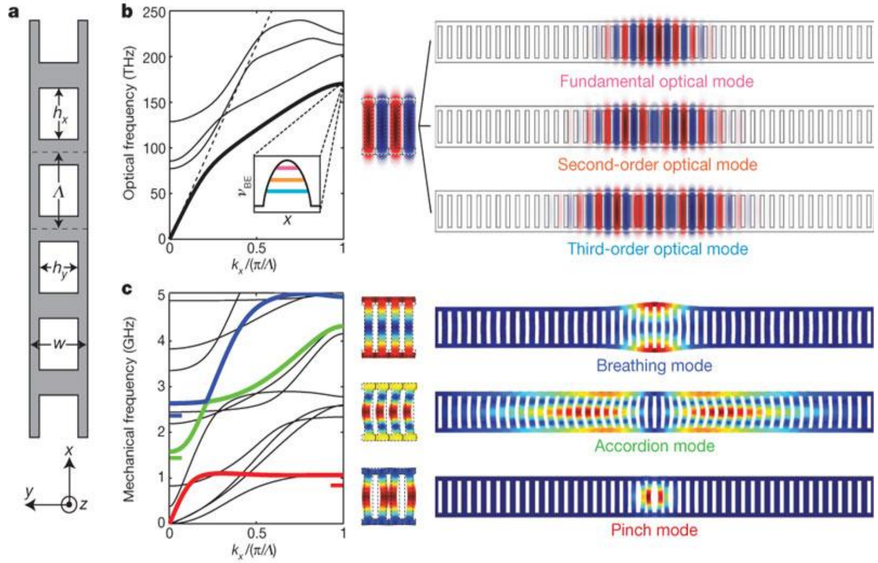

← Optical modes

← Vibrational modes

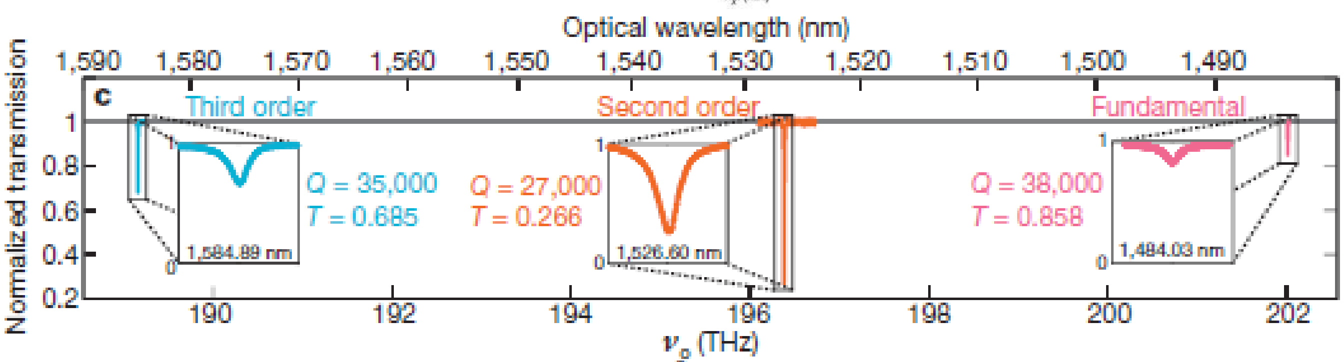

← Optical spectroscopy with the taper waveguide in contact

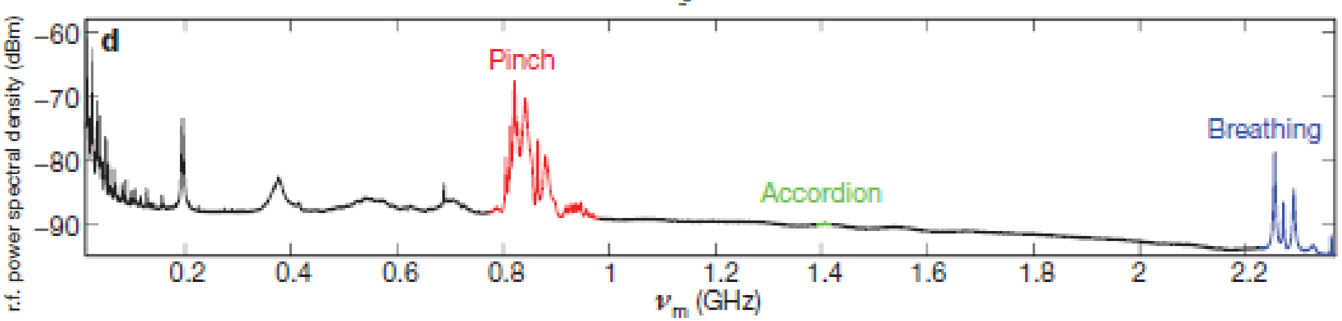

← Mechanical spectroscopy

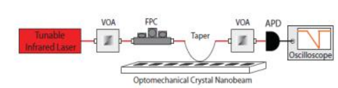

FIG. 4: Experimental setup used to measure optical, mechanical, and optomechanical properties of silicon optomechanical crystal nanobeam.

M. Eichenfield, J. Chan, R.M. Camacho, K.J. Wahala and O. Painter, Nature 462, 78 (2009)

Coupling in a Photonic crystal defect cavity

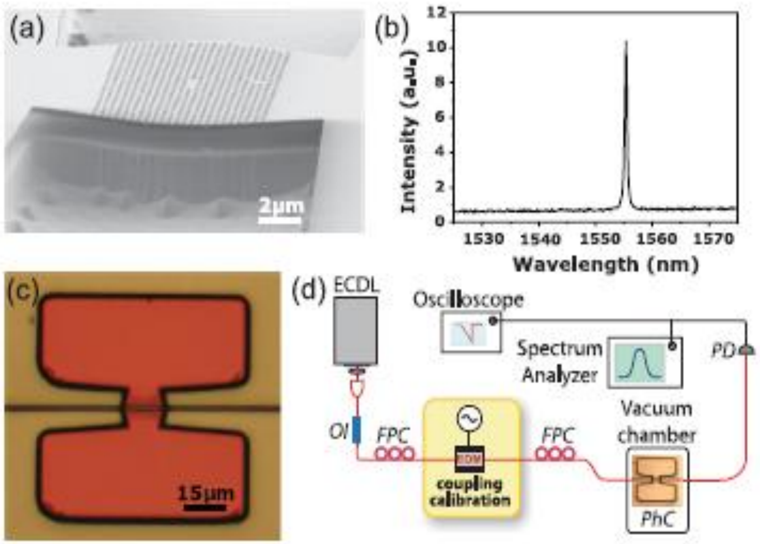

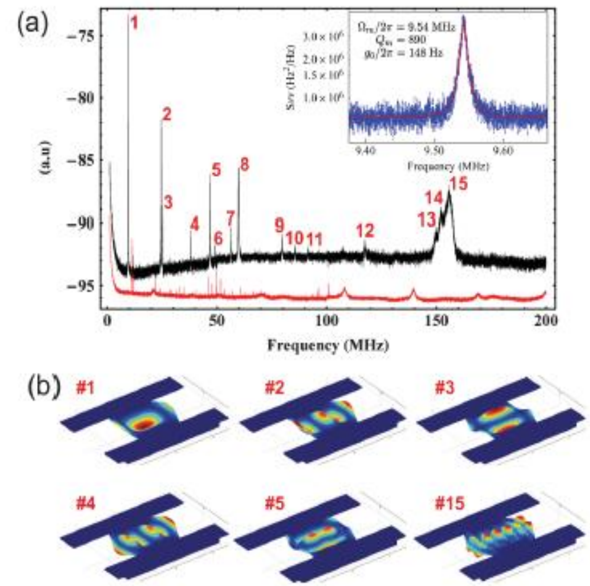

Frequency noise spectrum corresponding to different mechanical modes of the structure

- Upper figure: 1MHz-200 MHz
- Lower figure: 200MHz-1.2 GHz

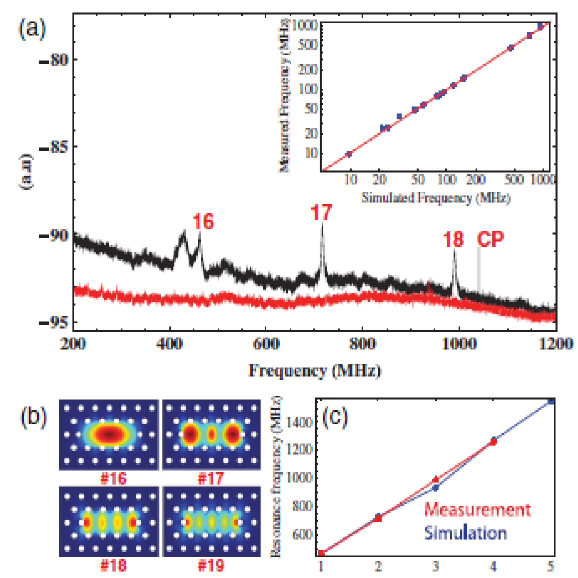

E. Gavartin, R. Braive, I. Sagnes, O. Arcizet, A. Beveratos, T.J. Kippenberg and I. Robert-Philip, Phys. Rev. Lett. 106, 203902 (2011)

Background

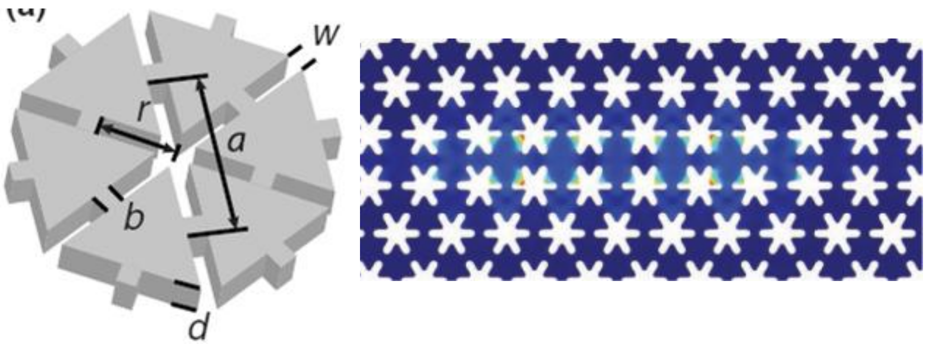

Amir H. Safavi-Naeini et al, PRL 112, 153603 (2014)

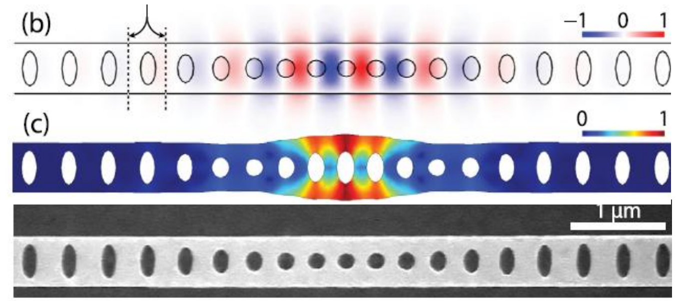

Chan et al, Appl. Phys. Lett. 101, 081115 (2012)

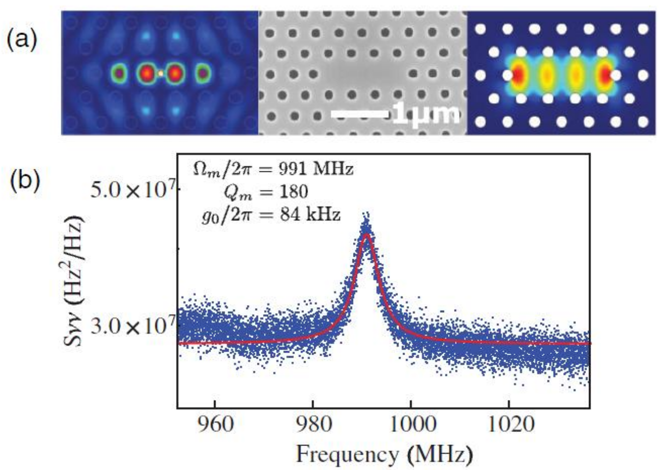

E. Gavartin et al, PRL 106, 203902 (2011)

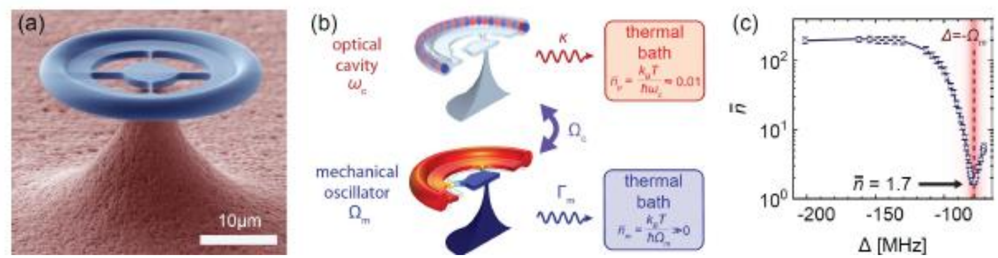

Ewold Verhagen et al, Proceeding IEEE 2014

Investigated phoXonic structures

PhoXonic crystal slabs

Periodic holes

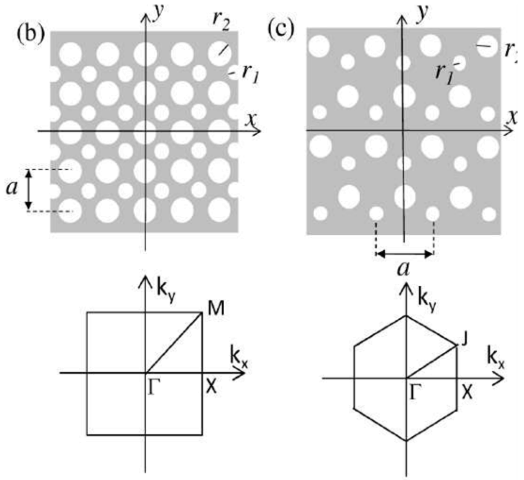

Pennec *et al*. Opt. Exp. **18**, 14301 (2010)
Mohammadi *et al*. Opt. Exp. **18**, 9164 (2010)
S. El-Jallal et al, Phys. Rev. B, 88, 205410 (2013)

Periodic pillars

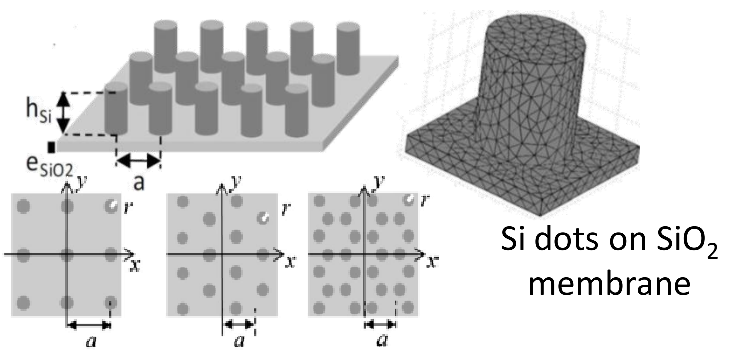

El Hassouani *et al*. Phys. Rev. B, **82**, 155405 (2010)

1D periodic nanowires

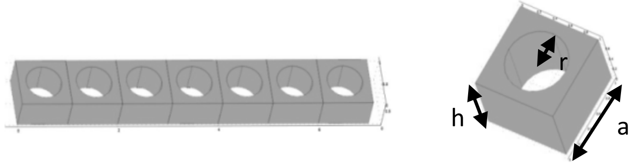

No Phononic band gap

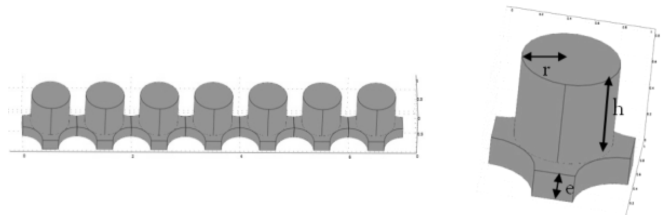

Wide Phononic band gap

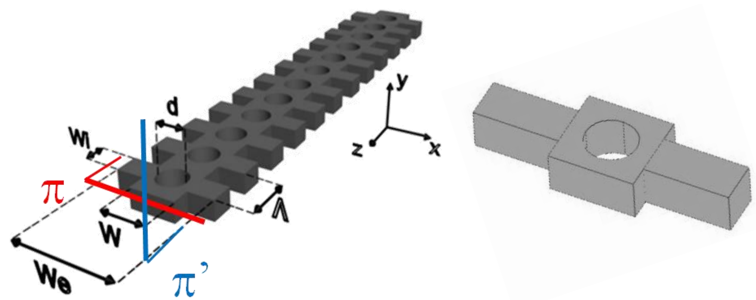

Simultaneous phononic and photonic gaps

Y. Pennec *et al*, AIP Advances 1, 041901 (2011)
M.Oudich et al, Phys. Rev B, 89, 245122 (2014)
J. Gomis et, Nature Communications, 5, 4452 (2014)
B. Djafari Rouhani, CR Physique 17, 555 (2016)

Optomechanic (acousto-optic) interaction

Mechanisms and methods of calculation

Two mechanisms contribute to the AO interaction:

1. **Photo-elastic (PE) effect:** (Pockels effect) the vibrational motion of the cavity induces a change in the dielectric permittivity $\Delta\varepsilon_{ij}$ proportional to the acoustic strain.

$$\Delta\varepsilon_{ij} = -\varepsilon_0 n^4 p_{ijkl} S_{kl}$$

2. Moving Interface (MI) effect: takes into account the dynamic motion of the silicon-vacuum boundaries around the holes.

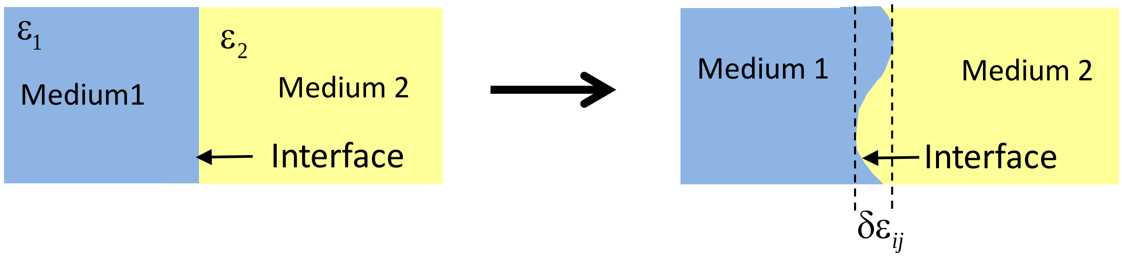

Two methods for the evaluation of optmechanical interaction strength

- Coupling coefficients quantification: the photoelastic (PE) and moving boundary (MB) effects are evaluated using the formulations introduced by Chan *et al* [Appl. Phys Lett. **101**, 081115 (2012)] :

$$g_{PE} = -\frac{\omega}{2} \frac{\left\langle E \left| \frac{\partial \varepsilon}{\partial \alpha} \right| E \right\rangle}{\int_V \mathbf{E}\cdot\mathbf{D}\ \mathrm{dV}} \sqrt{\hbar / 2 M_{\mathrm{eff}} \Omega}$$

Photoelastic coupling coefficient

$$g_{MI} = -\frac{\omega}{2} \frac{\oint_{\partial V} (\mathbf{Q}\cdot\mathbf{n})\left(\Delta\varepsilon \mathbf{E}_{\parallel}^2 - \Delta\varepsilon^{-1}\mathbf{D}_{\perp}^2\right) \mathrm{dS}}{\int_V \mathbf{E}\cdot\mathbf{D}\ \mathrm{dV}} \sqrt{\hbar / 2 M_{\mathrm{eff}} \Omega}$$

Moving interface coupling coefficient

- Modulation of the photon frequency by the phonon: the photonic mode frequency is calculated at several selected instants of an acoustic period under the assumption that the acoustic mode strain profile is being frozen at these instants. [Rolland *et al* . Appl. Phys. Lett **101**, 061109 (2012)]

Modulation of the photonic modes β et γ by the acoustic mode F

Acousto-optic coupling in 2D crystals
Example of a L1 cavity

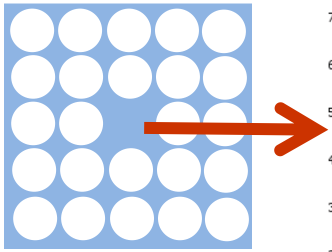

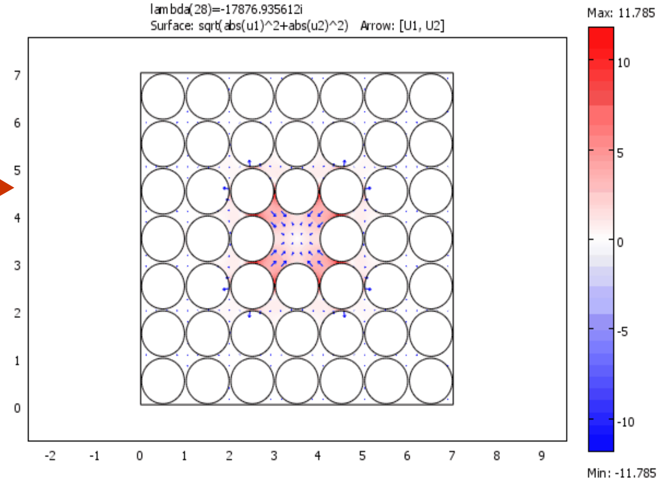

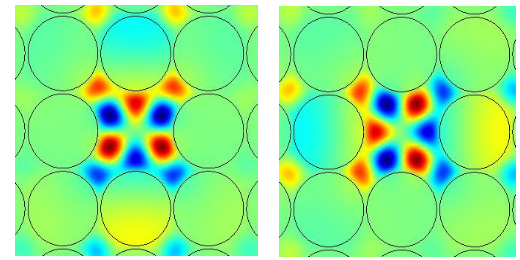

Optical modes β et γ

The degeneracy of the two modes is kept

g_{MI} = **0.71** THz/nm

g_{PE} = **0.58** THz/nm

$g_{MI} + g_{PE}$ = **1.29 THz/nm**

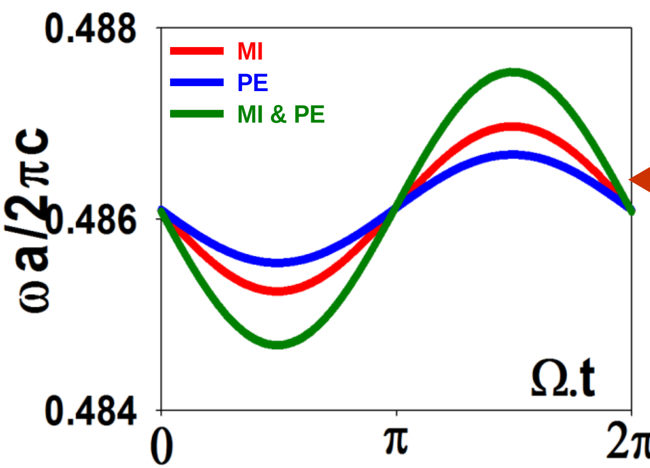

Frequencies of β et γ modes during one acoustic period

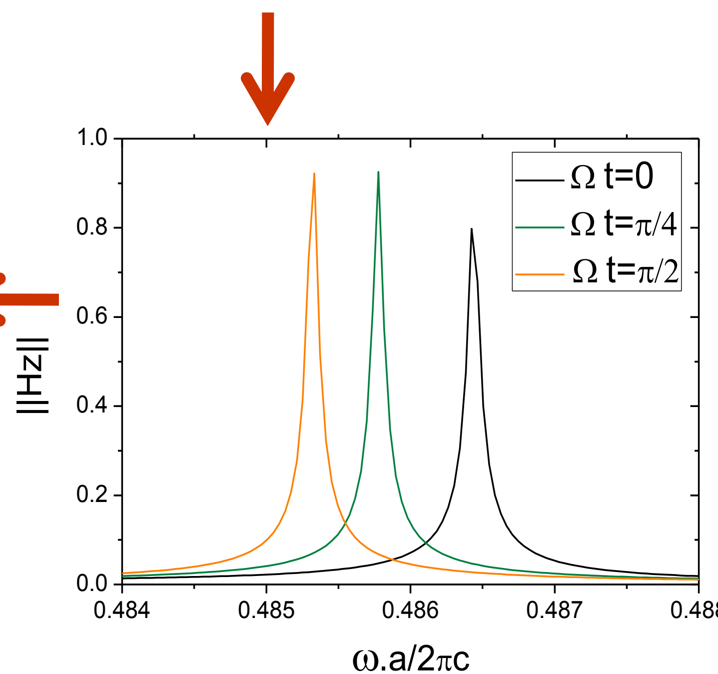

Transmission peaks ofmodes β and γ at different instants of an acoustic period

The MI et PE effects are in phase and add to each other

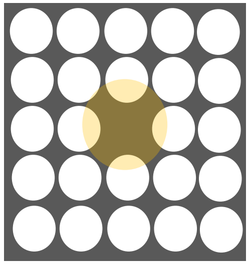

Acousto-optic coupling in 2D crystals
Example of a L1 cavity

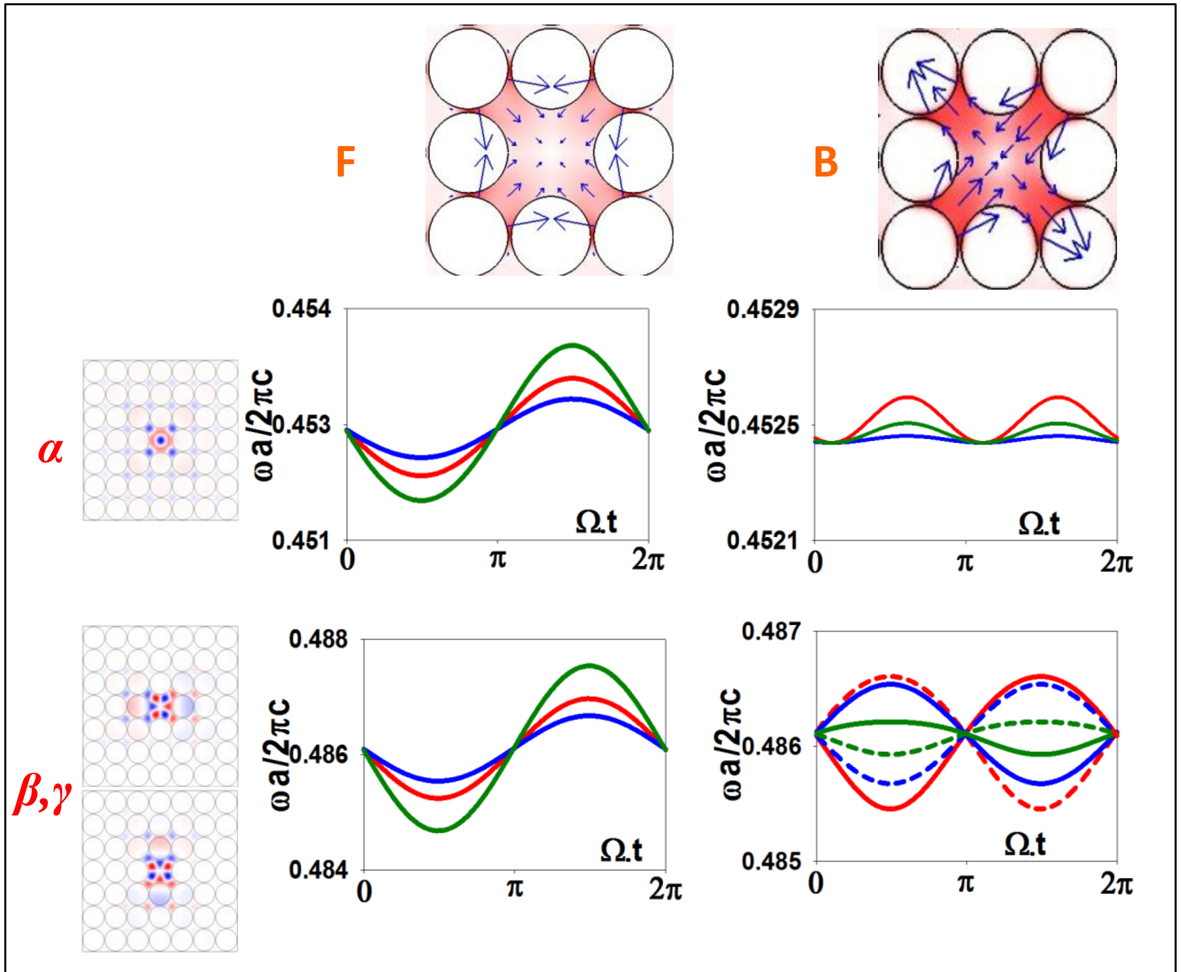

- MI+PE (green)
- Photoelastic effect (PE) (blue)
- Motion of interfaces (MI) (red)

F
- Sinusoidal Oscillation
- MI and PE in phase
- Strong coupling

B
- Double sine function
- MI and PE out of phase
- Weak coupling

$\left(\frac{\Delta\lambda}{\lambda}\right)_{MI}$	$\left(\frac{\Delta\lambda}{\lambda}\right)_{PE}$	$\left(\frac{\Delta\lambda}{\lambda}\right)_{MI+PE}$
0.35%	0.23%	0.58%

$\Delta\lambda$ = 9.1nm @ 1550nm

Q. Rolland *et al* . Appl. Phys. Lett **101**, 061109 (2012)
M. Oudich *et al* . Proceeding of IEEE IUS 2012

Acousto-optic coupling in 2D crystals
Example of a L1 cavity

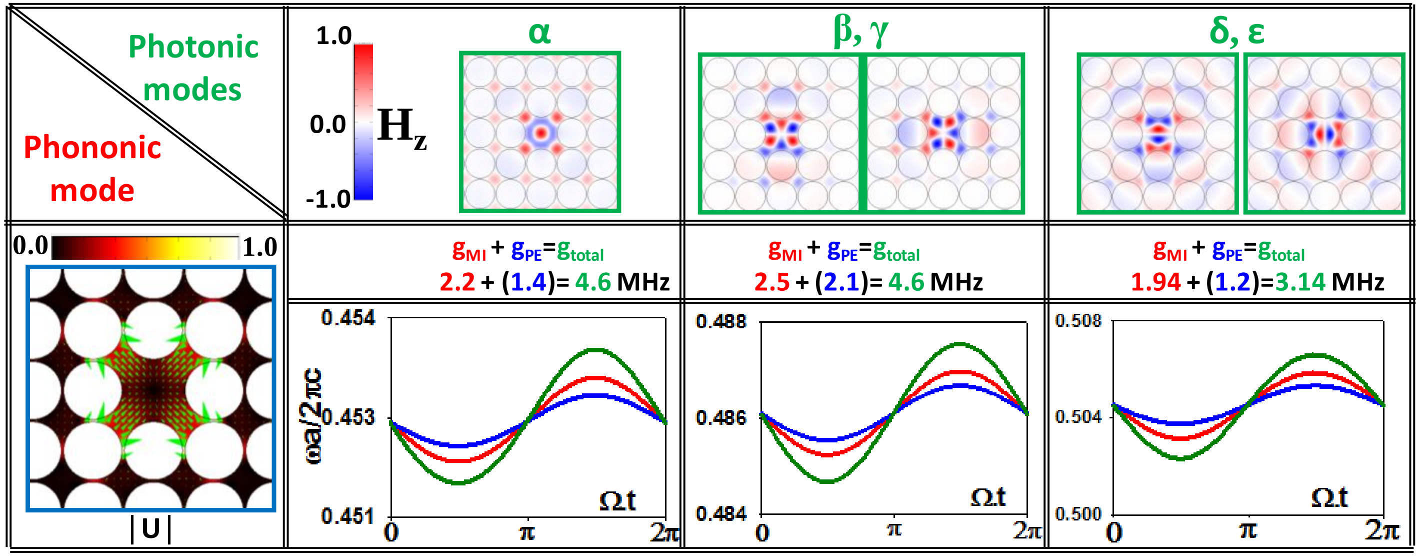

	Si (1150 nm)	GaAs (1150 nm)	GaAs (925 nm)
p_{11}	-0.1	-0.165	-0.273
p_{12}	0.01	-0.14	-0.316
p_{44}	-0.051	-0.072	-0.03

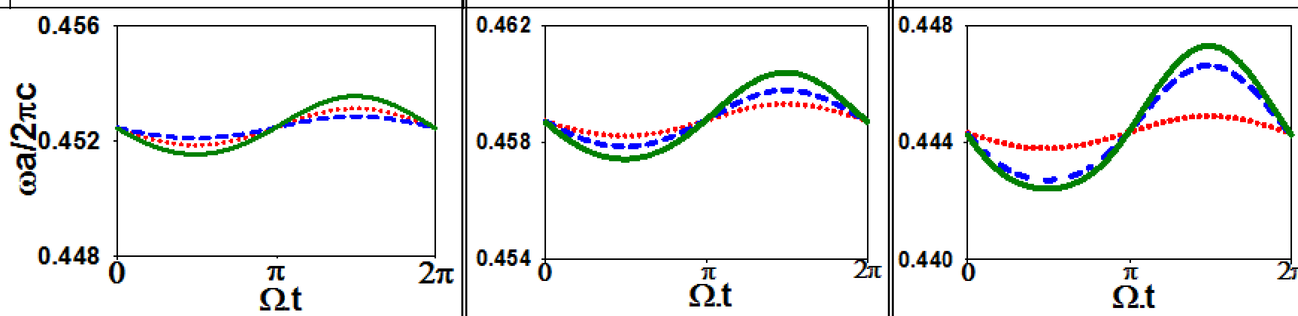

Q. Rolland, Appl. Phys. Lett. 101, 061109 (2012)
B. Djafari Rouhani, CR Physique 17, 555 (2016)

Acousto-optic coupling in crystal slabs. Example of an L3 cavity

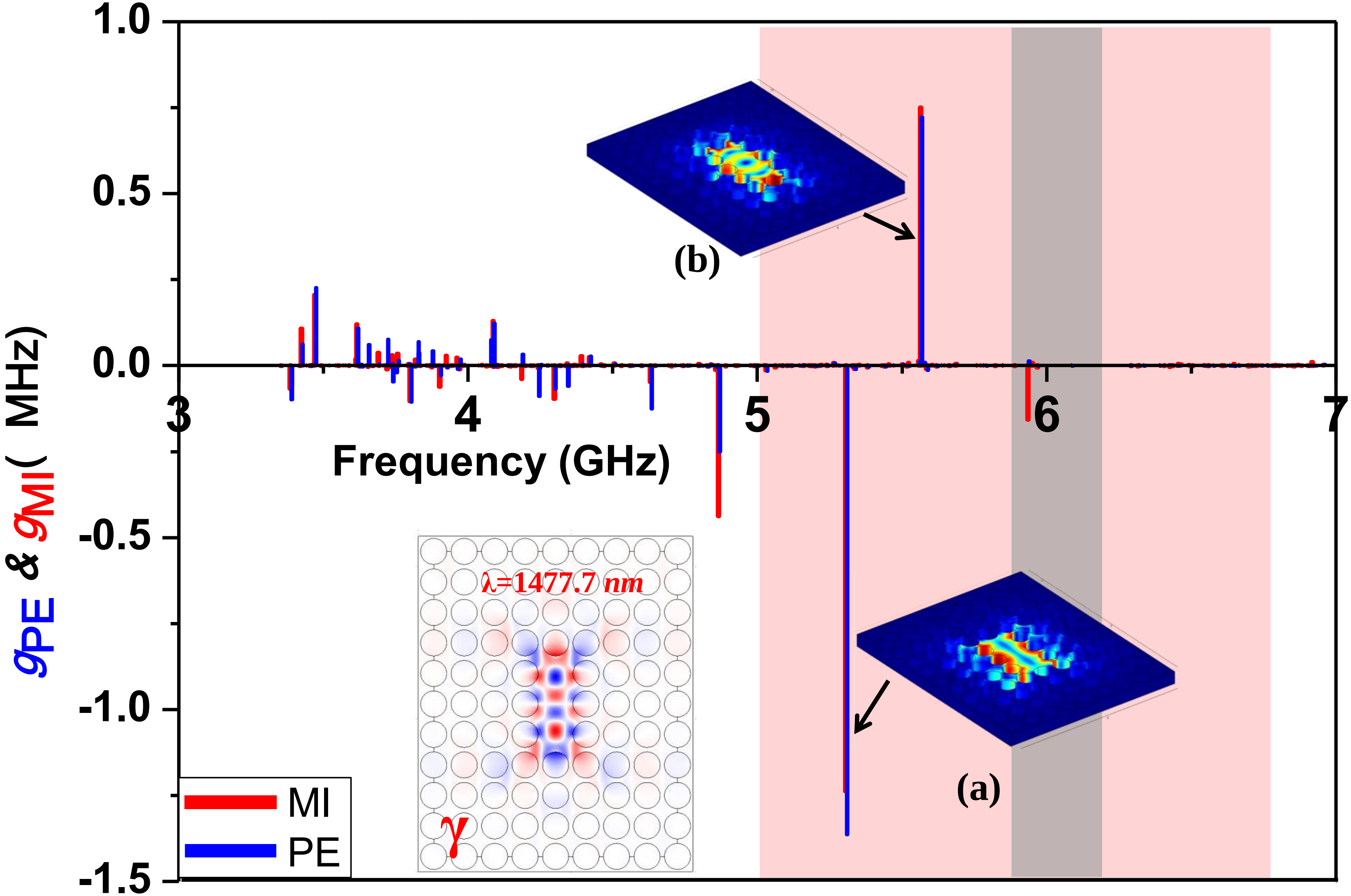

S. El-Jallal et al, Phys. Rev. B 88, 205410 (2013)
B. Djafari Rouhani, CR Physique 17, 555 (2016)

Acousto-optic coupling in crystal slabs. Example of a cross cavity

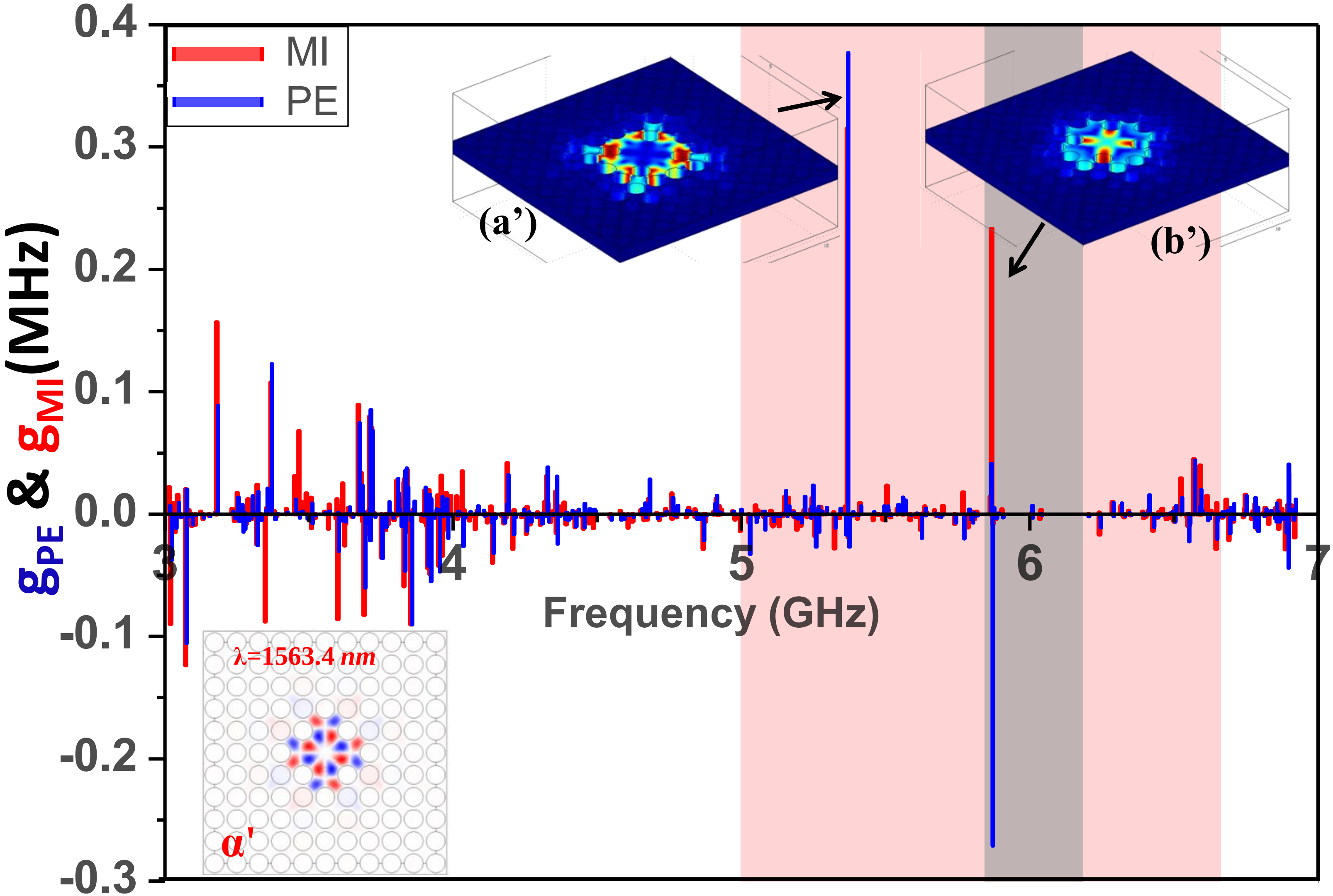

S. El-Jallal et al, Phys. Rev. B 88, 205410 (2013)
B. Djafari Rouhani, CR Physique 17, 555 (2016)

Nanobeam waveguides with periodic stubs and holes

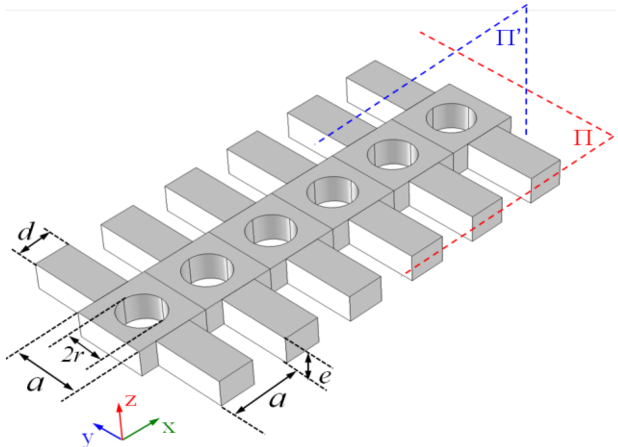

Two symmetry planes:

- Plane (xy): π

-plane (xz): π'

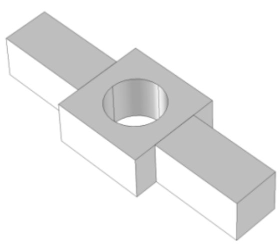

Unit cell

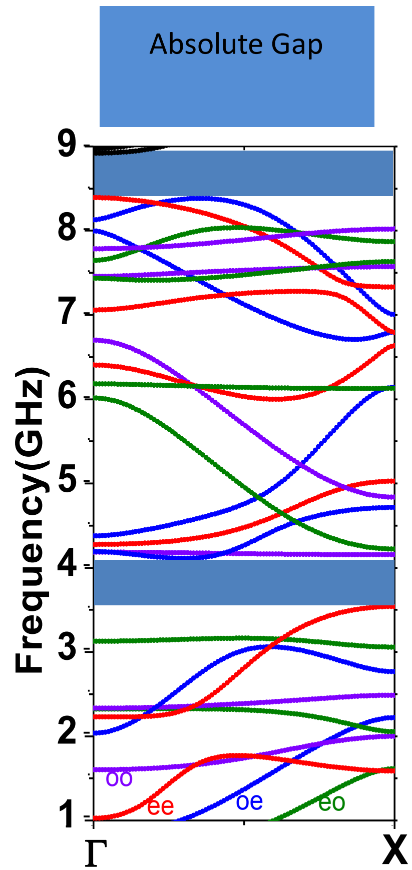

Phononic band structure

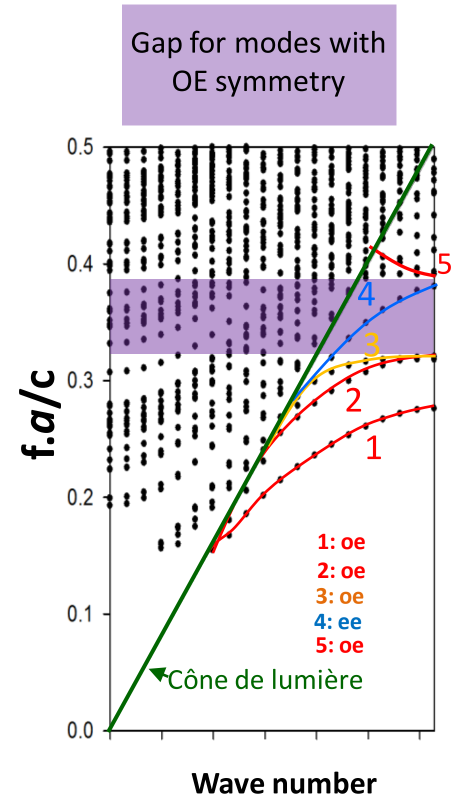

Photonic band structure

M.Oudich et al, Phys. Rev B, 89, 245122 (2014)
B. Djafari Rouhani, CR Physique 17, 555 (2016)

Nanobeam waveguides with periodic stubs and holes

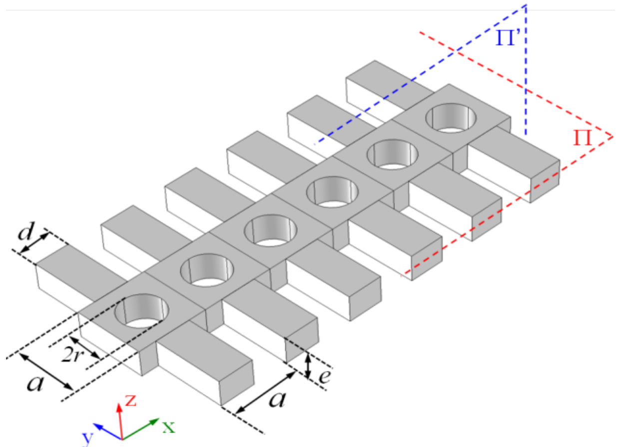

Two symmetry planes:

- Plane (xy): π

-plane (xz): π'

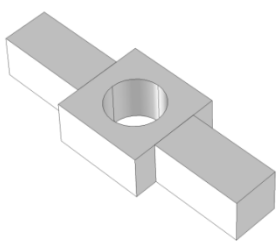

Unit cell

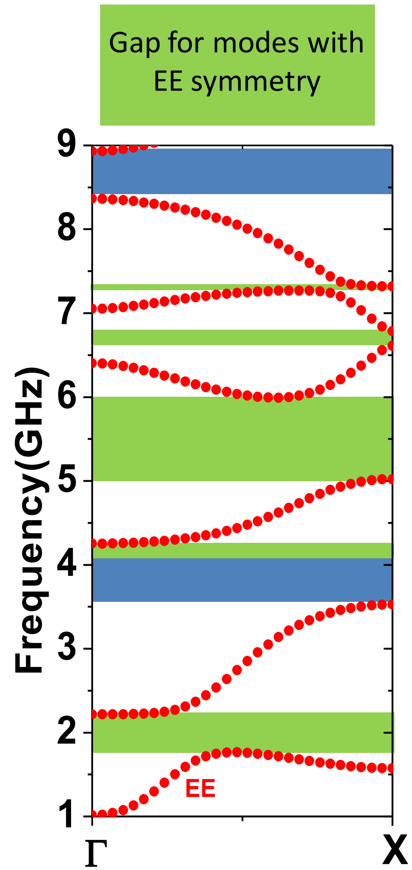

Phononic band structure

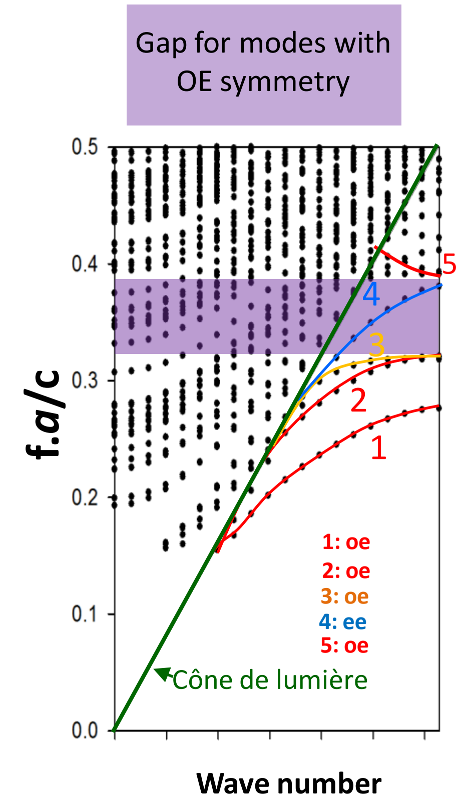

Photonic band structure

M.Oudich et al, Phys. Rev B, 89, 245122 (2014)
B. Djafari Rouhani, CR Physique 17, 555 (2016)

Nanobeam waveguides with periodic stubs and holes

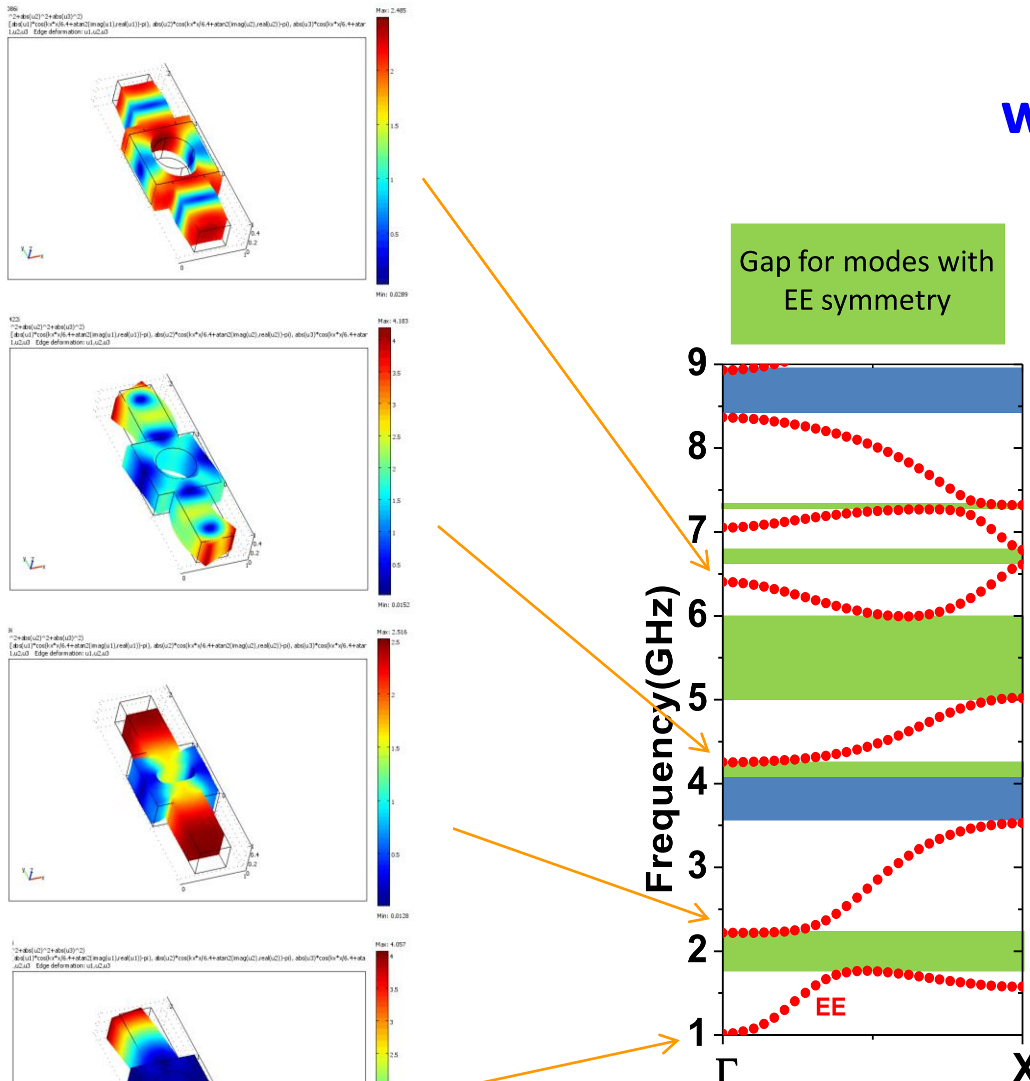

Phononic band structure

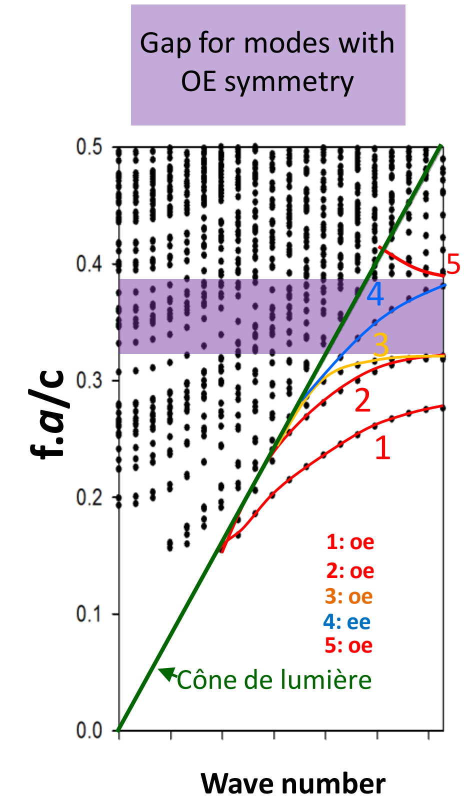

Photonic band structure

M.Oudich et al, Phys. Rev B, 89, 245122 (2014)
B. Djafari Rouhani, CR Physique 17, 555 (2016)

Tapered cavity to achieve high quality factor photonic modes

Parabolic tapering of the periodicity, hole radius and stub width

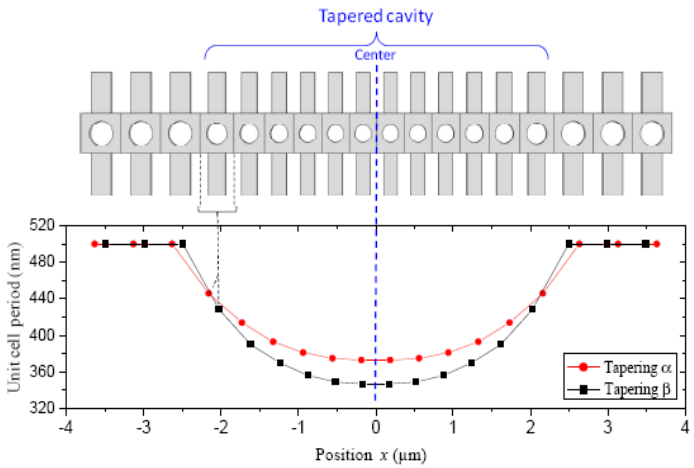

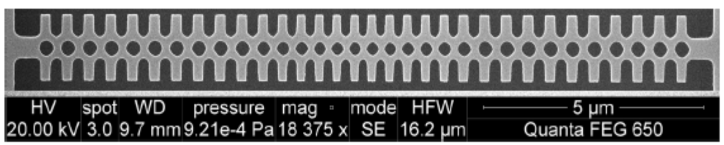

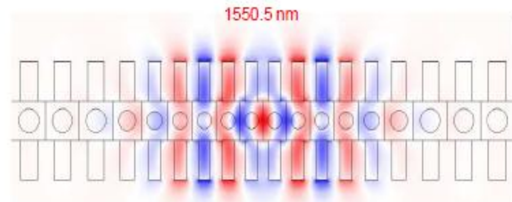

High Q photonic modes,
But Q degrades slightly for higher order modes.
The thermo-optic effect appears at high powers

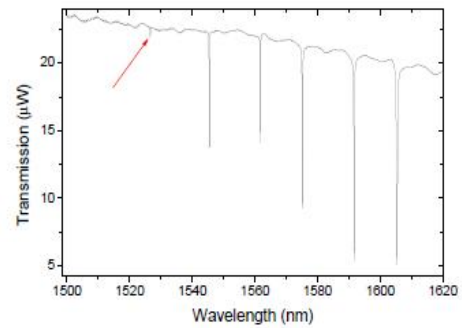

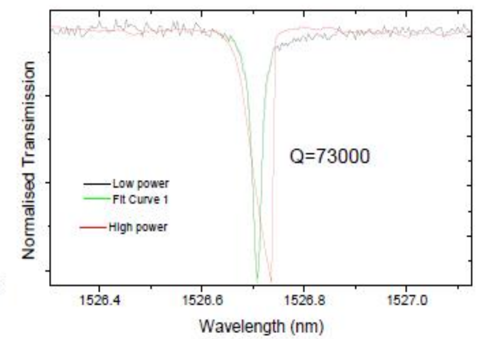

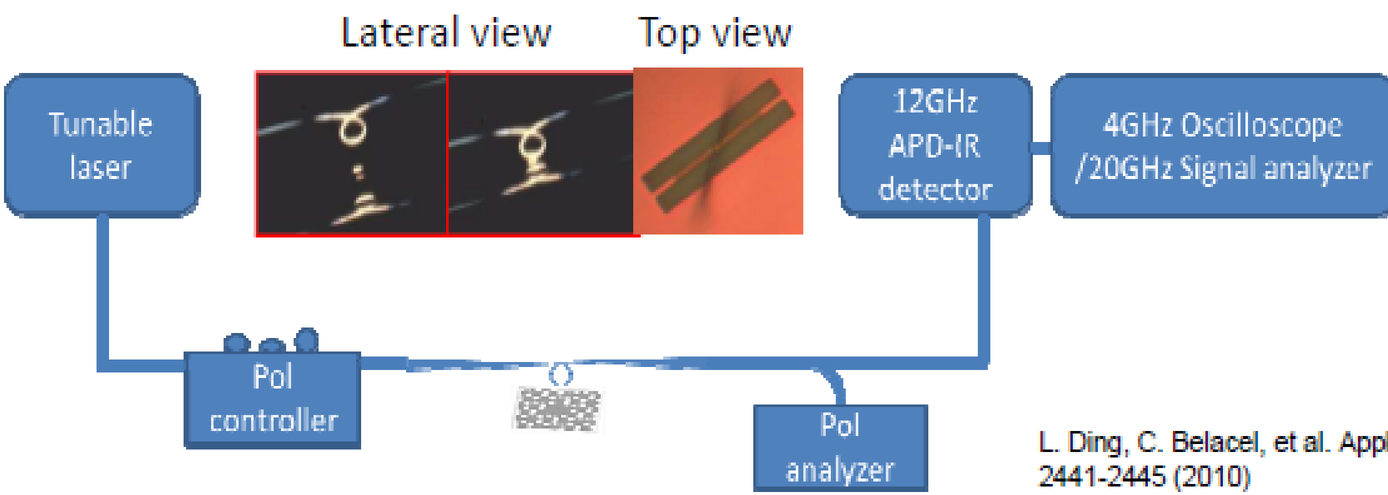

L. Ding, C. Belacel, et al. Applied Optics, 49, 2441-2445 (2010)

J. Gomis-Bresco, D. Navarro-Urrios, F. Alzina, C. M. Sotomayor-Torres, Catalan Institute of Nanotechnology

RF spectra of confined phononic modes

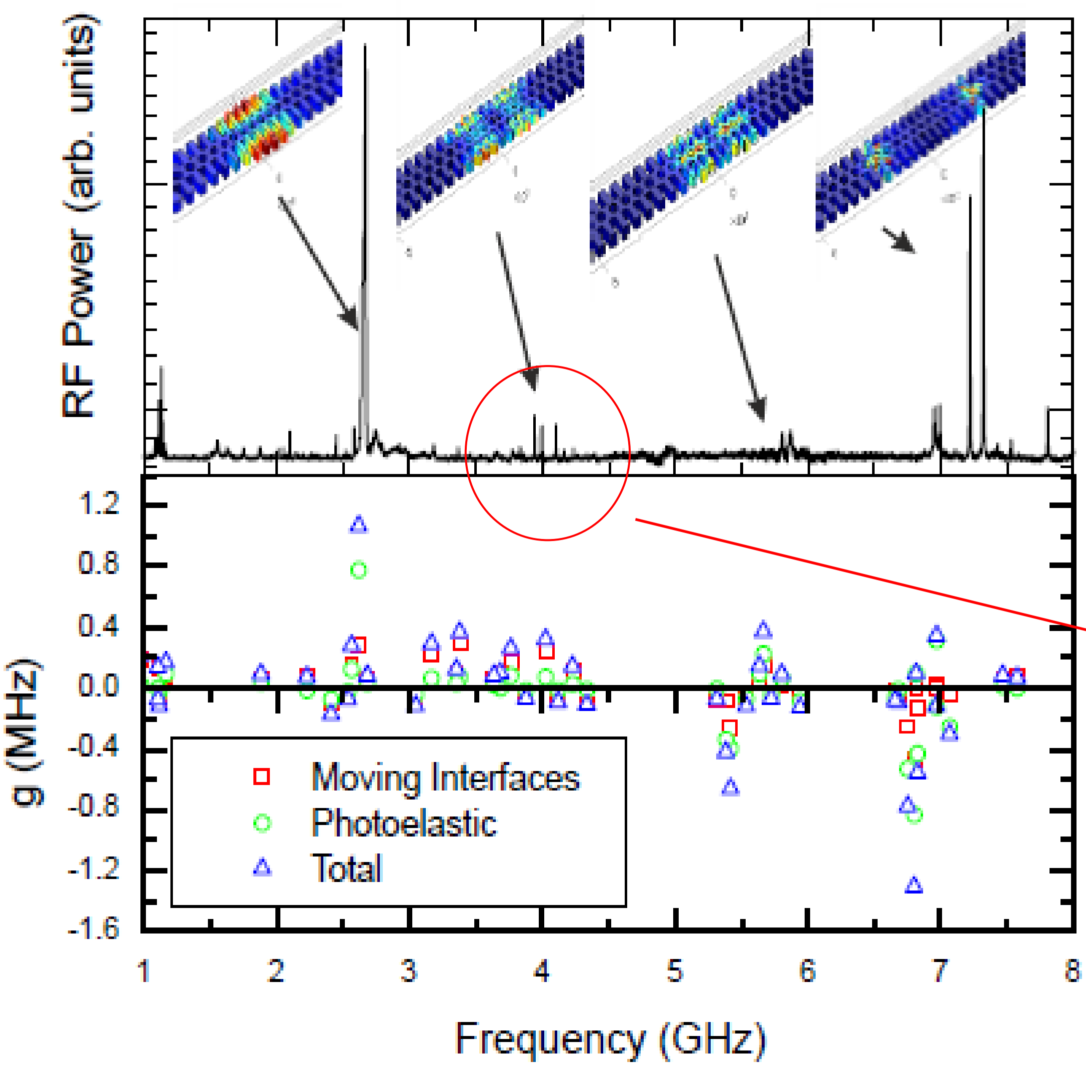

- Four different mode families observed

- Strengths depend on taper depth and selected optical resonance

Modes in the absolute band gap

J. Gomis et al, Nature communications, 5, 4452 (2014)

Characterization of phonon-photon interaction in phoxonic cavities (1D, 2D, Slab and Strip structures)

- Two methods of calculation;
  - Modulation of each photonic cavity mode by each phononic cavity mode
  - Calculation of the optomechanical coupling coefficient

- Both photoelastic and interface motions mechanisms contribute

- The relative magnitude of the the two effects can be different from case to case.

- The two contributions may be in phase or out of phase (constructive or destructive)

- The photoelastic contribution can be very dependent upon the choice of the material and the optical wavelength

- Symmetry consideration are important to discriminate the modes without coupling:
  In some cases, one-phonon process (which is the most likely in general) is forbidden due to the symmetry of the photonic and phononic modes

European Project FET OPEN « PHENOMENA »

All-Phononic circuits Enabled by Opto-mechanics (2016-2019)

Consortium: ICN2 Barcelona (Spain), polytechnic Valencia (spain), VTT (Finland), CNR and Univ. Pisa (Italy), UNIVPM Ancona (Italy) , University of Lille (France)

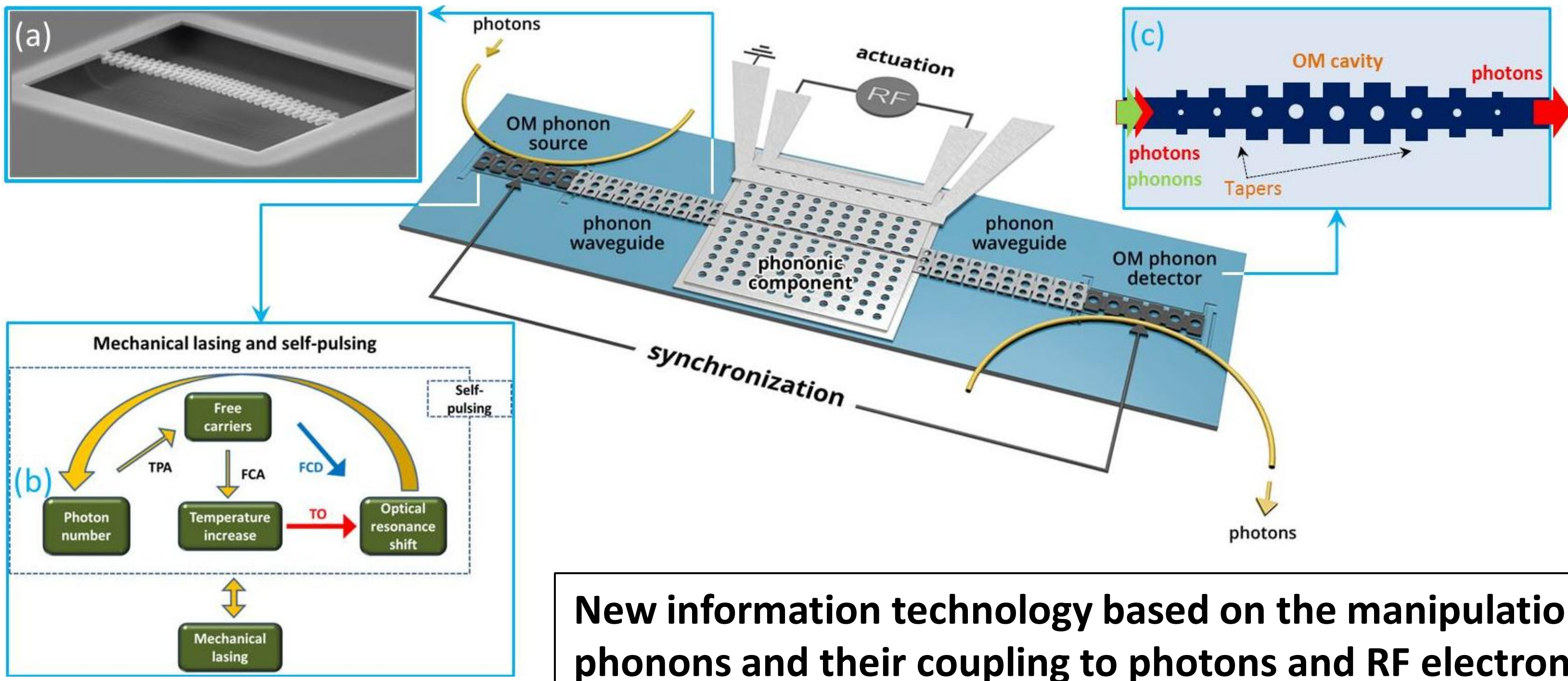

New information technology based on the manipulation of phonons and their coupling to photons and RF electronics

The PHENOMEN concept. *Information and energy of incoming photons are transformed into coherent phonons by cavity optomechanics. The phononic components process information (e.g., filtering, multiplexing, switching), and the output is transformed again to photons through optomechanics.*

Phonon-plasmon coupling

Metallic pillars separated from a Au film by a thin dielectric

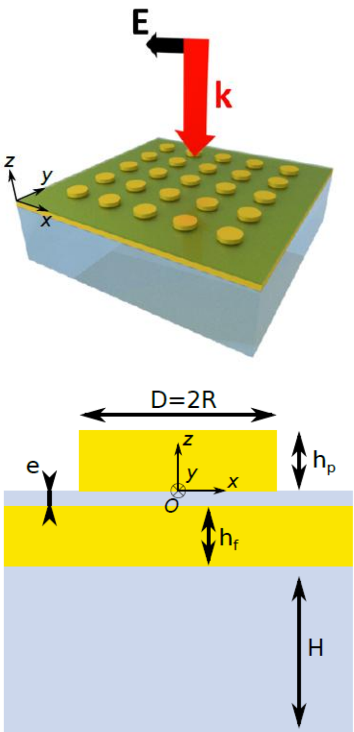

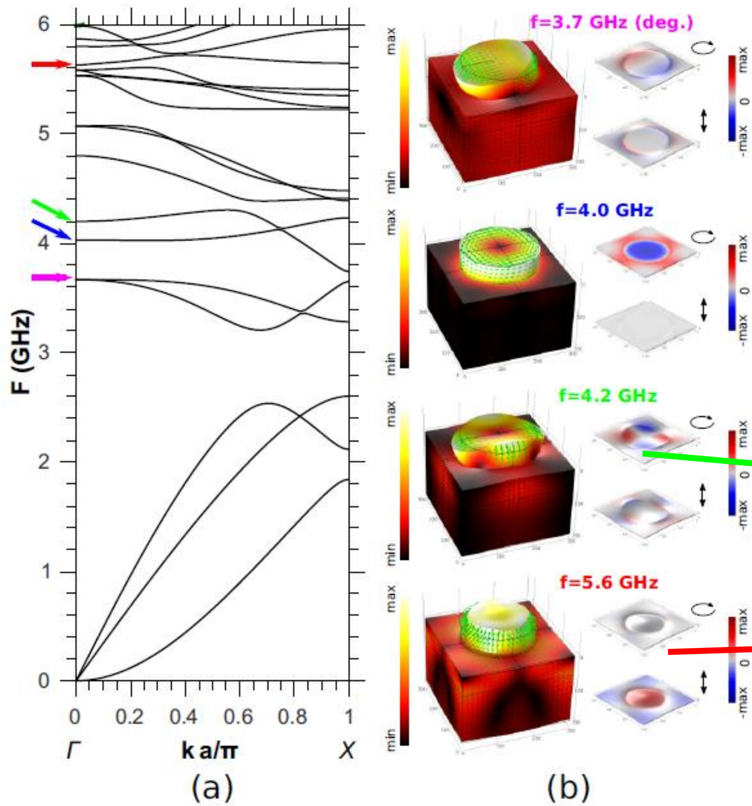

Very high sensitivity of Localized Surface Plasmons to compression modes

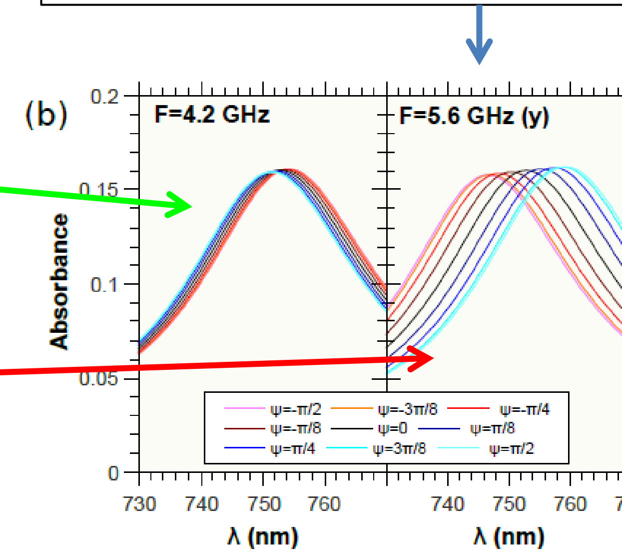

Modulation of the plasmonic attenuation by well-confined phonon

A. Mrabti et al., Phys. Rev. B 94, 075405 (2016)